

Low Density 2D-Electron Sheets on Liquid ^3He Surfaces

Der Universität Bayreuth
zur Erlangung des Grades eines
Doktors der Naturwissenschaften (Dr.rer.nat.)
vorgelegte Abhandlung

von

Sergiy Putselyk

geboren am 21 Dezember 1975 in Mogilev-Podolsk, Ukraine

Tag der Einreichung 13 Juli 2005
Tag des Kolloquiums 23 Januar 2006

1 Gutachter Prof. G. Eska
2 Gutachter Prof. P. Leiderer

Contents

1 Motivation	4
2 Electrons on ^3He surface: theoretical and experimental data	6
2.1 Excitation spectrum of a charged surface: the soft ripplon mode	6
2.2 Normal fluid ^3He	13
2.2.1 Vapour-Atom scattering regime	14
2.2.2 Ripplon-Limited regime	14
2.2.3 Wigner solid phase on Normal fluid ^3He	15
2.3 Wigner solid phase on Superfluid ^3He	17
2.4 Short Summary	21
3 Experimental Setup and Procedures	22
3.1 Nuclear Demagnetization refrigerator	22
3.1.1 Dilution Refrigerator	22
3.1.2 Nuclear Stage	22
3.1.3 Thermometry	24
3.1.4 The Magnet System	24
3.2 Experimental setup and cell	25
4 Discussion of different experimental conditions	28
4.1 Loading of electrons and determination of electron concentration	28
4.2 Recalculation of measured signal to resistance	33
4.3 Influence of cell tilting	35
4.4 Temperature gradients inside the cell	37

4.5 Overheating of electrons	39
4.6 Nonhomogeneous distribution of electrical fields and electron concentration	41
4.7 Influence of 1K-pot or cryostat oscillation	44
4.8 Short Summary	45
5 Results	46
5.1 Comparison of our results with results given in literature	46
5.2 Measurements with different film thicknesses	53
5.3 Measurements with different excitation voltages	58
5.4 Measurements with different excitation frequencies	60
5.5 Measurements with different pressing fields	65
5.6 Short Summary	69
6 Discussion	70
7 Summary and Outlook	76
Appendix A Determination of electron concentration	78
Appendix B Calculation of cell impedances and comparison of different models for signal-resistance recalculations	80
Appendix C Description of the cell	102
Appendix D Observed instability	103
Appendix E Wigner solid phase	109
Appendix F Original Data (X and Y Components)	111
Bibliography	123
List of Figures	128
List of Tables	131

Chapter 1

Motivation

Electrons on a bulk helium surface form a classical, two-dimensional system of particles, which has extensively been studied in the last two decades for ^4He [Leid92, Shir96]. These electrons offer the possibility of studying a two-dimensional (2D) degenerate electron fluid in the low-density limit, typically 10^5 - 10^9 electrons/cm². This system would be complementary to 2D electrons in heterostructures and MOSFETs for which the fluid phase has a higher density, for example, for GaAs/AlGaAs, 10^{10} - 10^{12} electrons/cm². In comparison with 2D electrons in GaAs/AlGaAs, electrons on He have higher effective mass 1.0 (GaAs/AlGaAs - 0.067 respectively), lower Fermi energy 10^{-7} - 10^{-3} mV (0.2-40 mV respectively), and usually higher mobility, 1-10000 m²V⁻¹sec⁻¹ (1-600 m²V⁻¹sec⁻¹ respectively).

The key feature of a 2D electron fluid on Helium is that the electrons are strongly interacting via the Coulomb force [Leid92]. At low temperatures, the transition to a 2D electron solid (Wigner crystal), occurs [Shir96]. This transition was observed by several groups [Leid92], [Shir96] for electrons on ^4He -liquid surfaces.

The possibility of studying quantum melting [Shir96], the effect of a magnetic field on the phase diagram [Shir96], and the 2D Hall effect [Lea91], made this an intriguing system to investigate to a great extent was done for electrons on ^4He .

For ^3He , Wigner crystallization was observed by the group of Kimitoshi Kono at all [Shir95] by mobility measurements. The author also performed plasma resonance experiments [Kir98, Kir00] as well as mobility measurements in the temperature range of superfluid ^3He [Kon00, Shir97].

Some questions are still open for 2D-electrons on ^3He -liquid surfaces: i) observation of Wigner solid transition (WS) for low electron density, (below $2 \cdot 10^7$ electrons/cm²), ii) whether temperature of non-crystallized electrons are higher than for crystallized ones, iii) unexpected behavior of resistivity in the superfluid phase [Shir98]. Theoretical prediction, proposed by Juri Monarkha [Mon01] of coincidence of effective collision frequency in the WS phase and in nondegenerate free electron one (plasma resonance measurements) also need to be checked. Systematic study of a mobility measurements for different excitation frequencies, electron densities, magnetic field and excitation voltage are still in need [Kon01].

Our work was aimed to the observation of Wigner solid transition in low density limit, below $2 \cdot 10^7$ electrons/cm², and under different conditions: 0.2-1.0mm, “bulk” helium film thicknesses, pressing electrical fields. In parallel we carried out measurements with different excitation voltages, frequencies of excitation voltages in order to illuminate different scattering mechanisms of 2D electrons. We also tried to used magnetic field, though these measurements were not extensive and could be used only as a hint for the future ones.

Chapter 2

Electrons on ^3He surface: theoretical and experimental data

2.1 Excitation Spectrum of a Charged Surface: The Soft Ripplon Mode

The surface of liquid helium has been proven as a nearly ideal substrate for surface state electrons (SSE) [Leid92]. Surface of helium could be considered as being completely inert and smooth, except for surface excitations (rippions), which act as the dominating source for SSE scattering at low temperature, where vapor pressure is too low that scattering of the electrons by the gas atoms is of any significance.

a) Neutral surface. Before discussing the influence of charges on the spectrum of surface excitation at the liquid helium surface, we briefly outline the situation for an uncharged surface. The motion of the surface, at rest located in the x-y plane, is governed by [Land59].

$$(\rho_- + \rho_+) \frac{\partial j}{\partial t} = -(\rho_- - \rho_+)gz + \sigma \frac{\partial^2 \zeta}{\partial x^2} \quad (1)$$

Here ρ_- and ρ_+ are the densities [kg/m^3] of the lower (liquid) and the upper (gas) phase, respectively, ϕ is the velocity potential, g is the acceleration due to gravity, σ [N/m] is the interfacial tension and ζ [m] the surface elongation of the interface from its equilibrium position (see also Fig. 1). In Eq. (2.1) we have assumed that ζ is varying only in the x axes, direction of wave propagation. The dispersion relation for interfacial waves (rippions) of frequency $\omega/2\pi$ and wave vector q , derived from Eq.(1), is

$$(\rho_- + \rho_+) \omega^2 = -(\rho_- - \rho_+)gq + \sigma q^3 \quad (2)$$

where we have made the simplifying assumption, that the distance d_- and d_+ of the surface from the ^3He -container bottom and top walls are large enough that $\tanh(d_+,q) \cong \tanh(d_-,q) \cong 1$.

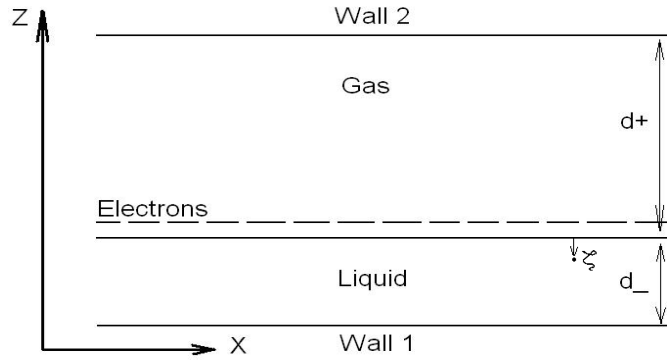


Fig. 2.1 Schematic diagram of gas-liquid (and electrons) interface. X -direction of signal propagation, z the surface elongation.

For small q the first term on the right-hand side of Eq.(2) dominates. For these “gravity waves” is $\omega \propto q^{1/2}$. For large q the dispersion of “capillary waves” is obtained $\omega \propto q^{3/2}$. The transition between these two types of waves occurs around $q=1/a$, where

$$a = [S / (r_- - r_+) g]^{1/2} \quad (3)$$

is the capillary length, describing the typical lateral range of static deformations of the interface. Incidentally, the phase velocity v_{ph} of interfacial waves has a minimum at $q=1/a$.

So far the damping of the riplons due to the viscosity of the bulk liquid has been neglected. If viscous forces can not be neglected, one has to consider additional term due to viscosity of liquid [Land59]. Equations. (1)-(3) not only hold for the “free” liquid surface (i.e. the liquid-gas interface) of helium, but also for the liquid-liquid interface of phase-separated ^3He - ^4He mixtures below the tricritical point, and in a slightly modified way, also for the interface between superfluid and solid helium [Leid92].

b) Charged surface. When the surface is charged, the electrons under the influence of a (homogeneous) external field perpendicular to the surface exert a pressure upon the interface. For a completely uniform charge distribution this

pressure is also uniform. Any local deformation of the interface, however, results in a rearrangement of the electrons, which are accumulated in the troughs and depleted in the crests of a, for example, sinusoidal perturbation [Leid92]. Therefore, the local pressure in the troughs is higher and in the crests is lower. The electrons thus tend to increase any deformation of the interface. Consequently, in the equation of motion of such a charged interface an additional term appears due to the pressure arising from the discontinuity in the electric field perpendicular to the interface

$$(r_- + r_+) \frac{\partial j}{\partial t} = -(r_- - r_+) g V + S \frac{\partial^2 V}{\partial x^2} + \{ [E_+(x)]^2 - [E_-(x)]^2 \} / 8p \quad (4)$$

where the (+) and (-) signs again refer to the upper and lower phase, E- applied electrical field pro unit surface. We shall assume in the following that the interface is charged to the saturation density n_s , i.e. the average field in the upper phase is screened completely, whereas in the lower phase it is

$$E_0 = 2pn_s e \quad (5)$$

(e is the elementary charge). One then obtains the dispersion relation of a charged interface

$$(r_- + r_+) \omega^2 = -(r_- - r_+) g q + S q^3 - 4p (n_s e)^2 q^2 \quad (6)$$

From Eq. (6) it follows that the aforementioned instability of the interface, related to the vanishing ripplon frequency $\omega(q_c) \rightarrow 0$, appears at a critical charge density $n_c e = [(r_- - r_+) g S / 4p^2]^{1/4}$, corresponding to a critical field

$$E_c = [64p^2 (r_- - r_+) g S]^{1/4} \quad (7)$$

The wave vector where this instability develops is $q_c = [(r_- - r_+) g / S]^{1/2}$, equal to the inverse capillary length defined in Eq.(3). Characteristic values for these quantities, calculated for the ^4He surface at $T=2.5\text{K}$, are $n_c=2.1 \cdot 10^9 \text{cm}^{-2}$, $\sigma=215 \cdot 10^{-6} \text{N/m}$, $E_c=3700 \text{V/cm}$ and $q_c=23 \text{cm}^{-1}$. For ^3He , $T=10\text{mK}$, $n_c=1.56 \cdot 10^9 \text{cm}^{-2}$, $\sigma=155 \cdot 10^{-6} \text{N/m}$ [Iino85, Mat01], $E_c=2.82 \cdot 10^3 \text{V/cm}$ $=2820 \text{V/cm}$, $q_c=22.7 \text{cm}^{-1}$.

Table 1 Critical values for instability phenomena of ^3He and ^4He .

	wave vector for instability	critical field*	critical concentration
^3He	22.7 cm^{-1}	2820V/cm	$1.56 \cdot 10^9 \text{ cm}^{-2}$
^4He	23 cm^{-1}	3700 V/cm	$2.1 \cdot 10^9 \text{ cm}^{-2}$

(* We would like to mention that during measurements we worked with much lower electrical fields, maximum 250V/cm).

c) *Electron scattering on ^3He -vapor atoms and riplons.* In order to solve Boltzmann equation for two scattering mechanisms, first of all, one has to find wave-function of electrons and interaction Hamiltonian. For that, one needs to solve Schroedinger equation.

Let us assume that liquid ^3He occupies the half space $z < 0$, and electrons are located outside the liquid. Since the dielectric constant of liquid ^3He , $\epsilon = 1.0426$ is larger than the vacuum value, the classical image potential acting on an electron

$$-\frac{e-1}{4e(e+1)} \frac{e^2}{4\pi\epsilon\epsilon_0 z} \quad (8)$$

is attractive, where e is electronic charge. We can consider $Q_0 = \frac{e-1}{4e(e+1)}$ as a effective charge and in our case it is $5.0 \cdot 10^{-3}$. Inside the liquid there is a potential which is repulsive because of negative electron affinity of helium caused by the Pauli exclusion principle. The motion along the surface is free-electron like and the wave function ζ in the z direction satisfies the Schrödinger equation,

$$\left[-\frac{\hbar^2}{2m} \frac{d^2}{dz^2} - \frac{\hbar^2}{ma_0 z} + V(z) + eE_z z \right] V(z) = EV(z) \quad (9)$$

where m is electron mass, a_0 the effective Bohr radius, $V(z)$ the barrier potential of the liquid, and E_z is the applied holding field and Hartree field due to other electrons, m – masse of He atom.

Since the barrier height is of the order of 1eV and a_0 ($a_0=9.5\text{nm}$) is much larger than the distance between He atoms, we can practically approximate $V(z)$ by an infinite barrier. The wavefunction should be solved with the boundary condition $V(0) = 0$ and for the ground state we obtain

$$V_g(z) = (4/b^3)^{1/2} z \cdot e^{-z/b} \quad (10)$$

with which variation ansatz yields

$$\frac{b}{a_0} = \frac{4}{3I} sh\left(\frac{1}{3} sh^{-1} \frac{9I}{4}\right) \quad (11)$$

where $I = \sqrt{2ma_0^3 e E_z / \hbar^2}$. For $E_z=0$, the exact solution of Schrödinger equation and the ground state energy for ^3He is $E_0 = \hbar^2 / 2ma_0^2$, which is about 0.47meV or 5.4K, b and a_0 are increased and normal Bohr radiuses.

To obtain the mobility of surface electrons we have to consider the Boltzmann transport equation with two scattering mechanisms: electrons-rippions scattering and electron- ^3He gas scattering. For more details see [Sait77].

$$T_e(E_x) = T(1 + (E_x / E_0)^2) \quad (12)$$

$$t(E_x, T) = t(T)(1 + b(E_x / E_0)^2) \quad (13)$$

where T_e is electron temperature, E_0 is the indicative field at which the warm electron effect becomes appreciable and $\tau(T)$ the Ohmic collision time, E_x is electric field along x-axis and β is effective parameter which depends on several values, such as surface tension, pressing electrical field, electron temperature, etc. In our experimental measurements with different excitation voltages (Chapter 5.3 and Appendix F, Fig. F4, p.116) we saw changing in measured signal slope (point, at which signal changes the slope, depends on temperature). Unless the electron-rippion scattering is present, β is identically zero and collision time is independent of the drift (excitation) field E_x . This is because when τ is energy independent (electron-He atom scattering), the averaged τ over the distribution function is still given by the Ohmic value. If β

is positive (negative) τ increases (decreases) as the drift field. Appreciable change in mobility occurs around $E_z \sim E_0 |\beta|^{-1/2}$.

d) Dimple lattice. The frequency of the soft ripplon mode at $q=1/a \equiv q_c$ vanishes when the electron density reaches a critical value n_c . For n just above n_c Eq.(6) predicts ω to become imaginary at a critical wave vector $q=q_c$, which implies that fluctuations in the elongation of the interface with that particular q -value will increase in time instead of decaying. As a result, a disruptive loss of charge from the surface develops, connected with a strong perturbation of the liquid.

A qualitatively quite different feature of the electrohydrodynamic instability is observed for ${}^4\text{He}$, when the surface is not charged to saturation, but only 8% of n_c or less. Although again interfacial waves with $q=q_c$ become unstable as the electric field is raised somewhat above a critical value E_c (and consequently the interface ripples spontaneously with a characteristic wavelength, which is again $\lambda_c=2\pi a$), the non-linear contribution to the restoring force stabilizes these deformations at a finite amplitude. Thus a new equilibrium state – dimple state in the charge distribution develops, different from the homogeneous layer of electrons for field below E_c .

An interesting property of the dimple lattice follows from the consideration of the charge distribution in this state. The charge density is not just slightly modulated along the surface, but is large in the region close to the dimple centres and zero elsewhere. Since the potential barrier between neighboring dimples is high, the amount of charge of each dimple is fixed, and as a result the interaction between the dimples is dominated by the Coulomb repulsion with only a small contribution from the deformation of the interface. The dimple lattice can therefore, be regarded as an example of a two-dimensional Coulomb crystal, and is in much respect a macroscopic counterpart of the (microscopic) Wigner crystal.

Some important features can be easily understood without developing a complete theory of the Wigner Solid (WS) on liquid ${}^3\text{He}$. First, in the case of liquid ${}^3\text{He}$, a high viscosity $\eta \propto 1/T^2$ makes the ripplon spectrum purely

imaginary for typical wavevector of ripplon and the WS $2\pi/a$, where a is a distance between electrons in the WS, which should crucially affect the low-frequency branch of the WS phonon modes.

Then transport properties of the WS could be limited by the mobility of dimple sublattice (no sliding, electrons move together with dimples), which could be determined by the interaction of ^3He bulk quasiparticles excitations (predicted by Monarkha for ^3He). The important point is that surface electrons cannot interact with bulk quasiparticles by themselves; above the solidification transition their mobility is still determined by the electron-ripplon interaction [Shir95]. In the solid state, the low-frequency motion of the electrons could be coupled with the dimple motion, the friction of which is determined by the bulk quasiparticle scattering. Therefore, the dynamic properties of the 2D WS on ^3He could be used as a powerful probe of the bulk properties of normal and superfluid liquid ^3He , as it was predicted by Yu. Monarkha [Mon97].

Given the typical electron spacing a is approximately 10^{-4}cm , therefore, three main temperature regimes could be expected for the WS transport above ^3He . The hydrodynamic regime theoretically predicted by Juri Monarkha for ^3He [Mon97] could valid if the quasiparticle mean free path, $l_f=5\eta/(\rho \hbar k_F)$ is shorter than the average dimple radius (here ρ is the density of liquid helium, 82kg/m^3 , $\hbar k_F$ is the Fermi momentum of quasiparticles, η - viscosity), which gives $T>20\text{mK}$. In this regime, the WS mobility is determined by the viscosity of ^3He . At lower temperatures, $T<20\text{mK}$, the system is primary in the long mean free path regime [Sh95]. In this case, the dynamic properties of the WS are determined by the reflection of the ballistic quasiparticles at the uneven dimple surfaces formed by the electron pressure. So WS mobility should depend on the quasiparticle Fermi-momentum and could be used as a probe of normal phase of liquid ^3He . The third regime occurs below superfluid transition, $T<0.93\text{mK}$. The appearance of the energy gap of the quasiparticle excitation spectrum could substantially reduce the number of excitation free to scatter from the dimple, which should reduce the momentum absorbed by moving dimples. At $T\approx 1\text{mK}$,

the mobility of electrons is far beyond the influence of the surface excitation, while the basic properties of the WS can be described in a rather stick way. Therefore, the WS mobility measurements can be used for experimental study of the superfluid phases of liquid ^3He .

It is worth to mention, that in the case of the very viscous ^3He , $\omega_q \ll 4\eta g^2/\rho$ (g - gravitational constant) leads to the important conclusion that low-frequency solution of the dispersion equation of coupled phonon-ripplon modes is purely imaginary ($\omega^2 < 0$) [Mon97]. This means that low-frequency resonances observed on ^4He by Grimes and Adams [Gri79] cannot exist in the case of normal liquid ^3He at sufficiently low temperatures. For typical electron density $n_e = 2 \cdot 10^8 \text{ cm}^{-2}$, this condition arises at $T < 0.13 \text{ K}$. Physically, this unusual behavior means that dimples of the ^3He surface are nearly stiff, even for low frequencies.

2.2 Normal Fluid ^3He

Surface state electrons (SSE) on liquid He have been gaining much interest of physicist for the resent three decades and the investigations have been done mostly on liquid ^4He , whereas little work has been done on ^3He . First measurements of escape rate and mobility of SSE on the ^3He have been done by Y. Iye [Iye80-1 and Iye80-2]. The phenomenon of electron scattering on ^3He vapor atoms, found in these works for temperature down to 0.5K, was parallel to those on ^4He and can be interpreted by taking into account, only the differences in the material constants; the liquid densities, saturated vapor pressure, surface tension, dielectric constants, and so on. Accordingly, no serious attention has been paid to the SEE on ^3He .

On the other side, measurements, done by K. Kono at all [Shir95] showed to be interesting. In Fig. 2.2 the SSE mobility is shown as a function of temperature for various electron densities [Shir95]. K. Kono divided the behavior into three temperature regions: the ^3He vapor atom scattering region, the ripplon-limited one, and the Wigner solid phase.

2.2.1 Vapor-Atom scattering regime

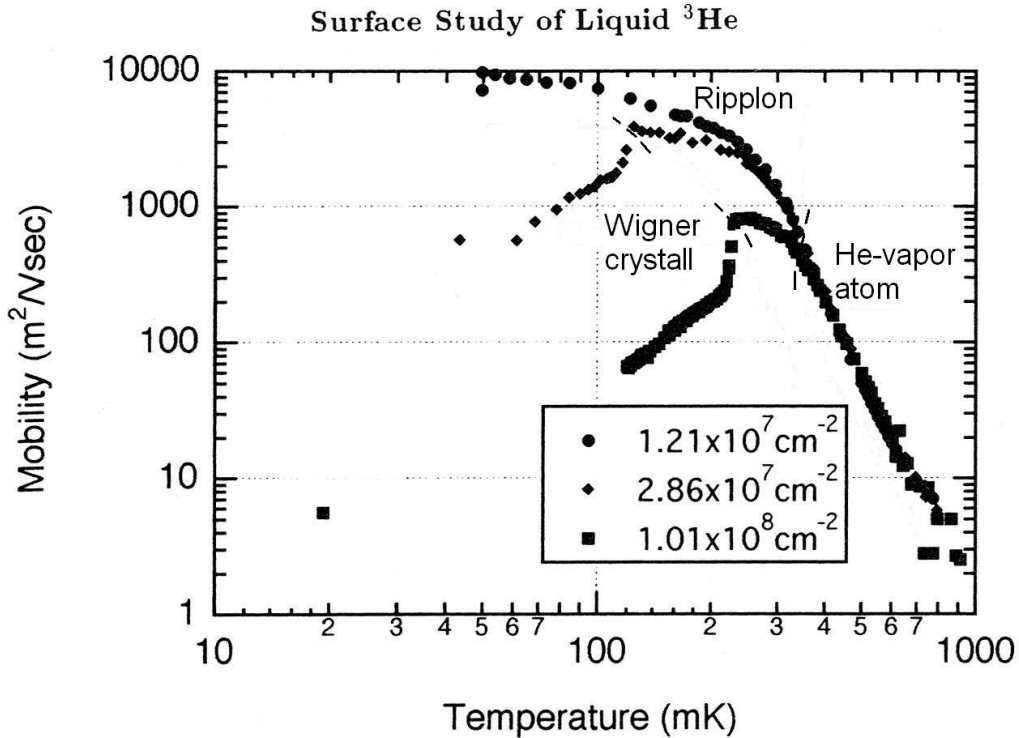


Fig. 2.2 Mobility, $m=1/(enR)$, as a function of temperature for three electron densities [Shir95], where R -resistance of electron layer, n -electron concentration, e -electron charge. Conductivity $S=1/R$ for two dimension layer. In further discussion we will use S as a conductivity, not as surface tension.

In Fig. 2.3 there is summary of experimental [Shir95] and theoretical [Sait77] data of electron scattering on vapor atoms of ^3He and ^4He . The theory predicted larger values by a factor of 1.5~2.0 than the experimental data (see Fig. 2.3, where calculations for ^3He were done by Motohiko Saito, using parameters of ^3He as well as his theory of He-gas-atom and ripplon-limited scatterings, developed for ^4He). From Fig. 2.2 and 2.3 one can see, that mobility in electron vapor atom scattering has power law dependence, not exponential or linear.

2.2.2 Ripplon-Limited regime

In Figure 2.2 we can see that the mobility changes from power law, (electron - vapor atom scattering) to gradual (electron - ripplon) increase below 300mK.

The position of transition region depended on the density of SSE. This transition region was shifted to lower temperatures for ^3He than for ^4He (and it can be explained by the difference in saturated vapour pressure). Also in these measurements K. Kono attributed density-dependent behaviour to the difference of the static electric field pressing the SSE toward the surface, which was proportional to n_s (Unfortunately, experimental parameters were not published and we can not directly compare our measurements with these ones).

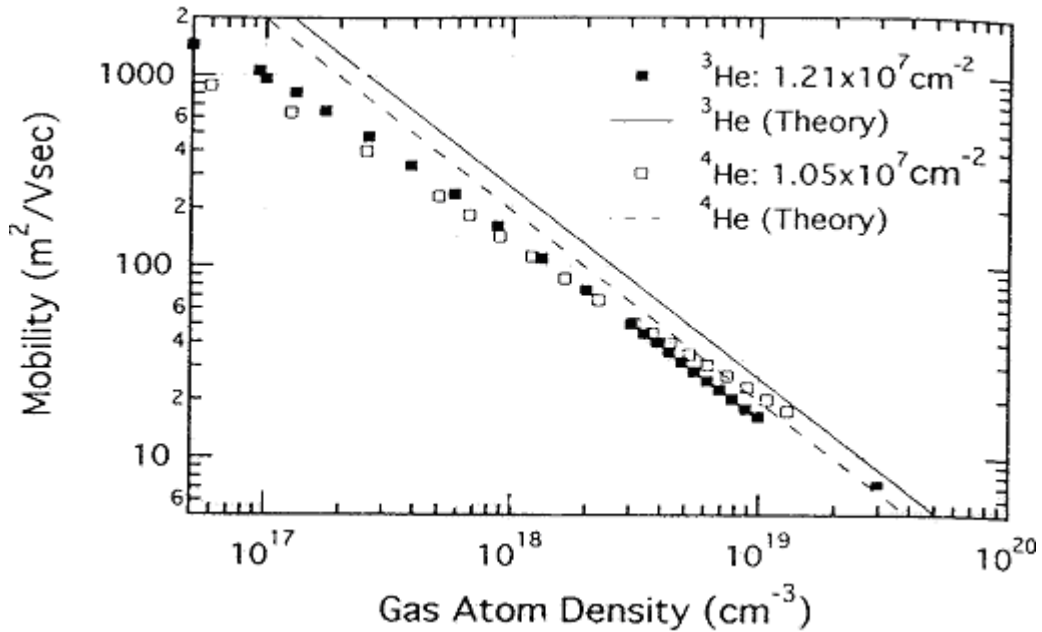


Fig. 2.3 Mobility of ^3He and ^4He [Shir95] in the vapor-atom regime as a function of vapor density. The lines represent the calculations [Sait77].

2.2.3 Wigner solid phase on Normalfluid ^3He

If we look in Fig. 2.2 on curves with densities $1.01 \cdot 10^8$ and $2.86 \cdot 10^7 \text{cm}^{-2}$ then we can observe two jumps of resistance at 250 and 130mK accordingly which were connected with WS crystallization. In his works Kimitoshi Kono distinguished two region of SSE mobility in the WS phase (See Fig 2.4): hydrodynamic regime and ballistic regime. Hydrodynamic regime was valid if the gasparticle mean free path was shorter than the average radius of dimples. At typical electron density 10^8cm^{-2} , it gave $T > 20 \text{mK}$. In this case, the WS

transport was determined by the viscosity of ^3He . At $T < 20\text{mK}$, the system was primarily in the regime of long mean free path (ballistic regime). In this case, the dynamic properties of the WS were determined by the quasiparticle reflection on the helium surface. Moreover at such a low temperatures [Mon97] the effective collision frequency of dimples with He quasiparticles (and reminding that electrons move together with dimples) was approximately two or three orders of magnitude higher than the contribution from scattering of electrons on surface excitation (ripples). Therefore, the bulk quasiparticle scattering at the dimples was the main cause for the electron resistance in these measurements (Fig. 2.4).

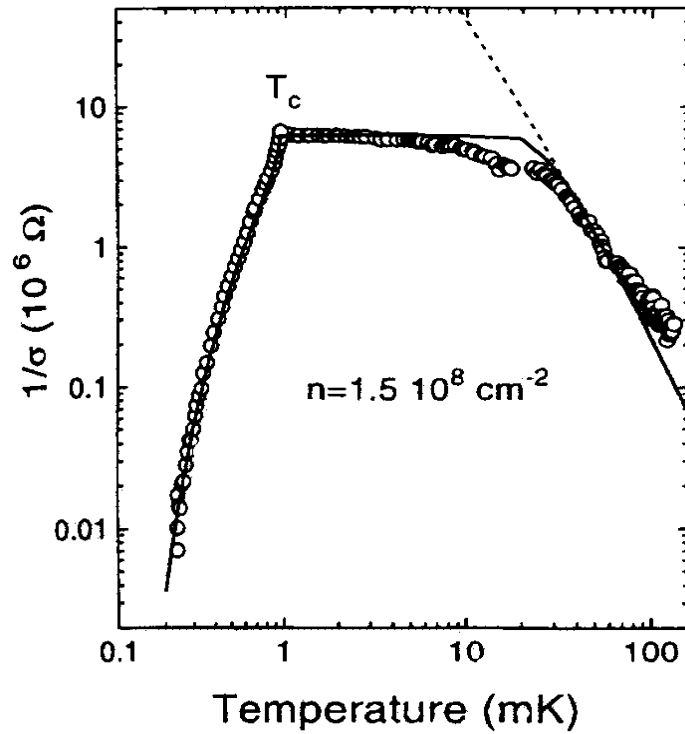


Fig. 2.4 WS resistivity versus temperature for the saturation case, $E=2p_{\text{en}}$. Solid line shows the theoretical results [Mon98].

2.3 Wigner solid phase on Superfluid ^3He

In the B-phase of superfluid ^3He (temperature below $T_c=930\mu\text{K}$) resistance R abruptly decreases by more than three orders of magnitude [Kon00]. The normalized to $R(T_c)$, (T_c is superfluid transition temperature) resistance obeys Arrhenius' law, see Fig. 2.4

$$\frac{R(T)}{R(T_c)} \propto e^{-\frac{\Delta}{kT}} \quad (14)$$

The parameter Δ increases from $1.76k_B T$ up to $2.0 k_B T$ as E_\perp increases from 180 till 498 V/cm. These values are close to the weak-coupling BCS energy gap at $T=0$, $\Delta(0)=1.764 k_B T_c$ and also to the estimated gap at the saturated-vapor pressure $1.774 k_B T$ [Shir97], [Mon98]. The theoretical curve is in a good qualitative agreement with the experimental data of the smallest electrical fields, E_\perp (in saturation case in which the electric field is completely terminated at the surface electrons) [Mon97].

$$\Delta(T) = \Delta(0) \tanh\left[\frac{3.067k_B T_c}{\Delta(0)} \left(\frac{T_c}{T} - 1\right)^{\frac{1}{2}}\right], \text{ where } \Delta(0)=1.764 k_B T_c \quad (15)$$

and the relation between the superfluid and normalfluid resistances is

$$\frac{R(T)}{R(T_c)} = \frac{2}{e^{-\frac{\Delta(T)}{kT}} + 1} \quad (16)$$

When the input excitation voltage V_{in} exceeds a certain threshold, the resistance shows no longer the exponential behaviour shown on Fig. 2.5 [Shir98]. At T_c , R starts to increase with a decreasing of the temperature and exhibits a step-like structure at about $800\mu\text{K}$. R subsequently decreases, obeying Arrhenius law similarly to that seen in the low V_{in} regime.

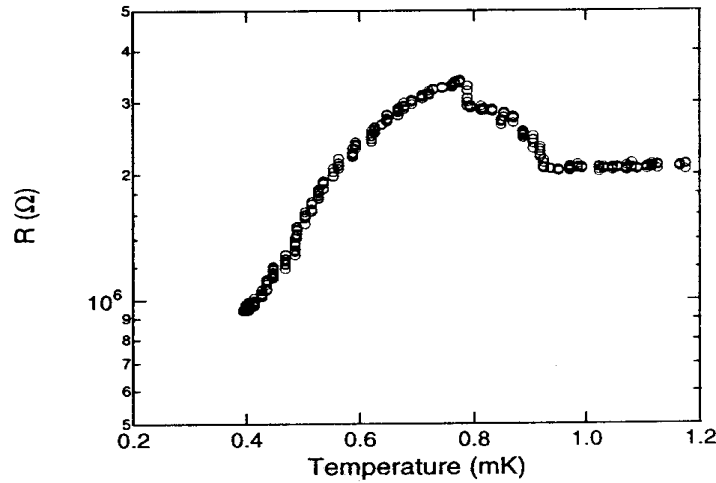


Fig. 2.5 Anomalous resistance of WS. $n_s=1.9 \cdot 10^7 \text{ cm}^{-2}$, $E_{\perp}=180 \text{ V/cm}$, $f=100 \text{ kHz}$, and $V_{in}=2.0 \text{ mV}_{p-p}$. [Shir98]. Deviation from Arrhenius' law, fig. 2.4 can be caused by excitation voltage, frequency, density and pressing electrical field [Shir98].

The threshold could also depend on various quantities such as the measurement frequency f , the pressing electric field E_{\perp} and the electron density n_s [Shir98], [Kon00] and under strong pressing field E_{\perp} the resistivity is smaller than the model prediction [Kon00].

From plasma resonance measurements of the coupled plasma-rippion (CPR) modes it becomes clear that below ^3He superfluid transition at 0.93 mK the relaxation time increases slightly [Kir98], Fig.2.6. Data obtained from a plasma resonance of transverse optical-plasma (TOP) mode also showed an increasing of the collision time τ below superfluid transition [Kir00], Fig. 2.7. It can be explained by a reduction of liquid ^3He surface fluctuations [Kir01] but further measurements and theoretical explanations for a big deviation of experimental curves and theoretical ones below 20 mK are required [Kir01].

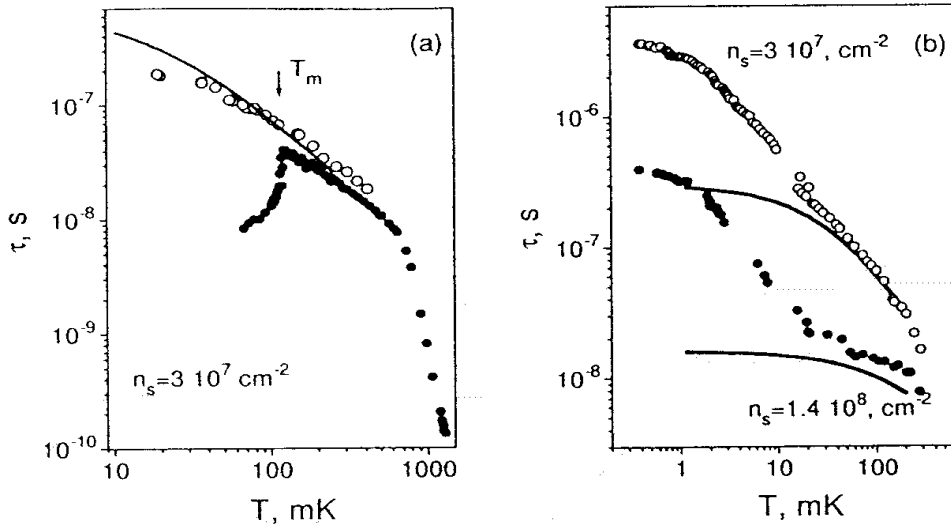


Fig. 2.6 (a) Collision time of surface electrons on the ^4He surface obtained from the linewidth of coupled plasmon-riplon resonance as a function of temperature (opened circle). The low frequency data of Corbino measurements (solid circles). (b) The collision time of surface electrons on ^3He surface as a function of temperature for two different densities [Kir98].

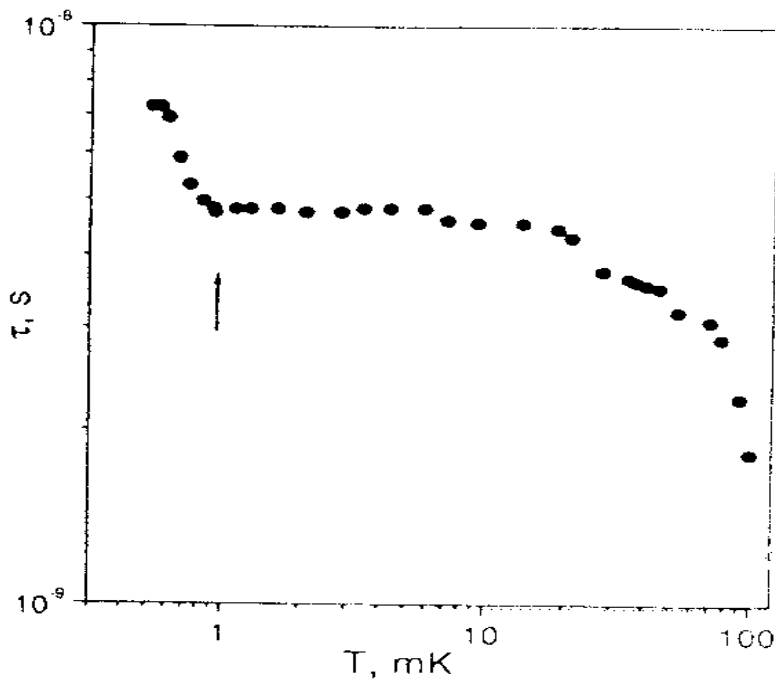


Fig. 2.7 Collision time t of surface electrons obtained from the line width of transverse optical-plasma resonance as a function of temperature. The temperature of the superfluid transition in ^3He is marked by an arrow.

Measurements of the WS conductivity in the A-superfluid phase of ^3He were also done [Shir00] but in a rectangular geometry. The A-phase was obtained due to the magnetic field applied parallel to surface of liquid ^3He . Relatively large WS resistance in the A-phase indicates that ^3He quasiparticles excited in the gapless direction substantially contribute to the resistance, see Fig.2.8. In this case the energy gap should be substituted by

$$\Delta(T, q) = \Delta(T) \sin q$$

$$\Delta(T) = 2.031 \tanh \left[1.687 \left(\frac{T_c}{T} - 1 \right)^{1/2} \right] \quad (17)$$

where θ is the polar angle with respect to \mathbf{l} , and \mathbf{l} is an angular-momentum quantization axis [Kon00]. Resistivity in the ^3He A-phase follows more or less the same curve from run to run, hence, it can be concluded that the texture has always the same configuration, at least at distances of the order of the quasiparticle mean-free path.

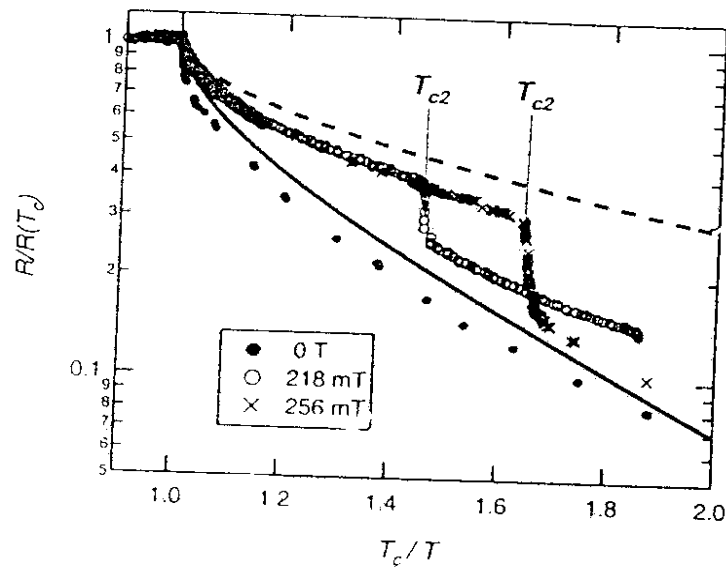


Fig. 2.8 The Wigner Solid resistance $R(T)$ normalized by $R(T_c)$, as a function of T_c/T , at $0T$ (filled circles), 218mT (open circles), 256mT (crosses). The solid and dashed curves are the calculated $R(T)/R(T_c)$ assuming l^2/n , and l/n , respectively (noting, this measurements are done in rectangular geometry) [Shir00], where \mathbf{n} is the surface normal vector, \mathbf{l} is gapless direction of A-phase.

2.4 Short Summary

- i) *summary of available experimental data in literature.* In the high temperature region, above 300mK electrons scatter on ^3He vapor atoms and from $\approx 300\text{mK}$ till 100-250mK there is scattering of electrons on ripplons. In Wigner solid phase, there are two scattering regimes – hydrodynamic and ballistic, in which electrons scatter indirectly on ^3He quasiparticles. In the ^3He superfluid temperature region, mobility of electrons is increased due to appearance of band gap of superfluid ^3He (A or B phase). Plasma resonance measurements gives much higher scattering times as theoretically predicted. Resistance of electron layer at ^3He superfluid temperatures can be unexpected.
- ii) *Existing problems.* Anomalous high scattering times of electrons in helium surface by plasma resonance measurements, unexpected behavior of resistance at temperatures below ^3He superfluid transition, measurements of Wigner Solid transition for low concentrations, below $2 \cdot 10^7 \text{electrons/cm}^2$, where sliding of WS can occur. Reproducibility of measured data should be also improved.
- iii) *Goals.* In this work we tried to observe Wigner Solid transition for low concentrations, below $2 \cdot 10^7 \text{electrons/cm}^2$. Attempts to measure anomalous resistance characteristics at ^3He superfluid temperatures were also carried out.
- iv) *Importance for the community.* For the area of 2D electron systems, measurements of electron densities and mobilities in very high as well as in very low density limit, below $2 \cdot 10^7 \text{electrons/cm}^2$, are of great interest. Usually, for quantumfluids we have lower densities, $10^7\text{-}10^9 \text{electrons/cm}^2$ in comparison with heterostructures, for example, AsGa/AlAsGa, $10^{10}\text{-}10^{12} \text{electrons/cm}^2$.

Chapter 3

Experimental Setup and Procedures

3.1 Nuclear Demagnetization refrigerator

3.1.1 Dilution Refrigerator

^3He - ^4He dilution refrigerator was bought from *Oxford Instruments GmbH*. Lowest possible temperature reached was approximately 3.8 mK [Wag95]. The cooling power of dilution unit is about 7 μW at 10mK with circulation rate of 550 μmol per second.

The temperature of the dilution unit was monitored by carbon (Speer) and RuO_2 thermometers. A detailed description of the dilution unit was done in [Wag95]. Further useful reviews of the principle of operation of a dilution unit may be found in [Lou74], [Bet76], [Pob92], [Sti86].

3.1.2 Nuclear stage

The experimental stage is attached under the dilution unit. This stage is made from 240 mol of oxygen-free high-conductivity copper. The stage consists of single pieces of copper which were also splitted to reduce eddy current heating. 40 mol are in a region where a magnetic field of 8.5 T may be applied. With the maximum field of 8.5 T and precooling time of approximately 60 hours it was

possible to cool the nuclear stage down to 15mK. Further demagnetisation of the nuclear stage enabled temperatures up to 0.7 mK with final field of 50mT. Three Indium ($B_c = 28.3\text{mT}$) heat switches are used to thermally couple and decouple the nuclear stage to dilution unit. The difference in heat transfer (“switching ratio”) is 60000 at 10mK. Helpful details about manufacture and operation of the nuclear stage are discussed in [Wag95].

In the context of the work described here the cryostat was operated in such a way that nuclear stage was magnetized and demagnetised two times to allow measurements (temperature sweeps) down to $\sim 0.7\text{mK}$. A typical sweep from temperature $\sim 1.3\text{mK}$ to 0.7mK and back to 1.1mK was carried out in approximately 6 hours.

The surface area ($\sim 400\text{ cm}^2$) of the circular experimental stage was used for mounting different experimental cells. The available height for such cells was 20cm. Cell was mounted in the side of experimental plate (Figure 3.1).

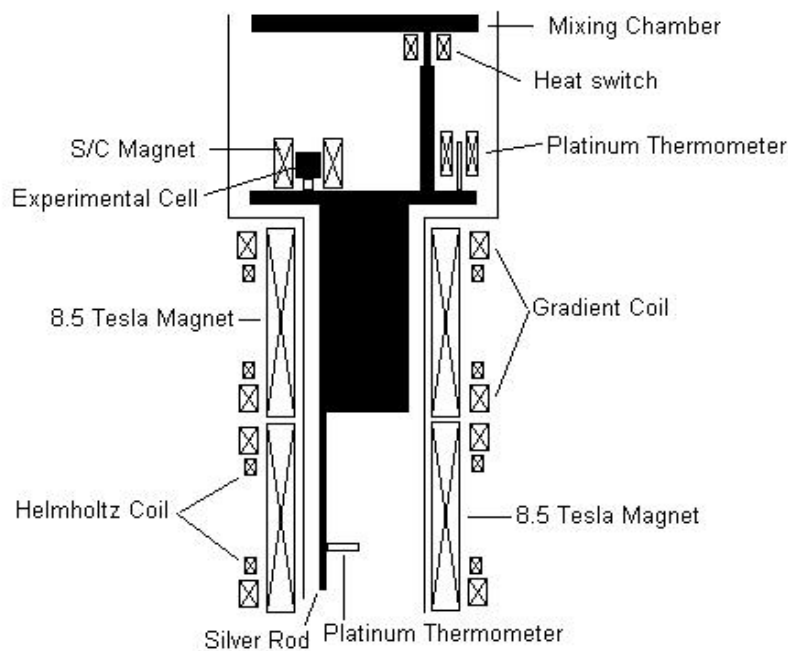


Fig. 3.1 *Schematic drawing of the cryostat. The mixing chamber is thermally connected to the nuclear stage via three In heat switches. The experimental cell is screwed in the side of the experimental stage. The superconducting magnet which encloses the cell is thermally linked to the dilution unit but not to the nuclear stage.*

3.1.3 Thermometry

Three different thermometric principles were used in order to monitor the temperature in the temperature region from 1-600mK. Firstly, a PdFe electron susceptibility thermometer, secondly, a Pt pulsed NMR thermometer located on the nuclear stage. Both of these thermometers monitored the temperature of experimental plate and two resistance thermometers: a Speer-carbon thermometer (1K-10mK); RuO₂ thermometer which was mounted directly in cell.

Measurements were also performed in the whole regime from 296 K down to 200 mK. A commercially available resistance thermometer (Pt-100) was used in the range from 296K-70K, in parallel with a germanium thermometer (296K-1.5K). The calibration of Pt-NMR thermometer was achieved with use of tungsten based fixed-point device, this fixed-point device depicted two fixed points, one at 17.1 mK and the other at 61 mK [Wag95].

In the low temperature region, i.e. < 4mK the Korringa constant of platinum (0.03 Ks) allowed a thermometry measuring sequence to be performed in no less than 180s [Eska88]. A linear extrapolation between two points was eminent and hence carried out in order to obtain the temperature between points. In our measurements for superfluid point transition of ³He, we made a demagnetisation sweep from 1.3mK to 0.77mK in 85min.

3.1.4 The Magnet System

There are plenty of different magnets for different application inside of Cryostat [Fig.3.1]. The “main-upper” (denoted as 8.5 Tesla Magnet in Figure 3.1) magnet used in order to demagnetise the nuclear stage. It sustains a magnetic field of 8.5 T with current of 64.2 A (=132mT/A). The induction of magnet is 42.3 Henry [Wag95].

The “Helmholtz” magnet is used in order to make field more homogeneous. The field to current characteristic of this magnet is 2.1 mT/A. It is also constructed so as to operate with maximum current of 64.2 A.

The “gradient” magnet is used so as to apply magnetic field gradients, which are sometimes required in NMR measurements. The gradient field produced by this magnet is 0.26 mT/(cmA). The maximum current is 64.2 A.

The “main-lower” magnet is located at the lower part of the cryostat and is essential for the NMR experiments lying at the low part of nuclear stage.

In addition 2D-Electron cell is located inside a small magnet (denoted as S/C Magnet in Figure 3.1) with a field to current ration – 0.651kG/A. The particular location of the cell (in the side of experimental plate) ensures that copper body of the cell was never subjected to fields large than $B \sim 50$ mT [Wag95]. The schematic drawing of the cryostat along with the position of the cell on the experimental plate (in the side) is given in Figure 3.1.

3.2 Experimental Setup and Cell

Figure 3.2 depicts the schematic diagram of the experimental cell (exact scheme with dimensions is presented in Appendix C, p.102). Excitation voltage is applied to the lower-left electrode from lock-in SR850 and picked up by the lower-right electrode and transferred back to the lock-in. After that experimental data are saved on the computer (we used available software written by the other Ph.D. students and G. Eska, which was only slightly changed for our experiment). For check of the cell and calibration of the ^3He film we used another setup, depicted on Fig. 3.3. Tungsten filament is used for evaporation (loading) of electrons on the surface of ^3He . We apply negative DC bias voltage V_g (Hewlet Packard E3612p) to the guard electrode. Usually two-third of this voltage was applied to upper electrode through voltage divider. Another DC power supply (Keitley 230) could produce positive or negative DC voltage on the lower middle electrode.

The experimental cell used in this work was made from copper, a typical material for low temperature measurements owing predominantly to its large heat conductivity, availability and due to the fact that it is easy to mechanically work with. The cell was divided into two parts [Appendix C, p102]. The lower part which contained the sinter, three lower electrodes and RuO₂ thermometer, the upper electrode and two filaments. The lower part was screwed into the upper part with indium oring. The whole cell was fixed on Nuclear Experimental plate. Outside of the sell there was superconducting magnet with maximum field in the middle of the cell 0.651KG/A (First version of the cell was done in 1998 and was changed several times. Current version was installed in spring 2001 and since then was not opened. Design and construction of the inner part of the cell was done by Anne Marie Valkering and Juergen Klier, University of Konstanz). We made most of the measurements as in “three electrodes” configuration (measuring from two opposite electrodes, #1 and #3) and some in “two electrodes” configuration (measuring from two adjust electrodes, #2 and #3)

Due to the large thermal boundary resistance at low temperatures between the copper part of the cell and the liquid ³He in contact with it, it was necessary to increase the surface area contact between the two media, solid and liquid, so as to improve the thermal coupling. This is typically achieved at low temperatures by the use of a silver heat exchanger. The heat exchanger used in these experiments was manufactured under high pressure of commercially available silver powder with grain size of approximately 70nm. This powder was pressed in the cell. The advantage, which may be inferred from this particular construction, was that the liquid was forced to flow through the sinter before it enters the experimental volume. The lower part of the cell containing the silver was annealed at 10⁻⁶ bar – 100⁰C for 12 hours prior to pressing of the sinter; this allows an enhancement of the heat conductivity of the material. If one assumes a surface area of 1.8 m² per gram [Fra84] then for this sinter of mass 5 g the total surface area amounts to 9.0 m².

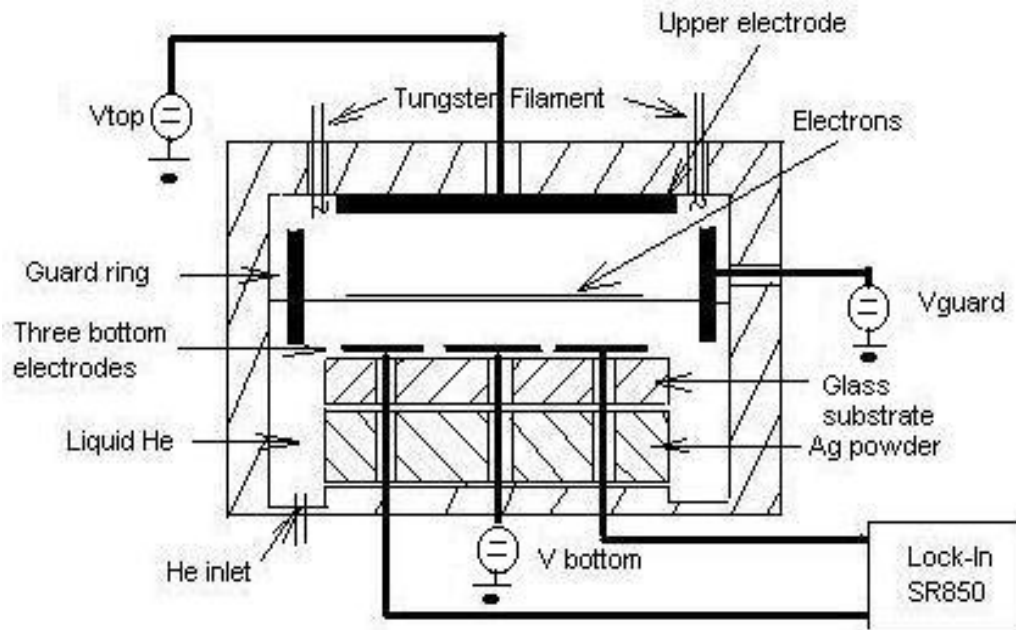


Figure 3.2 Schematic diagram (sketch) of the cell for mobility measurement. All electrodes have the same width – 17mm. Three bottom electrodes have the same length – 6mm, upper electrode has diameter – 17mm. Guard electrode (guard “ring”) has dimension of 17*17mm and high 4mm. Distance between top and bottom electrodes – 4mm (see also Appendix C, Fig. C1, p.102).

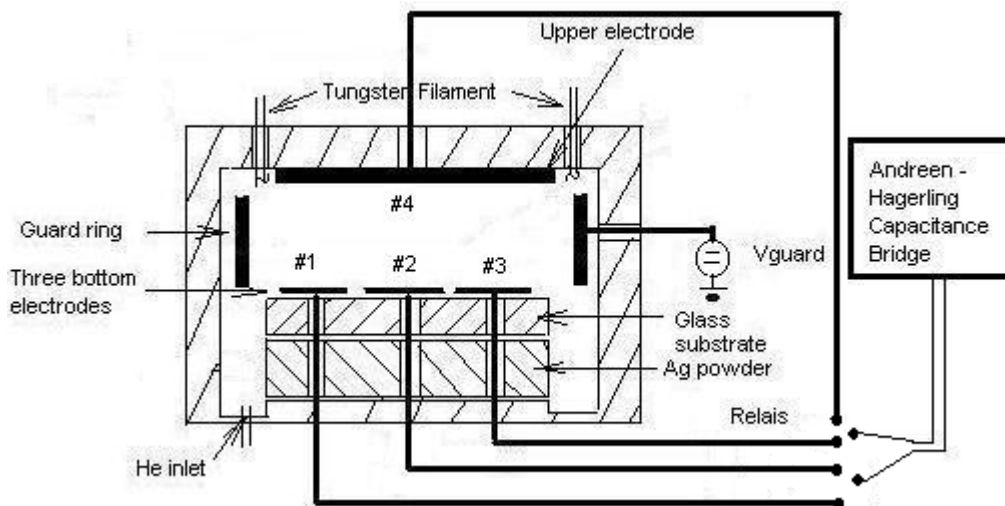


Figure 3.3 Schematic diagram (sketch) of the cell for mutual capacitance measurement.

Chapter 4

Discussion of different experimental conditions in our measurements

Before we start with analysis of experimental data, it is necessary to consider several factors that can influence our measurements.

In our experiments we usually worked with energies of less than few mJ during the electron loading, excitation field 10mV and typical Coulomb forces between electrons is 10^{-17} N for the electron densities 10^7 electrons/cm². These values are small and external sources, that can influence our measurements, must be considered.

First of all, one has to consider the problem of determination of electron concentration and recalculation of measured signal to resistance R (and knowing the concentration, n, using the formula $R=1/ne\mu$, where, e – electron charge and μ - mobility, we can obtain mobility of electrons).

Next questions could be influence of cell tilting, temperature gradients in the cell during the loading of electrons, overheating effects of electrons by the excitation voltage, nonhomogeneous distribution of electrical field profile inside the cell (and connected with it nonhomogeneous distribution of electron density), influence of noise of 1K-pot as well as oscillation of cryostat.

In this chapter we would like to consider all these factors.

4.1 Loading of electrons and determination of electron concentration

First question, which has to be stated, is whether all electrodes are mechanically not changed and whether we have the right helium layer of micrometer thickness, can be answered due to our capacitance measurements.

Capacitance bridge Andreen-Hagerling (see Fig. 3.3, p.27) was performed for the measurement of mutual capacitances of electrodes. Stable measurements till $1 \cdot 10^{-6}$ pF allowed us to see changing “aging” of the cell (maximal changing 1.5% pro year) as well as to determine He layer thickness better than 0.05mm.

The next questions, which have to be verified, are: how are electrons loaded, what is the electron distribution and is signal stable in time?

The standard loading (Fig. 4.1) was at temperature 350-450mK, with the loading pulse duration 70ms, amplitude of the pulse 4.7V, the filament resistance 88Ω , (corresponding power 0.25W, and the energy 17.6mJ). Under these conditions the electrons were loaded in two-three pulses till the signal saturates (further pulses resulted only in an insignificant increase of signal, within 5%, [PPE]). Our estimation for the given pulse power, geometry, and the tungsten filament showed, that we can load amount of electrons, typically $0.7-36.8 \cdot 10^7 [\text{cm}^{-2}]$ with three-four pulses.

For example, we can estimate how many loading pulses we need in order to load electrons till saturation. We take maximal density we worked with as $36.8 \cdot 10^6 [\text{cm}^{-2}]$. We have formula for the thermal emission current density

$$J = AT^2 \cdot e^{\frac{-e(\phi - V)}{kT}} \text{ [A/m}^2\text{]}$$

where ϕ - workfunction of tungsten (4.54V), V – applied voltage (in our case 4.65V), T – loading temperature (for our estimations we take surrounding temperature, 0.3K, which is not absolutely correct, because filament can have higher temperature during the loading), A ($\text{kA/m}^2\text{T}^2$) – proportionality coefficient, for tungsten A=600.

Because our applied voltage is the same as work-function (even a bit higher) we can neglect exponent for our calculations.

For our tungsten filament with 5mm length and 1mm diameter we have surface $4 \cdot 10^{-9} \text{ m}^2$. We can used conservative approach considering that only 1% of the surface emits electrons (other surface is dirty or oxidized). Than we have surface $4 \cdot 10^{-11} \text{ m}^2$. This surface emits $2.16 \cdot 10^{-6} \text{ A}$. For typical our loading pulse duration 70ms, we have $9.5 \cdot 10^8$ electrons. Due to geometrical position of

our filament, only fifth part of electrons go to the surface of helium (and this is again conservative approach, because we did not consider positive voltages on three bottom electrodes and negative voltages on the top electrode and guard ring) $2 \cdot 10^8$ electrons. And for the surface of $17 \cdot 17 \text{mm}^2$ we have density $0.7 \cdot 10^8$ electrons/ cm^2 .

So we can see that it is possible to load electrons to the expected concentration within few pulses.

However, it is worth to mention that saturation of signal does not mean a complete saturation of the electron density because loading of electrons particular on a thin film of nanosize thickness could be a complicated process due to the effect of localization of the electrons (or, in the other words, not all electrons or even groups of electrons are connected with each other and therefore part of electrons do not participate in the conductivity measurements). The situation becomes better when one works with a thick layer (1mm or so, and unfortunately we did electron density measurements only for 1mm, not for 0.2mm film thickness) where the electron localization effect is negligible. Though we would like to mention that due to nonhomogeneous electrical field distribution, namely three bottom electrodes are square and top electrode is round and does not cover the whole surface, it could be the case that part of electrons do not participate in the conductivity or part of helium surface is not covered by electrons at least during the loading. In order to illuminate it, 3D calculation of electrical field profiles could be very helpful. On the other side, even when we work with a thick layer (1mm), it is difficult to obtain absolute (full) electron density corresponding to the full screening of the applied electrical field. The reason is as follows: the loading is not homogeneous to the whole surface of electrodes (in one part, the electrical field can be screened, but in the other part it is not completely screened, and as a result, after the pulsing the average density is very close to the full screening, but is incomplete). To improve the loading (to be close to the full screening) one can load electrons at a higher temperature where the electron – helium-vapour-atom scattering is

higher (typically 550-600mK or even 1K) and a more smoother loading is possible. However, at loading temperatures, 550-600mK it is more difficult to determine the electron density (error is at least 20-25%, in comparison to 15% at 350-400mK) due to a higher scattering of electrons on helium-vapour-atoms and consequently resistance is very high and difficult to measure. Typically we did loading at 350-400mK. We took this temperature due to our experimental conditions, namely, at 550-600mK and above, our cell is not sensitive, resistance is so high, that one can see near no signal, and after loading cryostat must be cooled in order to obtain signal, for loading at 350-400mK we have signal and can determine the electron concentration with smaller error, 15%.

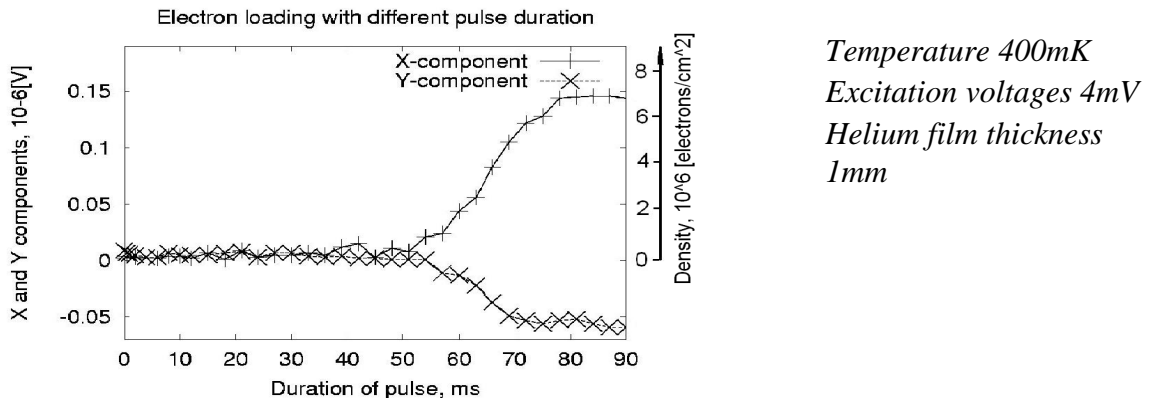
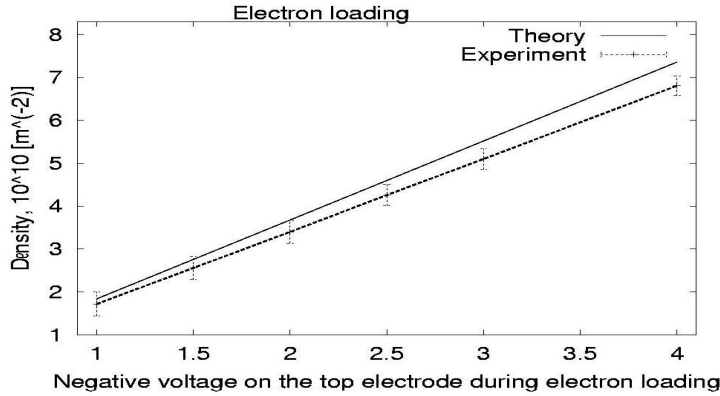


Fig. 4.1 *Dependence of the X and Y components of the signal versus the pulse duration. The signal measurement was done from smaller impulse to a higher one. After each measurement (for particular pulse duration), electrons were removed. For each pulse duration, loading of electrons was done with 3-4 pulses. On the right, additional scale shows electron density.*

We performed several tests in an attempt to determine and to check whether we have the expected electrons' density after the loading (so, conditions are "close to saturation", and unfortunately only for 1mm helium film thickness): (i) the loading with different top electrode voltages and their subsequent recalculation to the resistance and density; (ii) the loading with different top electrode voltages and with direct determination of electron density (see Appendix A, p.78). All measurements showed that we have had the correct density after the loading (for example, see Fig. 4.2). Electron loadings (Fig. 4.2)

were done at 350mK and corresponding error was 15% (for the densities below $2 \cdot 10^6$ electrons/cm², the error was 20%). Another our loading at 450-500mK leaded to a slightly higher density (closer to the full screening of the electrical field on the top electrode) but at the same time, the error bar was increased to 20-25%. Usually our loadings were done at lower temperatures (350mK) and the errorbar was about 15%.



*Helium film thickness 1mm
Temperature 350mK*

Fig. 4.2 *Electron density versus the voltage at the top electrode. Loading was up to the signal saturation. To determine the density, lower middle electrode (with negative voltage) was used (for details, see also Appendix A, p. 79, formula 18). Theoretical curves shows electron density for the loading till saturation (Appendix A, p. 79, formula 19).*

We would like also to mention that there is an additional method of determination of electron concentration and mobility. It is based on the fact that Drude formula is valid for the electrons on the surface of ³He in magnetic field (which is also must be proved for the temperatures, below 200mK and for magnetic fields >800G). Basing on Drude formula for each point in temperature, one can separately determine electron concentration and mobility (to be more precise, first the calculated conductivity (or resistance) from transmittion line model, then with the help of Drude formula $R = \frac{1 + (mB)^2}{nem}$ one calculated separately mobility and concentration of electrons). This method was sometimes used by K. Kono in his measurements [Shir95].

On the other side we can not ignore some critical notes about determination of electron concentration made by other people, for example, V. Sivokon (Kharkov Group, Ukraine, private communication), mentioned, that all methods

mentioned above give only order of magnitude (because they are "secondary" in density determination), but only Wigner crystallization gives the right electron density because of dependence of only two parameters, temperature and electron density.

4.2 Recalculation of measured signal to resistance

After electron signal is measured, namely X and Y components of Lock-In amplifier, it is necessary to recalculate it to resistance of electron layer (and knowing the electron concentration, to mobility). There are two models: lumped-equivalent (sometimes called Sommer-Tanner) and transition line model. First model is very simple, but is valid for small resistances (in our case, $R \ll 2M\Omega$, See also Appendix B, Chapter B.1.1, p.80). Second one is quite difficult and also calculated for the case, when electrons cover all surface of electrode (see also Appendix B, Chapter B.1.2, p.82). In our computations we used first model, Sommer-Tanner, but we improved it considering all additional capacitances and resistances between electrodes and cables and as a result, we can use it for all ranges of resistances and "our" model is very similar to transmission line model (for more details, see Appendix B, Chapter B.1.3, p.83).

Before we consider our experimental data, we would like to mention, that in lumped-equivalent scheme (Sommer-Tanner) as well as transmission line model, resistance of electron layer is considered as pure real part, no imaginary component (possible influence of imaginary component is considered in Appendix B, Chapter B.1.5, p.89). Here we also treat resistance of electron layer as pure resistive.

Here we would like to present one of our experimental data and theoretical curve. On the figure below we plotted X and Y components of signal (bottom scale) as well as theoretical curve (top scale). We can see, that power law dependence of resistance on temperature takes place in the temperature 300-500mK (in this measurement, deviation from power law above 500mK we attribute to our experimental condition, namely, insensitive thermometer though

in other measurements power law behavior can be seen, Fig. 5.3, p.54). In temperature region below 300mK, resistance was stable.

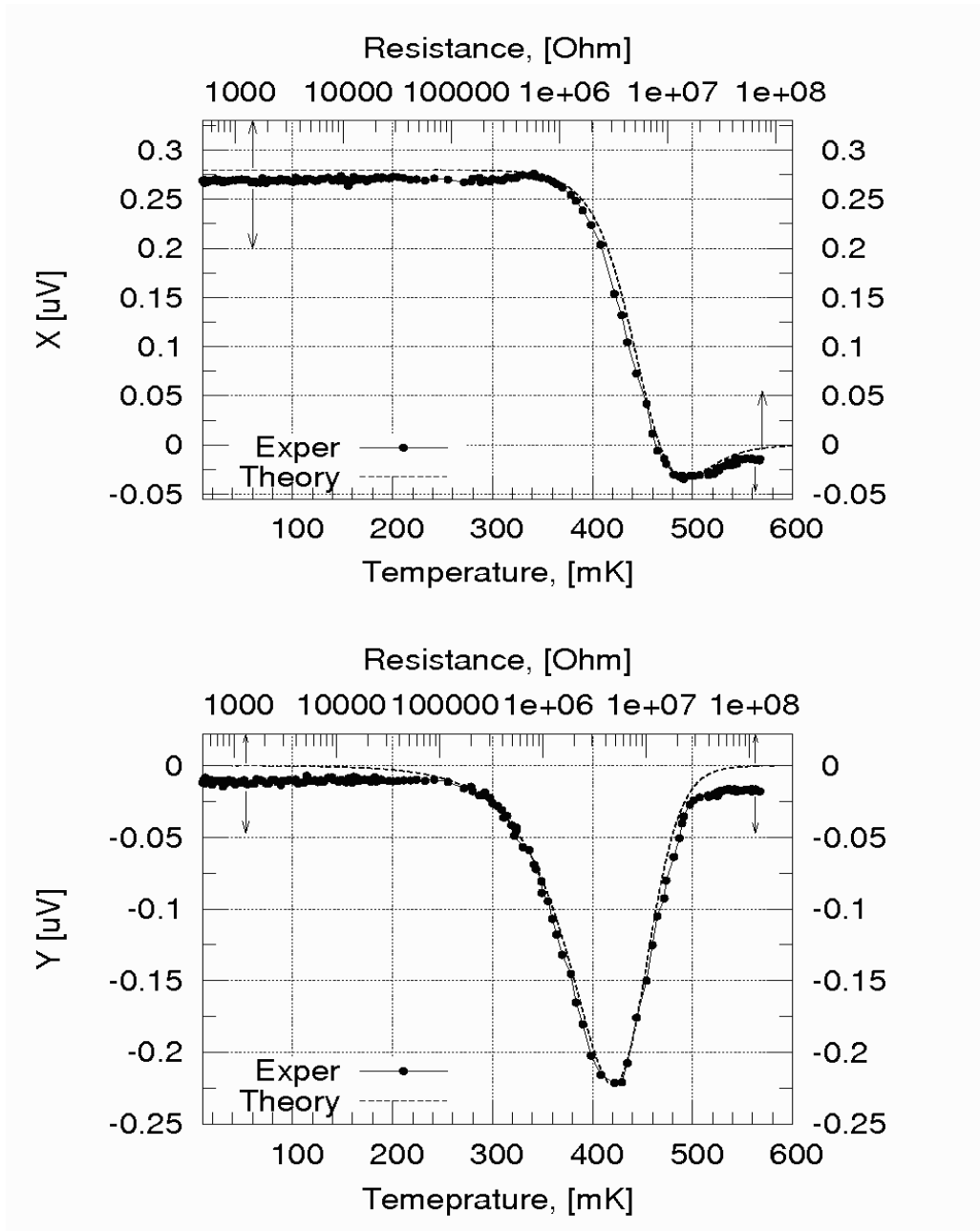


Fig. 4.3 Typical measured X (top) and Y (bottom) components of electron layer signal. In each of two pictures, bottom scale (temperatures) refers to measured signal, top (resistance) to recalculation (theoretical) curve. Deviation of experimental curve from theoretical one at temperatures above 500mK, in this measurement we attribute to our measuring conditions (insensitive thermometer), but not to the true deviation from power law (see also final resistance-temperature curve on Fig. 5.1, #4, p.50). In the temperature region below 250mK we have stable resistance.

4.3 Influence of cell tilting

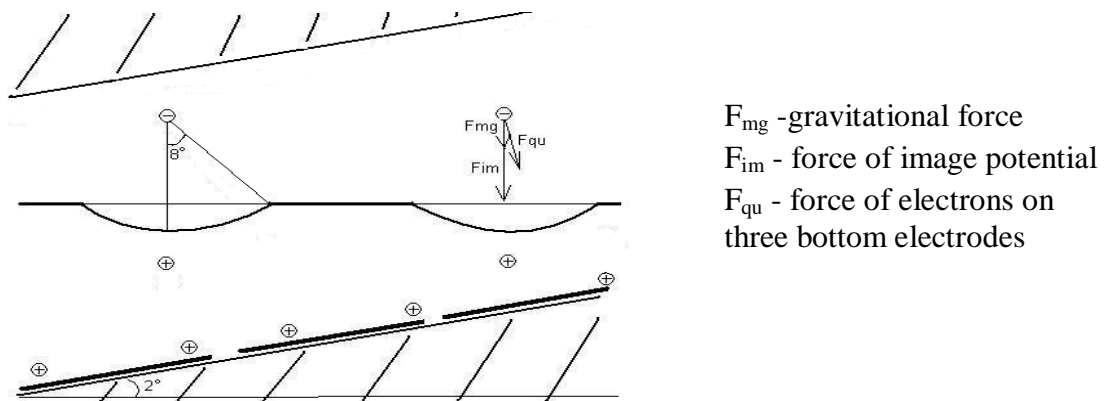


Fig. 4.4 Schematic picture of cell tilting and forces acting on electrons.

In order to consider the influence of cell tilting, we should also determine all forces acting on electrons.

First of all, let us made estimation of angle, that can influence the electron, sitting in the dimple. Typical depth of dimple in Wigner solid regime is 0.02nm, for the field below 200V/cm (without Wigner crystallization, electrons, with typical amount 10^6 can make a “big dimple” of micrometer size, for more details, please, see Chapter 2.1, p.11) and typical distance between electrons and helium surface is a couple nanometers, so let us take 2nm and for simplicity we assume, that dimple has spherical form (see Fig. above). Than the angle between lines connecting electron with bottom and edge of dimple would be 8^0 . Or by the other words, if we tilt the surface on 8^0 than electron will be just on the edge of dimple and will not “feel” dimple at all and can move along the surface (On the other side, it is hardly possible that tilting of our cell can be more than 8^0 usually it is 1- 2^0). First of all, we also note, that without Wigner crystal, dimple does not exist and for our measurements, we do not see Wigner crystallization (see also Chapter 5.1 p. 46). Second, dimple can be non spherical. Therefore influence of dimple does not come in question.

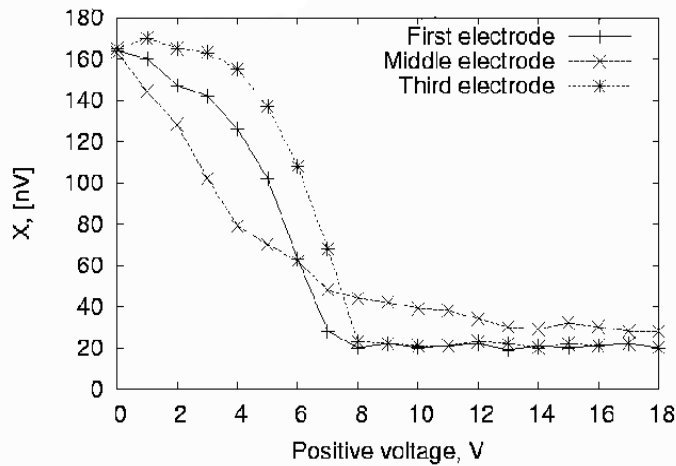
On the other side, let us consider that we have 2^0 tilting of the surface, which is due to mechanical construction of our cell. If we have length of three bottom electrodes 17mm, than difference of height could be 0.6mm. For typical our

film thickness 1mm it means, that one edge of first electrode can have distance from electrode to surface 0.7mm, and opposite edge of third electrode has 1.3mm.

Let's now estimate forces, acting on electron. Gravitational force $F_{mg}=10^{-29}$ N. Force of image potential is $F_{im} = \frac{e-1}{4e(e+1)} \frac{e^2}{4\pi\epsilon_0 r^2}$ and for estimation we take as a

distance between electron and its image in helium as 3nm, than we have $F_{im} = 1.3 \cdot 10^{-13}$ N. The next force is between electron on the surface and positive charge under the surface of helium on three bottom electrodes. This force is different, due to tilting of cell and accordingly distance could be from 0.7 to 1.3mm. Therefore, in the worse case, forces will be in the range from $F_{qu} = 4.7 \cdot 10^{-22}$ to $1.36 \cdot 10^{-22}$ N and difference between them 3.5 times. We would like to mention that image and gravitational force is perpendicular to the surface and does not have component along the surface when cell is tilted. Force between electrons and electrodes has component parallel to surface and, hence, contributes to the forces between electrons itself. On the other side, force between electron and electrode can be different up to 3.5 times and therefore can contribute to the Coulomb force between electrons and therefore to nonhomogeneous density of electrons on the surface. In order to qualitatively estimate, how this force contributes to the Coulomb forces between electrons, one should made 3D calculation of electrical field profile in the cell.

In our experiments we made test whether we have the same symmetry (and correspondingly the same density) of our two opposite electrodes. We applied positive voltage to one of our bottom electrodes and observed at which voltage we loose our signal (so, there are no electrons on the opposite electrode). On the figure below, we can see, that applying a positive voltage on the middle bottom electrode leads to faster decreasing of signal, in comparison with the same voltages on the first and third electrodes (we note, that offset of our signal is 20nV). Applying of positive voltage on first or third electrode led to nonsymmetrical behavior: electron density above the first electrode is higher than on the third electrode.



Temperature 10mK
Excitation 10mV
Top electrode -4V
Guard electrode -6V
Concentration $3.1 \cdot 10^6$ electrons/cm²
Zero offset of signal for X-component - 20nV

Fig. 4.5 *Electrical signal (X-component) versus applied positive electrical field on one of the bottom electrodes. During the measurement voltage on two other bottom electrodes was kept zero.*

From experimental observation of other group [Oleg Kirichek, Tokio University, group of Prof. K. Kono, private communication] they can conclude that tilting could play a crucial role around Wigner crystallization temperature but can be of minor importance for other temperature regions [Kir04].

4.4. Temperature gradients inside the cell

During the loading of electrons it could be possible that applied energy was too high and it could lead to temperature gradients inside the cell. We consider this problem from two points, temperature of filament and relaxation to the ambient temperature.

We consider two steps: (i) maximal temperature of filament and (ii) relaxation times through copper cables and stycast.

We have the following data:

	Tungsten	Stycast 2850GT
Specific heat capacity	0.132 J/gK	0.004 J/gK
Density	19.3g/cm ³	2.4g/cm ³
Thermal conductivity	14.4-97.1W/cmK	$78 \cdot 10^{-6} T^{-1.8}$ W/cmK

Tungsten:

Density at 25⁰C=19.3g/cm³, [Handbo], page 12-220

Specific heat capacity at constant pressure at 25⁰C is 0.132 J/gK (here we overestimated heat capacity just to take the worst case, at low temperature its value in 10-100 times less), [Handbo], page 4-135 or 12-220

Thermal conductivity in the range 1-10K is 14.4-97.1W/cmK [Handbo, Pob92]

Stycast 2850GT

Thermal conductivity in the range $K_{\text{stycast}} = 78 \cdot 10^{-6} T^{-1.8}$ W/cmK [Pob92, Table 3.2, page 56]

Density – 2.4g/cm³.

Specific heat capacity is 0.004 J/gK at 10K.

Solution

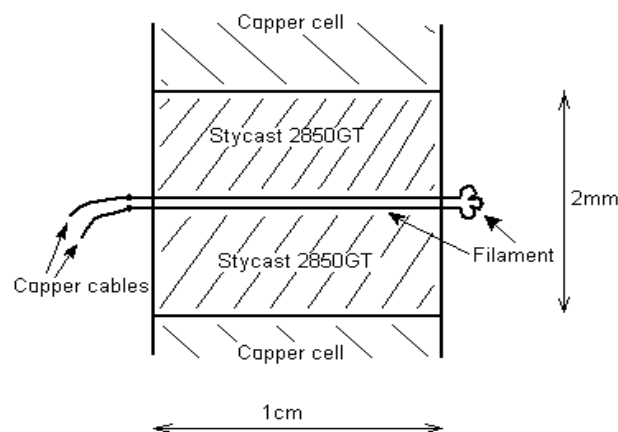


Fig. 4.6 *Filament schema for calculation of filament temperature and relaxation time.*

Let us determine the temperature of the filament after one pulse (pulse duration 70ms and energy of 17.6mJ). Diameter of filament is approximately 0.1mm, length 1cm, then Volume is approximately 10⁻⁴ cm.

Mass of the filament is $19.3 \cdot 10^{-4} = 1.93 \cdot 10^{-3}$ g.

Heat capacity of the filament is $C_p \cdot m = 2.55 \cdot 10^{-4}$ J/K

The temperature of the filament is $T = Q/C \approx 69$ K.

Let us calculate time constant for the case, when energy is released from filament to copper wires, which are at the surrounding temperature, 400mK. So,

energy flows from hot sport to the cold one, which is sold to the copper wire. We used copper wire because of good thermal conductivity.

If we take thermal conductivity of the filament at 10K (averaged) as 50W/cmK, then for our case, $50\text{W/cmK} \cdot \text{Surface/length}$ of tungsten wire = $50 \cdot [3.14 \cdot (10^{-2})^2 / 4] / 1 = 5 \cdot 10^{-3} \text{ W/K}$

And time constant $C/k = 2.55 \cdot 10^{-4} / 5 \cdot 10^{-3} = 5.1 \cdot 10^{-2} \text{ s} = 51 \text{ ms}$.

For the case of thermal conductivity of the Stycast to the cell, we used formula for the conductivity for cylindrical geometry.

Thermal conductivity = $k_{\text{stycast}} \cdot 2 \cdot \pi \cdot \text{length} / \ln(d_{\text{out}}/d_{\text{in}})$ and for the data $d_{\text{in}} = 0.1 \text{ mm}$ (inner diameter, tungsten filament), $d_{\text{out}} = 2 \text{ mm}$ (outer diameter, copper cell), $T = 10 \text{ K}$, length = 1cm, we have mass is $7.8 \cdot 10^{-2} \text{ g}$, thermal conductivity – $2.6 \cdot 10^{-6} \text{ W/K}$, heat capacity – $3.12 \cdot 10^{-4} \text{ J/K}$ and correspondingly time constant $1.2 \cdot 10^2 \text{ s} = 120 \text{ s}$

Time between two successive pulsing was 15 seconds, therefore, we can see, that time of temperature relaxation through stycast could be slow and temperature gradients can be present.

Temperature gradients could lead to changing of geometry of cell (for example, guard electrode could be changed and consequently could not hold electrons to the whole extend) as well as properties of surrounding details (for example, during the loading, overheated Stycast could easier "catch" electrons which can than stay for a longer time or even prevent further loading of electrons). In our measurements we tried to overcome such kind of problems, but further clarification or even measurements could be helpful.

4.5 Overheating of electrons

Another important parameter, that could influence our measurement is possible overheating of our electrons by the excitation voltage. The increased electron temperature is given by the formula [Mon91] for ^4He

$$\Delta T = \frac{E_x^2 t}{R k_B n_s}$$

where E_x electrical excitation field in propagation direction (in our case, 10mV/12mm=0.83), k_B – Boltzmann constant, R – measured (existing) resistance, n_s – concentration of electrons, and τ is the thermal relaxation time of electrons on riplons.

We would like to notice that this formula was derived for electron-riplon scattering on the surface of ^4He . Though, as it was shown by Juri Monarkha [Mon97, Mon01] for ^3He , due to high viscosity, it is questionable whether riplons can exist below 300mK. Unfortunately, because there are not any other formulas for ^3He and theoretical consideration as well as experimental data for overheating effects (for example, thermal relaxation time), we will use this one considering as “valid” for ^3He at least for our estimation.

We can consider the worse case – concentration is small, $1 \cdot 10^6 [\text{cm}^{-2}] = 1 \cdot 10^{10} [\text{m}^{-2}]$ and three resistances 1K Ω , 100K Ω , 10M Ω . Then the final increase of temperature could be seen from figure below.

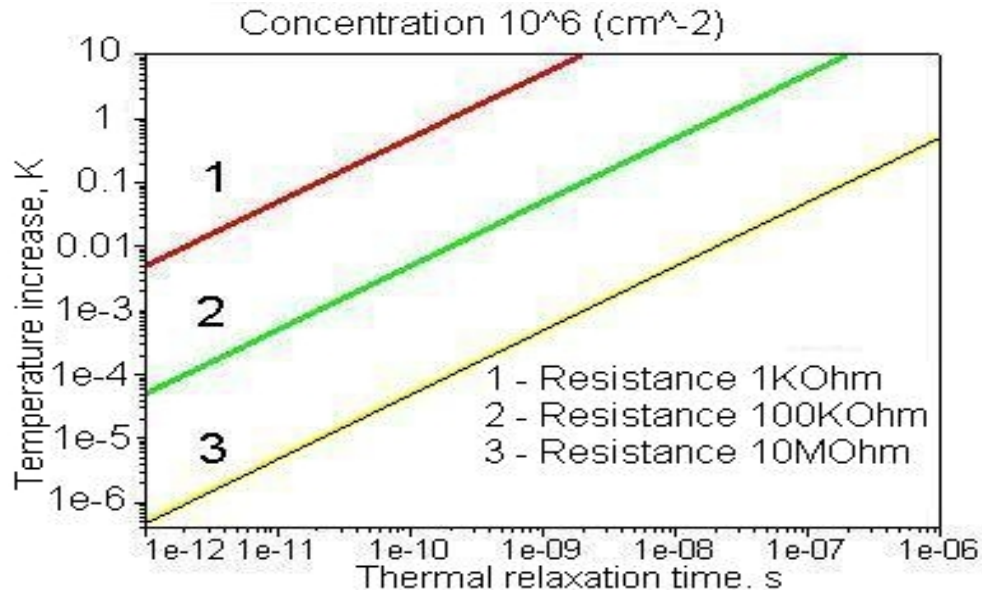


Fig. 4.7 Temperature increase of electrons, due to overheating by excitation voltages. 1 – resistance of electron layer to the surface is 1K Ω , 2 – 100K Ω , 3 – 10M Ω . Excitation field 0.83mV/mm

We can see, that it is very simple to overheat our electrons at low resistances.

Increasing of concentration leads to decreasing of temperature difference between electrons and helium surface. Unfortunately, next parameter – relaxation time of electrons on ^3He was not measured and we could only speculate about it.

So, we can see, that if the formula is valid, then for some condition it could be possible (for example, higher relation time and higher excitation field) to overheat electrons.

Our measurement with different excitation voltages, Chap5.3 p.58, gave us the following values of resistances at different excitation voltages and temperatures

	18mK	104mK	254mK
10mV	3.46M Ω	3.48M Ω	3.46M Ω
1000mV	504K Ω	522K Ω	662K Ω

In this measurement, we did not have an overheating effect due to excitation voltage. Though overheating can be caused also by excitation frequency. In order to exclude overheating effects caused by excitation voltages and excitation frequencies one needs further measurements.

4.6 Nonhomogeneous distribution of electrical fields and electron concentration

Any chosen geometry has its own boundary (for example, guard electrode) where electrical field changes in order to keep electrons. This leads to changing of electron density from maximum to null. These electron density changes were calculated for circular geometry (two dimensions calculations) by R. Metrotra [Met82, Met87] but unfortunately not for rectangular geometry (where three dimensional calculations must be done).

Next point could be distribution of driving electrical field along the direction of wave propagation. In circular geometry excitation field is parallel to wave propagation and inhomogeneity of electron density does not play any role. Unfortunately, for rectangular geometry, excitation field is parallel to the propagation direction only in the center. Moreover, due to density changes on boundary, we could also have different pressing electrical field (z-component) as well as changing of absolute value of excitation field. Unfortunately, for our experiment, it was very difficult to estimate such an inhomogeneity, because we need 3D calculation of electrical field profile, but we think, that this did not influenced our results much. Nonhomogeneous distribution of electrical field in z direction can be crucial. In chapter 2.1, p.11 we discussed influence of pressing electrical field on SSE not in WS phase. When electrical field is close to critical one E_c , than our electrons on the surface can be non stable and disruptive loss of charge develops. Therefore, electron concentration can be lower. On the other side, when electron concentration is around 8% of saturation one, than our surface can be stable, but new state – dimple state develops, with typical amount of electrons, 10^6 and depth of micrometer size. This was observed for electrons on ^4He surface and one can also use it for ^3He . Critical value of electron concentration $n_c=1.56*10^9\text{cm}^{-2}$ and electrical field $E_c=2.82*10^3\text{V/cm}$ (Table 1, p.9) are high. We never applied such a high field (maximal 250V/cm), but we have corners in the cell, which due to singularities can locally produce it. 8% of critical concentration give us $1.2*10^8\text{cm}^{-2}$. We usually worked with even smaller concentrations, below $1*10^7\text{cm}^{-2}$. Therefore, we can not exclude losses of electrons and existence of new dimple state.

On the other side, rectangular geometry implies that there could be also two electron conductivities, one through the center, where we have homogeneous (constant) electron density, and one through the electron boundary layer, along the guard electrode, where electron density changes from maximum to null. Which of these conductivities can prevail is questionable, particular because we do not know how or whether at all electron mobility depends on electron

density. As a prove, that conductivity through the boundary layer could play a role, can be measurements with different pressing electrical fields. If we apply positive electrical field on three bottom electrodes (and we have more homogeneous distribution of pressing field, see Appendix C, p.102 for more detailed description of our cell) than resistance increased (see also Chapter 5.5, p.65), which is qualitatively in agreement with theory. On the other hand, applying pressing negative field on top electrode, leads to less homogeneous distribution of electrical field, because upper electrode is circular and does not cover the whole surface of electron layer. So, electron from center move to the boundary and conductivity of center and boundary layers of electrons are changed even due to change of electron concentration and instead of increase of resistance we have decrease (see Fig. 5.8, p.68). For example, let us take R_{bulk} as a “bulk” resistance and R_{boundary} as a “boundary” one. We consider that applying of electrical field on three bottom electrodes does not lead to redistribution of electrical charges and $R_{\text{bulk}} < R_{\text{boundary}}$ (boundary resistance is higher and we measure bulk one). This can be only due to either smaller mobility of boundary electrons or smaller concentration (which is true). When we applied negative field on top electrode, electrons can move from the center (bulk) to boundary. The resistance in center is increased, due to less electron concentration and resistance in boundary is decreased, situation is changed and now $R_{\text{bulk}} > R_{\text{boundary}}$. In our measurements we tried to keep pressing field on top electrode constant (usually 10V/cm).

Of course, here we should also point out that top electrode (with which we usually kept electrons) did not cover the whole surface of electron layer (corners are not covered). This means, that in addition to changing of electron concentration along the guard electrode, we have increase of electron concentration in the corners. This could also somehow influence our results.

4.7 Influence of 1K-pot or cryostat oscillation

Let us consider energies of different sources in the cell.

The electrical energy. For an typical excitation 10mV and a typical resistance 1M Ω , we have 10^{-10} W.

The gravitational-surface wave energy. For 1kHz and amplitude 10^{-10} m (actually it is even exaggerated, because the depth of the dimple is a couple angstroms and the gravitational-surface wave amplitude will be therefore, even smaller) we have $4.2 \cdot 10^{-14}$ W, and for 35Hz – $0.5 \cdot 10^{-18}$ W [Land59].

Let us estimate frequencies and wave-lengths of gravitational-surface waves that can exist in our cell. For the longest wave-length, 50mm, (circular geometry, for more details about eigenmodes of gravitational-surface waves in such resonator, see [Land56]) we have frequency 35Hz. For the wave-length 0.23mm we have frequency 1KHz, and for the wave-length $1\mu\text{m}$ we have 3.34kHz (apply of electric field does not change wave-length, but leads to a decrease of frequency, the so called “softening” – see Eq.6). Usually for the standing wave in a resonator, we have a fundamental frequency (35Hz) and its two or three harmonics. Hence, typical oscillations of 1K-pot (a few kHz, [Eska04], [Pere04]) do not come into resonance with this waves and we can neglect the direct influence of 1K-pot on gravitational-surface waves.

Cryostat oscillation are usually below few Hz and we can also neglect it.

As an additional argument of disproving of external resonance influence on gravitational-surface wave (and, for example, connected with it possible loose of electrons) could be a standard formula for damping (in 1/s) given by

[Land56] for gravitational-surface waves $g = \frac{2\eta w^{4/3}}{r s^{2/3}}$, where η is the viscosity

of ^3He which is equal to $3.3 \cdot 10^{-7}/T^2$ Ns/m², ρ stands for the density ($\rho = 82\text{kg/m}^3$), and σ for the surface tension, ($\sigma = 155 \cdot 10^{-6}$ N/m).

Table 2: *Quantitative comparison of different damping coefficients of gravitational-surface waves versus different temperatures and frequencies.*

γ , (1/s)	f=35Hz, $\lambda=0.05\text{m}^{-1}$,	f=115Hz, $\lambda=1*10^{-3}\text{m}^{-1}$,	f=1000Hz, $\lambda=0.23*10^{-3}\text{m}^{-1}$	f=3340Hz, $\lambda=1*10^{-6}\text{m}^{-1}$
600mK	0.068	0.326	5.78	28.80
100mK	2.45	11.72	208.15	1036.70
10mK	245	1172	20815	103670

So, we can see, that even if we have an influence of 1K-pot (or other external influences), gravitational-surface waves are very good damped at our temperatures. More detailed calculations, made by Juri Monarkha [Mon97], showed that the spectrum of surface oscillations on ^3He is imaginary for the wave-vectors above $25*10^4\text{cm}^{-1}$ for low temperatures as well as for low frequency branch of coupled plasmon-riplon mode.

Therefore, in our opinion, noise, caused by the oscillations of the whole cryostat or by 1K-pot did not come in resonance with gravitational surface wave and did not noticeably influence our measurements.

4.8 Short Summary

- i) In the absent of Wigner crystallization jump, estimation of electron concentration is possible, though error is no less then 15%
- ii) Influence of cell tilting, cryostat oscillations and 1K-pot noise are of minor importance. Overheating effects during the electron loading is estimated of small influence.
- iii) Overheating of Surface State electrons due to excitation voltage can be the biggest difficulty for the temperatures below 300mK. Nonhomogeneity of electrical field profiles can also be crucial.

Chapter 5

Results

5.1 Comparison of our results with results given in the literature for 2D electron on ^3He

In our experiments we tried to repeat measurements published in the literature.

We begin with summary of similarities and differences between experiments done by Kono's group [Shir95] and our experiments:

1. Densities: K. Kono's group published data for the same density $1.5 \cdot 10^8$ electrons/cm² (for high temperatures and just to show the Wigner solid transition he used even smaller density $1.21 \cdot 10^7$ electrons/cm²). We usually used with smaller density in the range 0.01 - $3.7 \cdot 10^7$ electrons/cm².
2. The guard electrode voltage: K. Kono did not mentioned this parameter. We used the following two values: -4V or -2.6V .
3. Excitation frequencies and voltages: in both Kono's group and our experiments the same frequency, 100kHz and we used usually the same excitation voltage 10mV in comparison with 2 - 10mV in Kono's ones.
4. Difference in the cell. Kono used circular geometry, we employed the rectangular one.
5. Difference in the pressing electrical field. Kono did measurements for the field ranging from 90 to 488V/cm . Typical our measurements were for fields from 10 to 25V/cm . But we also did sweeps 100 and 255V/cm .
6. Helium film thickness. We used the same film thickness – 1.0mm .

For comparison we can look at our several measured curves. All these measurements were done with 10mV excitation voltage, 100kHz frequency and the applied voltage of guard electrode was -6V and the top electrode -4V and correspondingly to the field -10V/cm

Below we gave description of our experiments and meantime we also tried to compare our data with proposed by K. Kono theory of electron-ripplon and electron (in dimple) - ^3He quasiparticle scatterings (hydrodynamic and ballistic regimes) [Kon02].

For all measurements below 300mK, for electron-ripplon and electron - ^3He -quasiparticle scatterings, we do not have neither right power law dependence of resistance (mobility) on temperature nor right beginning and end of particular scattering mechanism or regime. We discuss only presence of particular scattering mechanisms in our measurements (qualitative estimation).

Fig. 5.1, #1: The electron density was $3.6 \cdot 10^7$ electrons/cm². Voltage on the middle bottom electrode was +6V (or field +15V/cm). Sweep was done immediately after the loading, from high to low temperatures in 8 hours. Below 300mK (300-190mK) we had only slightly decreasing resistance region that could be attributed to the possible electron-ripplon scattering. From 190 till 175mK we have increasing of the resistance (in time this corresponded to 1hour). We attributed it to the loosing of electrons, which was smooth in time (so, not in one step). Than again, in the temperature region 175-165mK signal was constant (40minutes) and in the region 125-150mK we had smooth loosing of electrons. At temperature 120mK we had abrupt loosing of electrons and below 120mK we had slightly increasing resistance region, which could be attributed to the beginning of electron (in dimple) - ^3He quasiparticle scatterings (hydrodynamic regime). So, during the sweep we lost the big part of electrons and the final electron density was around $2.5 \cdot 10^6$ electrons/cm². During the following sweep from low to high temperature, signal (and accordingly resistance) was constant (at 0.5M Ω) in the temperature region 5-310mK and power law increase of resistance in the temperature (310-500mK).

Fig.5.1. #2: The electron density was $7.3 \cdot 10^6$ electrons/cm². Voltage on the middle bottom electrode was 0V. Sweep was done immediately after the loading (loading at 350mK), from high to low temperatures in 8 hours. Below

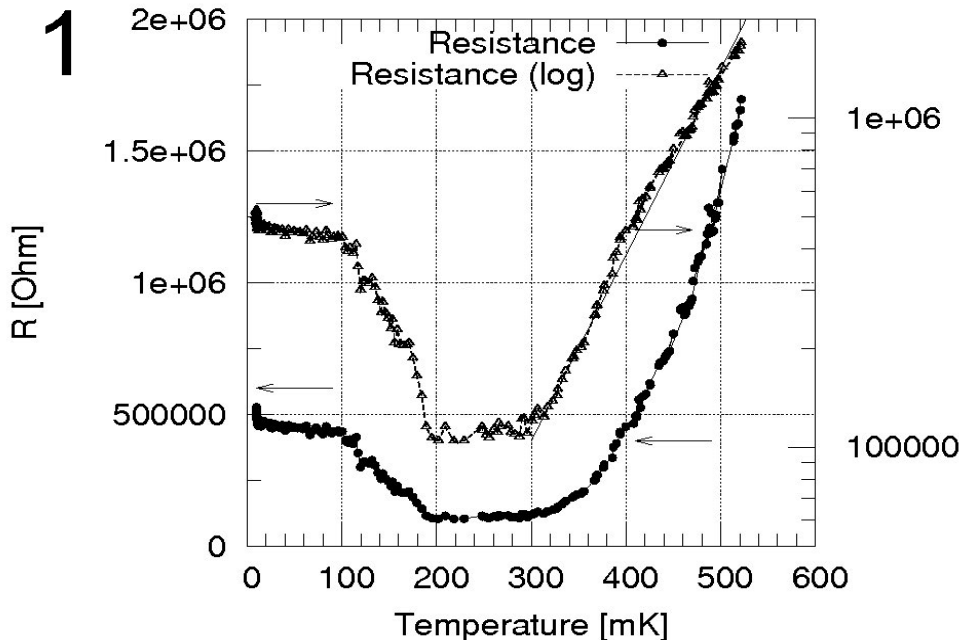
300mK (300-210mK) we had constant resistance region which is not expected (to be absolutely sure about electron-ripplon scattering we should have the right temperature dependence, which we do not have). In temperature interval 210-190mK we had three small jumps which could be related to the loosing of electrons. Than in temperature region 125-190mK we had constant resistance and at 125mK we had loosing of electrons near in one step (10minutes). So, during this sweep we lost the part of the electrons and the final electron density was approximately $3.2 \cdot 10^6$ electrons/cm². During the following sweep from low to high temperature, resistance was constant (5-310mK) and power law increase in temperature 310-500mK.

Fig.5.1. #3: The electron density was $4.5 \cdot 10^6$ electrons/cm². Voltage on the middle bottom electrode was 0V. Sweep was done from high to low temperatures in 8 hours. Below 330mK we had constant resistance region, which is not expected. The following sweep from low to high temperature reproduced the resistance.

Fig.5.1. #4: The electron density was $3.2 \cdot 10^6$ electrons/cm². Voltage on the middle bottom electrode was 0V. Sweep was done from high to low temperatures in 8 hours using Ithaco 3961B Lock-In amplifier. In this measurement, deviation from power law above 520mK we attribute to our experimental conditions (namely, insensitive thermometer) but not to the true deviation of resistance from power law. Below 330mK (330-5mK) we have increase of resistance, first faster (330-280mK) then slower (280-5mK). It could be related it to the possible electron (in dimple) - ³He quasiparticle scatterings (ballistic regime). The following sweep from low to high temperature fully reproduced the signal.

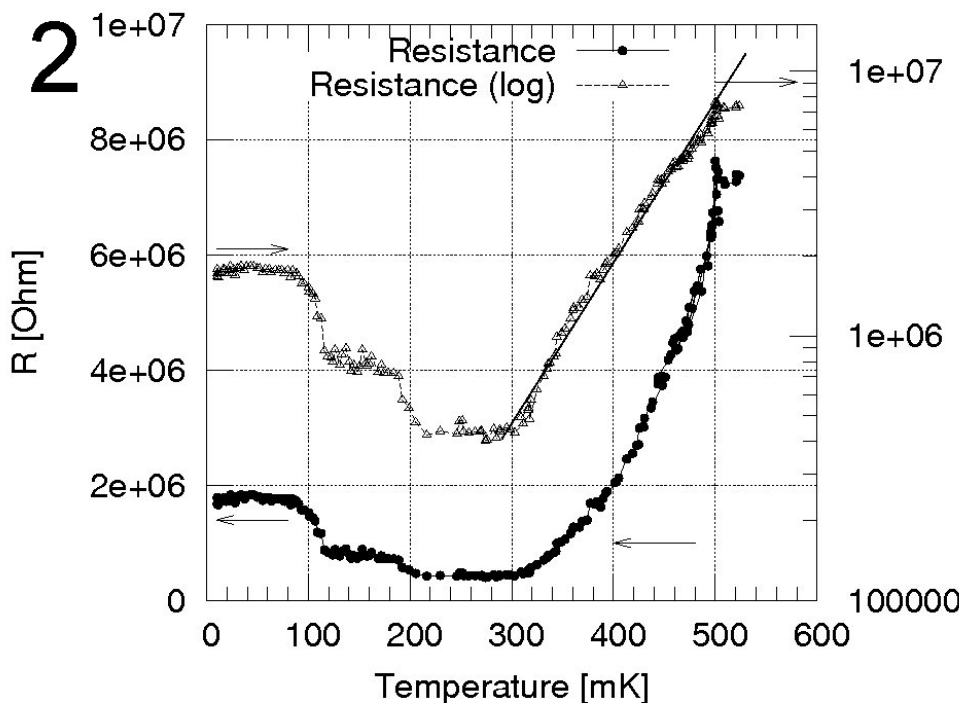
In these and following measurements we estimated the final electron concentration after loose of electrons in the following way. For the same temperature 350-400mK, namely electron – He atom scattering regime, we have the same mobility, but different resistance values before and after electron

loosing. Then knowing the initial electron concentration, we can estimate, which part of electrons was lost, $R=1/ne\mu$. Later in experiments, we used also negative voltage on middle bottom electrode for estimation of electron density (see Appendix A, p.78).



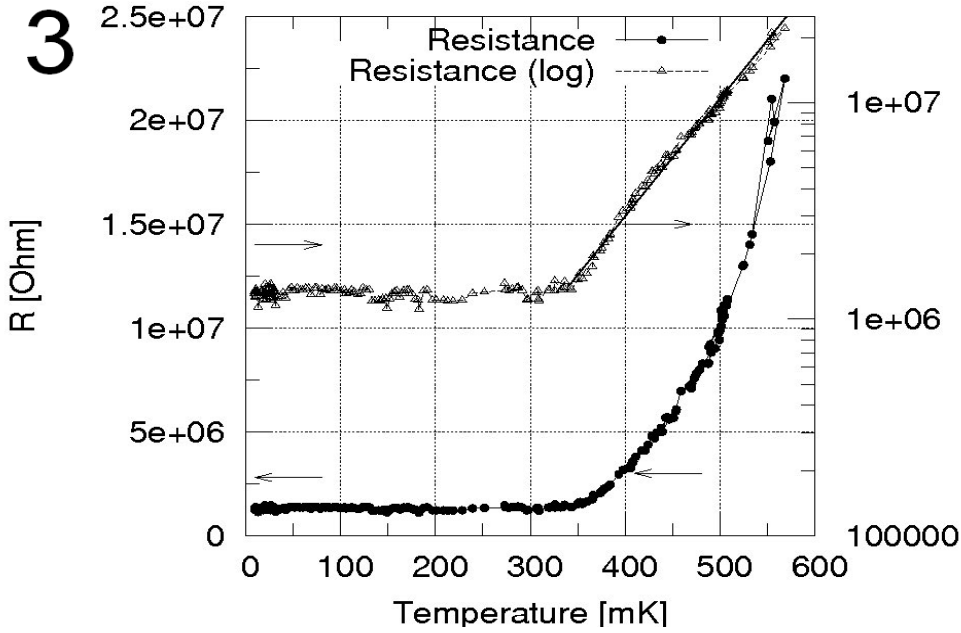
Density - $3.6 \cdot 10^7 \text{ cm}^{-2}$.
Electrical field on middle bottom electrode +15V/cm.

Frequency 100kHz,
Excitation voltage 10mV,
Film thickness 1.0mm,
Electrical field on top electrode -10 V/cm.
Lock-In - Stanford SR850

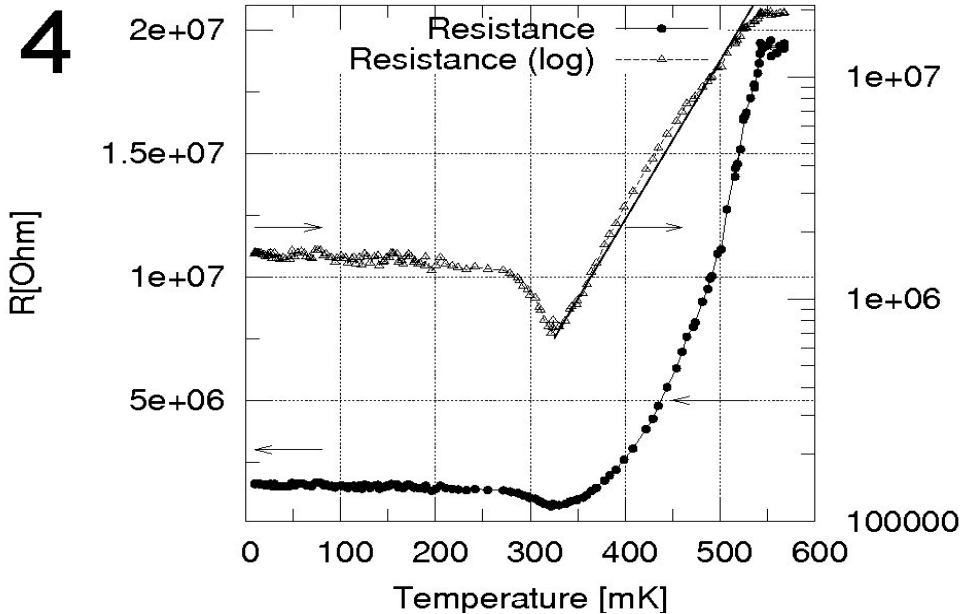


Density - $7.3 \cdot 10^6 \text{ cm}^{-2}$.
Electrical field on middle bottom electrode 0 V/cm.

Frequency 100kHz,
Excitation voltage 10mV,
Film thickness 1.0mm,
Electrical field on top electrode -10 V/cm.
Lock-In - Stanford SR850



Density - $4.5 \cdot 10^6 \text{ cm}^{-2}$.
 Electrical field on middle
 bottom electrode 0 V/cm .
 Frequency 100kHz,
 Excitation voltage 10mV,
 Film thickness 1.0mm,
 Electrical field on top
 electrode -10 V/cm .
 Lock-In - Stanford SR850



Density - $3.2 \cdot 10^6 \text{ cm}^{-2}$.
 Electrical field on middle
 bottom electrode 0 V/cm .
 Frequency 100kHz,
 Excitation voltage 10mV,
 Film thickness 1.0mm,
 Electrical field on top
 electrode -10 V/cm .
 Lock-In - Ithaco3961B

Fig. 5.1 Our resistance measurements.

1- Loosing of electrons in temperatures: 175-190mK, 125-150mK, 120mK. Constant resistance in 190-230mK is not expected.

2- Loosing of electrons in temperatures: 190-210mK, 125mK. Constant resistance in 300-210mK and 125-190 is not expected. At temperature 6-90mK possible we have electron - ^3He quasiparticle scatterings (ballistic regime).

3- Constant resistance value below 340mK was not expected.

4- Increase of resistance in 330-280 and 280-5mK could be similar to electron- ^3He quasiparticle scatterings (hydrodynamic and ballistic regimes). Deviation of resistance from power law above 550mK we attribute to our experimental conditions, namely insensitive thermometer.

So, our measurements were consistent with given in the literature (K.Kono) in the high temperature region (above 300mK) for electron- ^3He vapor atom gas scattering (Fig. 5.1, Fig.5.2 and Fig. 5.3). However, for measurements for 1mm film below 300mK we had different behaviors: We observed that signal can be stable or to decrease to some level and then stayed constant. Very often we saw, that for a high density $0.7\text{-}3.2 \cdot 10^7$ electrons/cm² (usually after the loading) the signal decreases (resistance increases) in one or several steps. We cannot attribute it to the Wigner crystallization due to the facts: (i) electron density corresponding to these steps should be higher and (ii) if we performed a next sweep in another temperature direction (from low to high temperature) and we did not observe any jump in conductivity. Therefore, we relate such kind of jumps with the loose of electrons. We also observed that process of electron loose can be very fast, almost in one step (3-5 min) or long, for instance in 50mK range (which corresponds to 40min-1hours), see Fig. 5.1, #1,2.

We would like to note, that Kimitoshi Kono also did not observe the Wigner solid transition for low densities, for example, for $1.21 \cdot 10^7$ electrons/cm² [Shir95]. In our measurements, concentrations were usually even smaller than $1.21 \cdot 10^7$ electrons/cm², so absence of Wigner solid transition agrees with published in the literature for low concentrations.

So, our data differ from published one in the temperature below 300mK and it could be attributed to different experimental conditions: pressing electrical field, excitation voltages, geometry of cell and last, but not the least electron density. It is also possible that in our case we do not have good coupling between electrons and underlying helium surface. This assumption can be supported by the explanation of K. Kono [Shir95, Kon02] of sliding mode of Wigner crystal. In this mode, electrons can form a Wigner crystal but due to weak coupling to helium surface, Wigner crystal moves freely along the surface. Sliding mode can easily obstacle the existence of Wigner solid phase. Increasing of pressing electrical field can increase coupling to surface, though our measurements showed, that we can only slightly increase the field, maximal

-50V/cm. Above this value, we cannot see any signal anymore. Decreasing of this pressing field recovers the signal (for more details, see Appendix D, p.103).

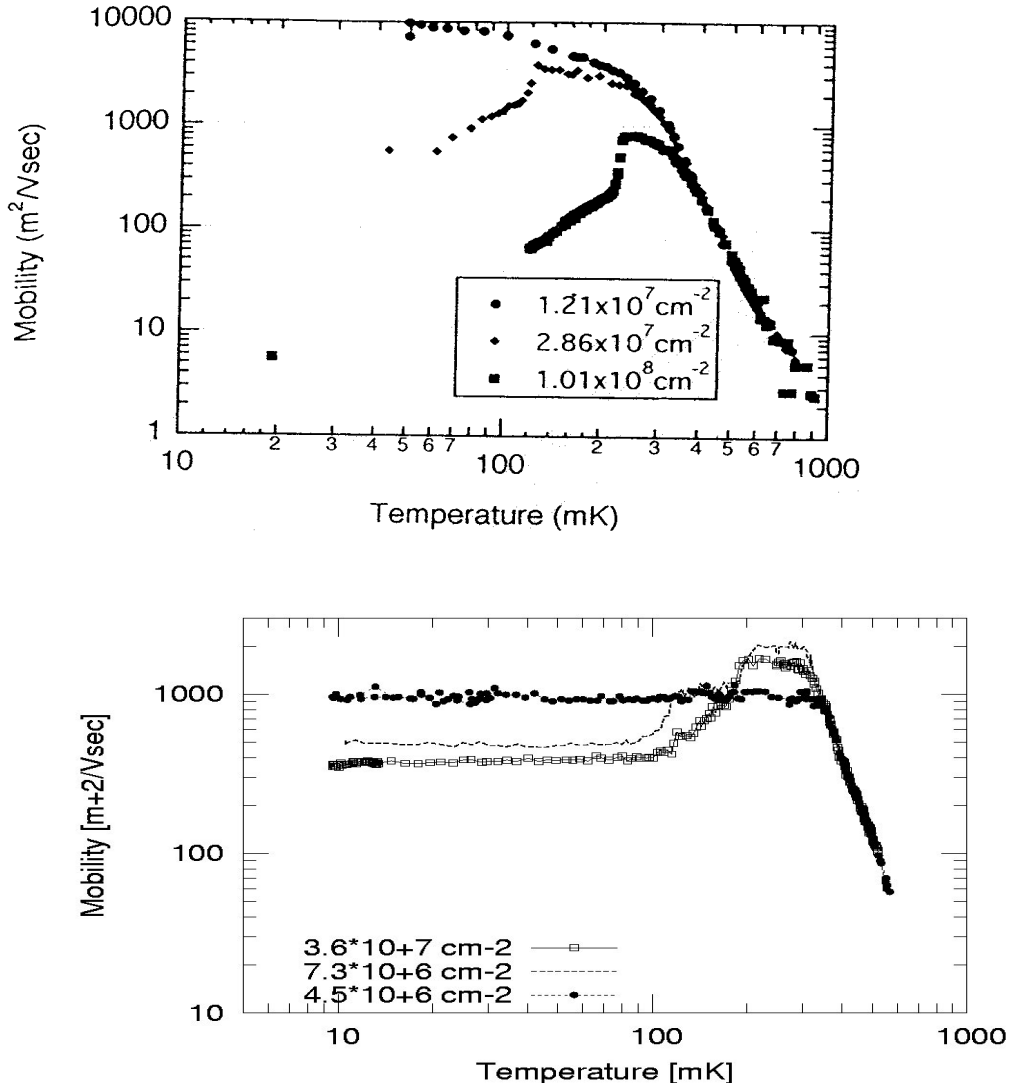


Fig. 5.2 *Top – Mobility for three electron densities [Shir95], bottom our measurements (for description, see Fig. 5.1).*

We would like also to note, that one interesting feature was very often observed: transition from electron- ³He vapor atom scattering (T>300mK) to possible sliding mode (T<300mK) is not smooth one, but very often a kink like, for example, see Fig. 5.2, temperature around 300mK. At the moment we still need an explanation.

From our measurements we can conclude that we do not see electron-rippion scattering. Very often, in the temperature region 200-350mK, where we expect

existence of ripplon, our resistance is either stable or does not have the right temperature dependence. Therefore, in the future discussion for explanation of our data, we will not use electron-ripplon scattering mechanism as explanation. We also conclude that we do not see electron- ^3He quasiparticle scattering (hydrodynamic und ballistic regimes). Beginning and end of scattering as well as temperature dependence of resistance is not right.

5.2 Measurements with different film thicknesses

Measurements with different film thicknesses (0.2; 0.5 and 1.0 mm) were performed in order to check two things: (i) to measure signal in low resistance range and in higher absolute amplitudes (see also Chapter B.2, Appendix B, p.93) and (ii) to verify, whether our 0.2, 0.5 and 1.0mm films were still “bulk” films and formulas for the bulk helium films (Chapter B1.3, Appendix B, p.83) can be used.

Our measurements showed that absolute value of signal in maximum can be increased in the same ratio as film thickness decreases (for more details, please see Chapter B.2, Appendix B, Fig. B7, p.94 and Table 3, p.95) and we can measure lower resistances. Electron- ^3He vapor-atom scattering did not depend on the helium film thickness (see Appendix F, Fig. F.3, F.8, p.115) as well as magnetic field (less than 92 Gauss, approximately 60 Gauss), see Fig. 5.3.

On the other side, our measurements in the low temperature (below 300mK) again showed that we had different behavior, which cannot be explained by the theory of Wigner solid scattering on ^3He -quasiparticle and ripplons (here we would like to mention that for the calculation we used only real part of resistance of electron layer. For consideration of resistance of electron layer with the imaginary part, please see Appendix B, p.89). In the previous chapter we tried to analyze our data from point of view, proposed in literature (K.Kono), though explanation was not very successful. Below we gave description of experimental conditions and our comments for the temperature region below 300mK.

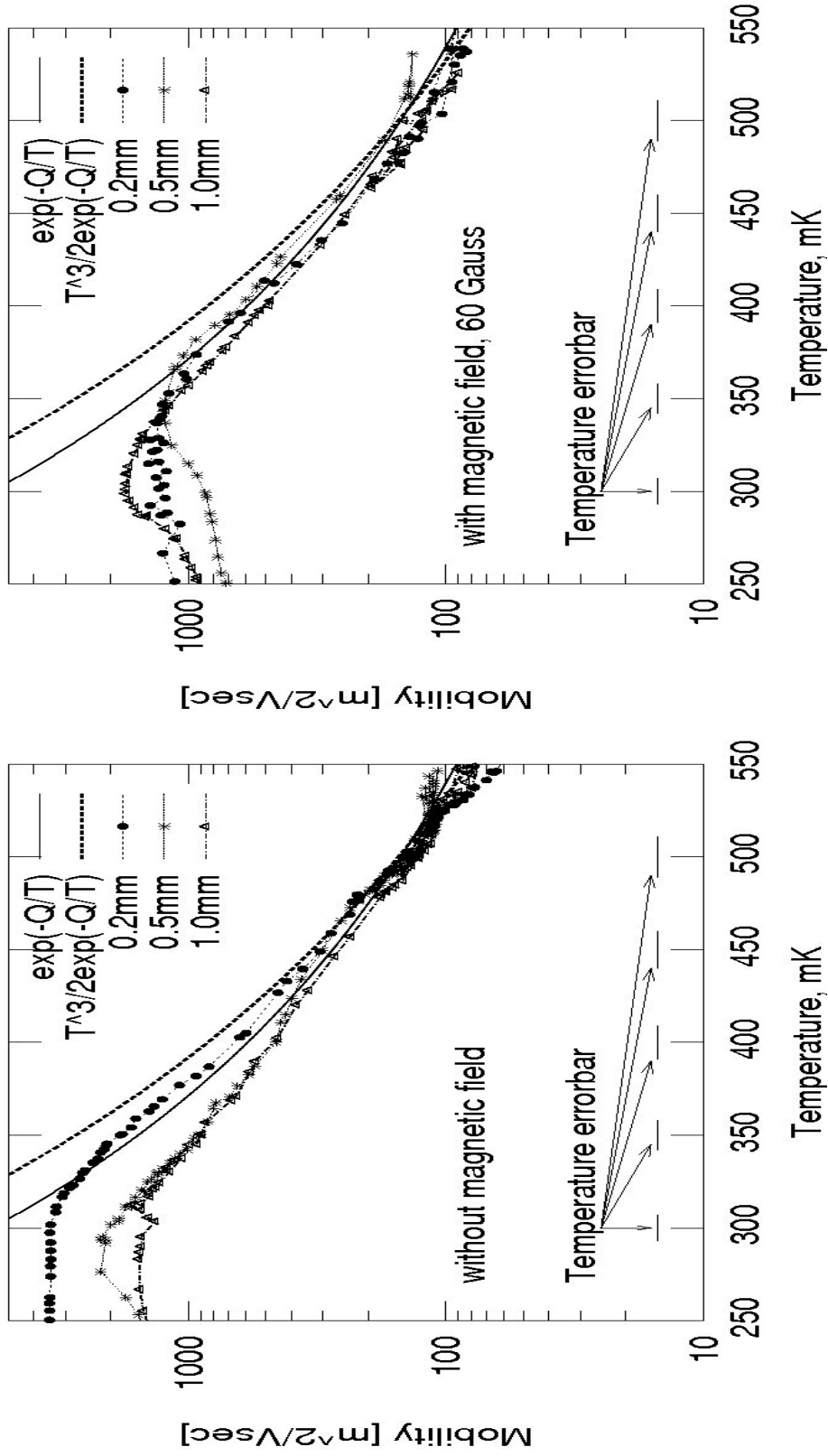
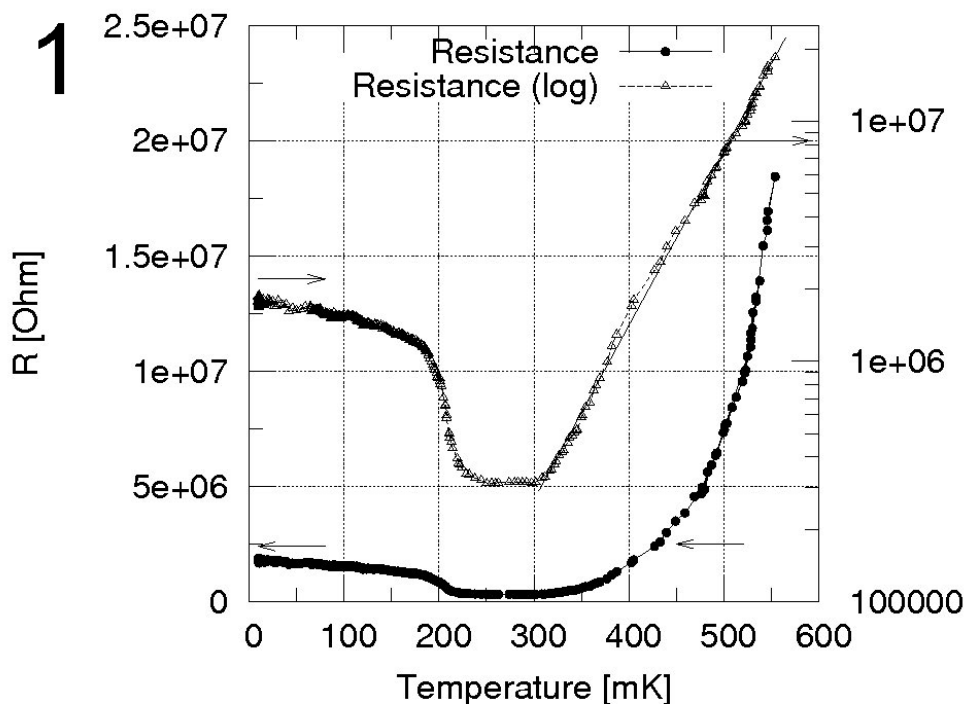
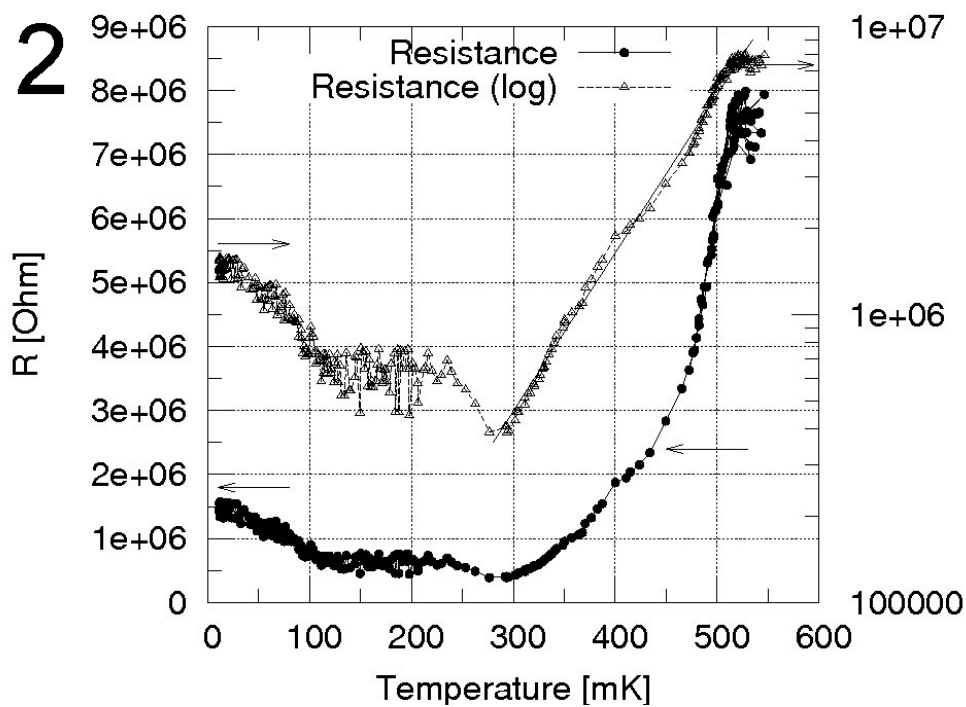


Fig. 5.3 Electrons' mobility for helium films with different thicknesses (0.2, 0.5 and 1.0mm). Left without magnetic field and right with magnetic field (less than 92Gauss, approximately 60Gauss). For more description, see also Fig F.3 in the Appendix F, p.115 and Fig. 5.4. Dashed line is presented to show pressure dependence of ${}^3\text{He}$ vapor atoms assuming the formula $n_{\text{gas}} \sim AT^{-3/2} \exp(-Q/T)$, and solid line describes dependence of ${}^3\text{He}$ vapor atoms assuming correspondingly formula $n_{\text{gas}} \sim A\exp(-Q/T)$, where T - temperature, Q - vaporization energy, and we took it as 2.74K, A -proportionality constant. We can notice that resistance has power law dependence on temperature, but not an exponential or linear.



Density - $5.8 \cdot 10^6 \text{ cm}^{-2}$.
 Electrical field on top electrode -8.5 V/cm .
 Film thickness 0.2 mm

Frequency 100 kHz ,
 Excitation voltage 10 mV



Density - $7.3 \cdot 10^6 \text{ cm}^{-2}$.
 Electrical field on top electrode -10 V/cm .
 Film thickness 0.5 mm

Frequency 100 kHz ,
 Excitation voltage 10 mV

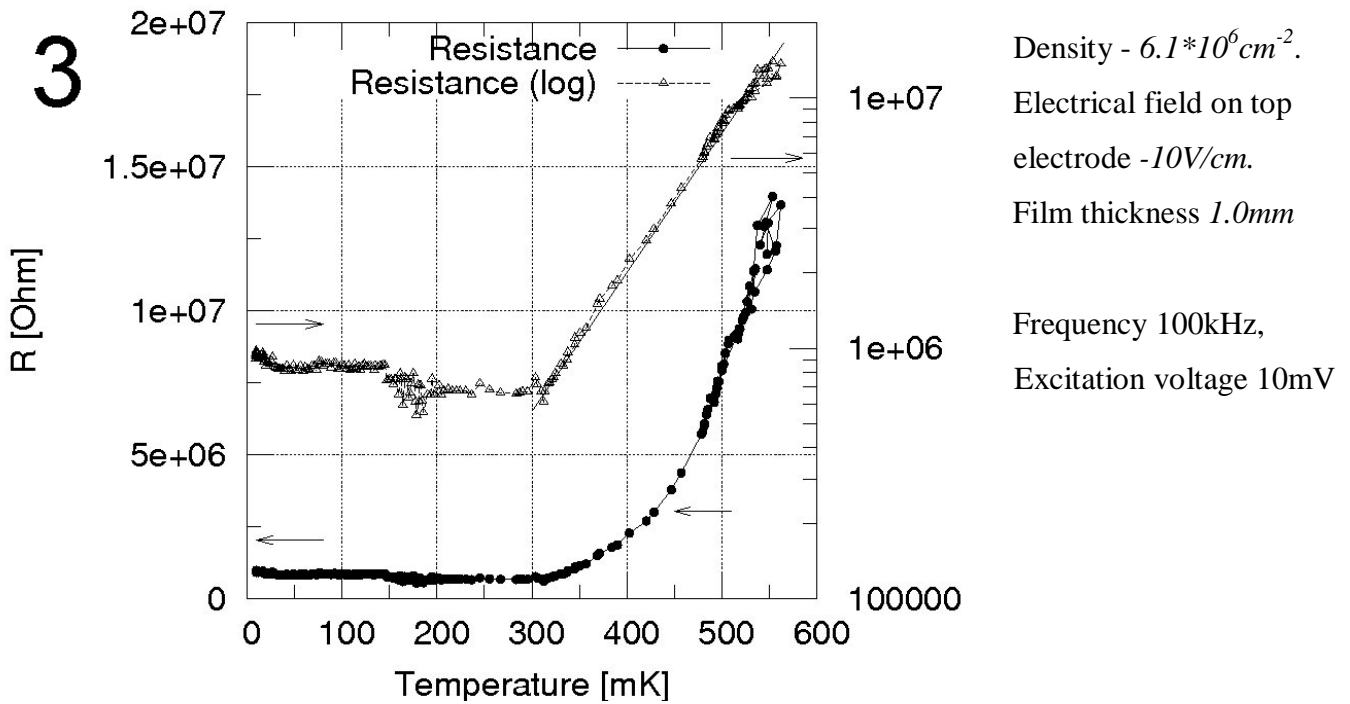


Fig. 5.4 Measurements of electron layer resistance with ^3He films of different thicknesses. Deviation of resistance from power law in temperatures above 530mK for 0.2mm film (#2) we attribute to our measuring condition, namely insensitive thermometer. Increase of resistance at 150mK for 1mm film (#1) is connected with loose of small part of electrons.

For 1mm film thickness, a sweep was done from high to low temperatures in 12 hours. Three bottom electrodes were kept at zero voltages, the voltage of the guard electrode was -6V and the top electrode at -4V (or field -10V/cm). The offset for the x-component of signal was 100nV. The electron density was $6.1 \cdot 10^6$ electrons/ cm^2 .

For 0.5mm film thickness, a sweep was performed from high to low temperature during 15 hours. Three bottom electrodes were at zero voltage; the voltage of the guard electrode was -6V and top electrode -4V (field -10V/cm). The offset for the x-component of signal was 200nV. The electron density was $7.3 \cdot 10^6$ electrons/ cm^2 .

Finally, for 0.2mm film thickness, a sweep was done from high to low temperatures in 22 hours. Three bottom electrodes were at zero voltage; the voltage of guard electrode was -4V and top electrode -2.6V (field -8.5V/cm).

The offset for the x-component of signal was 220nV. The electron density was $5.8 \cdot 10^6$ electrons/cm².

In the temperature region above 300mK the electrons were scattered on ³He vapor atoms. However, in the temperature range 5-300mK we have different characteristics: for 1.0mm film, the resistance did not change (unless some part of the electrons was lost, Fig. 5.4, #3 at 150mK); for 0.5mm film, the resistance increased with decreasing of temperature (this change was approximately 30% or less); for 0.2mm, the resistance is also increased.

Fig. 5.4 #3, 1.0mm He-film: Constant value of the signal below 310mK was not expected (electron (in dimple) - ³He quasiparticle and electron-rippion scatterings should depend on temperature). Decrease at 150mK was connected with loose of electrons. The following sweep from low to high temperature with magnetic field (Fig. F.8, Appendix F, p122) showed the same constant value below 310mK.

Fig. 5.4 #2, 0.5mm He-film: Small resistance increase in the temperature region 280-240mK could be related to the possible beginning of electron (in dimple) - ³He quasiparticle scattering. Constant value of resistance in the temperature region 105-240mK was not expected and subsequent increase of the resistance in 105-5mK could be again attributed to the possible electron (in dimple) - ³He quasiparticle scattering (hydrodynamic regime) and constant value 15-5mK could be related to electron (in dimple) - ³He quasiparticle scattering (ballistic regime). The following sweep from low to high temperature with magnetic field (Fig. F.8 #2, Appendix F, p.122) showed again constant value of resistance in increased temperature region (not only 5-15mK), the increase of the resistance in the temperature region 300-150mK (so, with magnetic field, this region was shifted to the higher temperatures), and small resistance increase (without magnetic field at 280mK-240mK) now was shifted again to the higher temperatures, 340-300mK.

Fig. 5.4 #1, 0.2mm film: Constant value of resistance in the temperature region 310-250mK is not expected (electron-rippion scattering should have the

right temperature dependence, which we did not have). Resistance increase in the temperature region 250-180mK could be attributed to the probable electron (in dimple) - ^3He quasiparticle scattering (hydrodynamic regime) and relatively constant value between 5-180mK could be related to electron (in dimple) - ^3He quasiparticle scattering (ballistic regime). The following sweep from low to high temperatures with magnetic field (Fig. F.8 #3, Appendix F, p.122) showed again constant value of resistance in the temperature region 5-130mK and unexpected increase in the resistance (130-220mK) and following resistance decrease (220-300mK). So, with magnetic field, resistance decrease at 250mK was shifted to higher temperatures.

As a conclusion, one can see, that our data differ from published one and could not be explained by the electron/ripplon and electron - ^3He quasiparticle scatterings

5.3 Measurement with different excitation voltages

In order to check M. Saito's model, we have performed measurements with different excitation voltages of signal. In his model for ^4He , Saito [Sait77] predicted that there should be a transition region in excitation voltages (different slopes), where one should see an electron scattering on He vapour atoms and on riplons. This transition value should depend on the temperature. On the fig. 5.5 (an original data also in Appendix F, Fig. F4, p.116) we can see resistance of electron layer for different excitations.

Measurements with different excitation voltages were done together with measurements of pressing electrical field on top electrode (chapter 5.5) and sweep in frequency from 1Hz to 100kHz (chapter 5.4). All sweeps (excitation voltage, frequency and pressing electrical field) were done in the following way. We started from low temperature to high one. For each point in temperature, first measurement with different excitation voltages was done

(measuring from smaller value to higher one, and then in one step back to the original voltage 4mV, each sweep in voltages was performed in 10min); than measurement with different pressing voltages on the top electrode (voltage was negative, and was increased from small value, -2V (-5V/cm) to higher -14V (35V/cm) one, and then in one step back to the original voltage -2V, each sweep in voltages was performed in 8min); and finally, sweep in frequency from 1Hz to 100kHz was performed (from smaller frequency to higher, and back in one step, and each sweep was 5min long). So, for each point in temperature, all measurements were approximately half an hour and changing of temperature was small (below 10%). All these measurements were done in 41hours. Concentration of electrons was $1.04 \cdot 10^6 (\pm 15\%)$ electrons/cm², film thickness 1mm.

Two increases in resistances at 10mK and 130mK, see Fig 5.5 (8% of the total resistance) were connected with loose of small part of electrons (these electrons, 8%, were lost during time period between changing the temperature, rather than during the measurements itself).

Resistance for different excitations and Temperatures

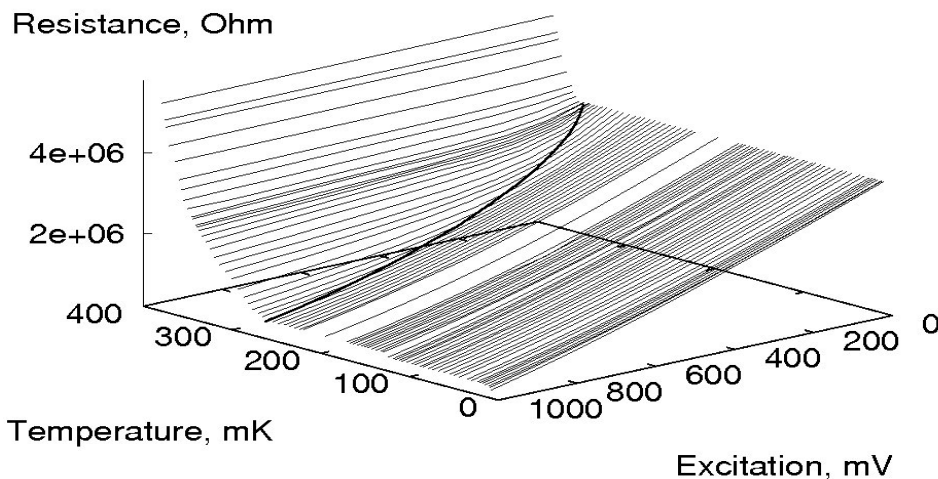


Fig. 5.5 Resistance of electron layer versus different excitation voltages. Two jumps at 10mK and 130mK are connected with loose of a small part of the electrons (8% total). Line separates regions of different slopes of measured resistances. Concentration of electrons was $1.04 \cdot 10^6 (\pm 15\%)$ electrons/cm², film thickness 1.0mm. Voltage on the top electrode was -4V (field -10V/cm), on guard electrode -6V, on three bottom electrodes - 0V, frequency - 100kHz.

As it can be seen, for the temperature below 250mK the resistance was proportional to the excitation voltages from 4 till 1000mV and in region above 400mK, resistance did not depend on excitation voltage. In the temperature region between 400 and 250mK we had two linear regions with different slopes (see also original data in Appendix F, Fig. F4, p.116). For smaller excitation voltages, slope was near the same as one below 250mK and for the higher voltages, slope tended to be parallel to excitation axis (so, no resistance dependence on excitation voltage as it was in high temperature region, above 400mK). Transition from one slope to another one depended on temperature. We attribute higher temperature region (above 250mK) to electrons - ^3He vapor atoms scattering, below 250mK to another one, which is still under the question, and temperature region 400-250mK as transition from one scattering mechanism to another one.

5.4 Measurement with different excitation frequencies

We also carried out measurements with different excitation frequencies. First of all, we wanted to check the fact that ripplons cannot exist at low temperature (below 250mK) due to the high value of viscosity of ^3He , and second, that low frequency electron-ripplon mode also cannot exist. To check this idea we made a sweep in frequency from 1Hz to 100kHz for each temperature point (for details of experiment, see Chapter 5.3). Concentration was $1.04 \cdot 10^6 (\pm 15\%)$ electrons/cm², helium film thickness 1.0mm, and temperature 5-450mK. Our measurements showed that there were not any peaks that were connected with ripplons or low frequency coupled electron-ripplon mode.

On the other side we made different sweeps in temperature with different frequencies (during changing of temperature, frequency was kept constant). The initial idea was to check our equivalent scheme for signal to resistance

recalculation. Increasing of frequency led to possibility to measure lower resistance values of electron layer (see also Appendix B, Fig.B7, p.94, Table 3).

Our frequency measurement were done unfortunately only for 0.2mm ^3He -film, the excitation voltage – 10mV and for the voltages on the top electrode – 4V (10V/cm), and on the guard electrode –2.6V (only measurements for 10kHz were done with voltages –6V on top electrode and –4V on the guard electrode). Measurements for the frequencies 10kHz and 100kHz were done during the sweep from high to low temperatures, 50kHz and 75kHz measurements were done during the sweep from low to high temperatures. 10kHz measurement was separately done (but the same cool-down), 50kHz, 75kHz and 100kHz in series (only between 50kHz and 75kHz sweeps, additional 50kHz sweep was carried out, which was absolutely identical to previously measured 50kHz sweep). From experimental curves we can find a general feature: for all frequencies we had the same high-temperature region where electrons scattered on ^3He vapor-atoms (so, resistance decreased with power law with decreasing of temperature, deviation from power law dependence for some our measurement above 500mK, we attributed to the experimental conditions: our measuring thermometer started to be insensitive). Our measurements in the high temperature range are very similar to previous measured one, see also Fig. 5.2. Below 250mK we did not have the same characteristics: signal could slightly decrease and then again increase and sometimes was very similar to Kono's measurements (for example, 75kHz sweep) or to decrease and disappear at all (like for 100kHz sweep, where we can see a loose of electrons at 120mK).

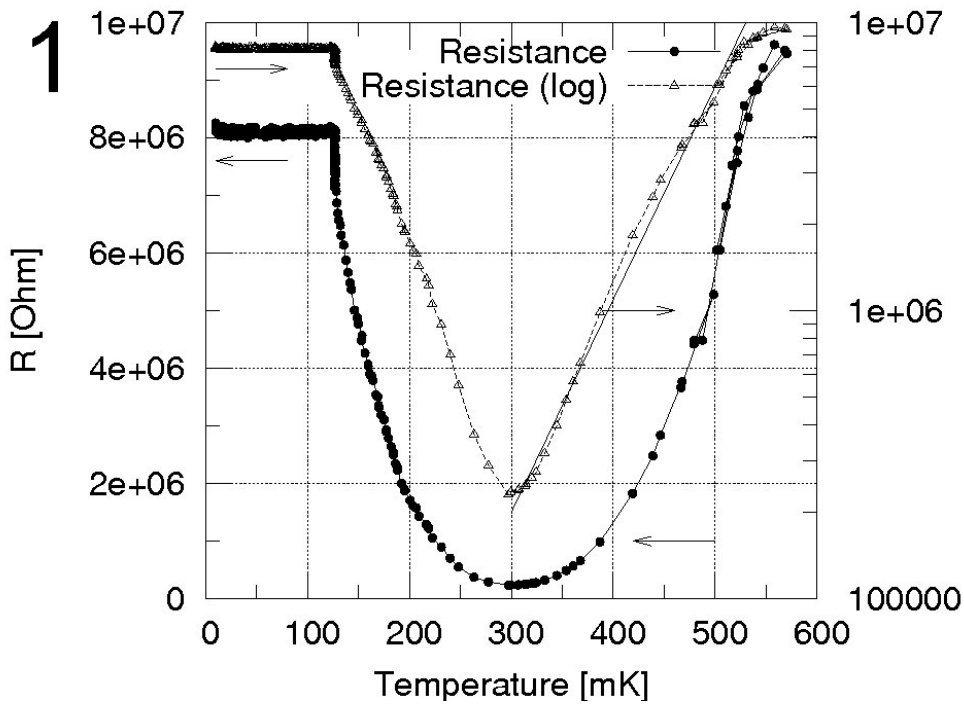
For each sweep in frequency we can consider low temperature region (below 250mK) in more details. We note, that here we would like to consider our resistances, which were recalculated from our equivalent scheme, considering only real part of electron layer resistance. For another possible explanation (which took into account also imaginary part of electron resistance) are given in Appendix B and Chapter B.1.5, p.89

Fig. 5.6 #4, 10kHz measurement: Gradual decrease of resistance from 320 to 250mK is not explainable (to be absolutely sure about electron-ripplon scattering we had to have also the right temperature dependence, which we did not). Gradual increase in the resistance from 270 to 50mK could be attributed (according to K.Kono) to electron (which was in dimple) – ^3He quasiparticle scattering (hydrodynamic regime) and constant value below 100mK to electron- ^3He quasiparticle scattering, ballistic regime (like K. Kono did). If we had had abrupt increase (jump) in the resistance (Wigner crystallization) around 250mK and density $1.5 \cdot 10^8$ electrons/cm², it would have been similar to K. Kono's measurements.

Fig. 5.6 #3, 50kHz measurements: Small increase in the resistance in the temperature region 320-240mK could be attributed to the beginning of the electron (in dimple) - ^3He quasiparticle scattering. Although we could not explain the following (start at 240mK) decrease of resistance and again (at 150mK to 5mK) resistance increase.

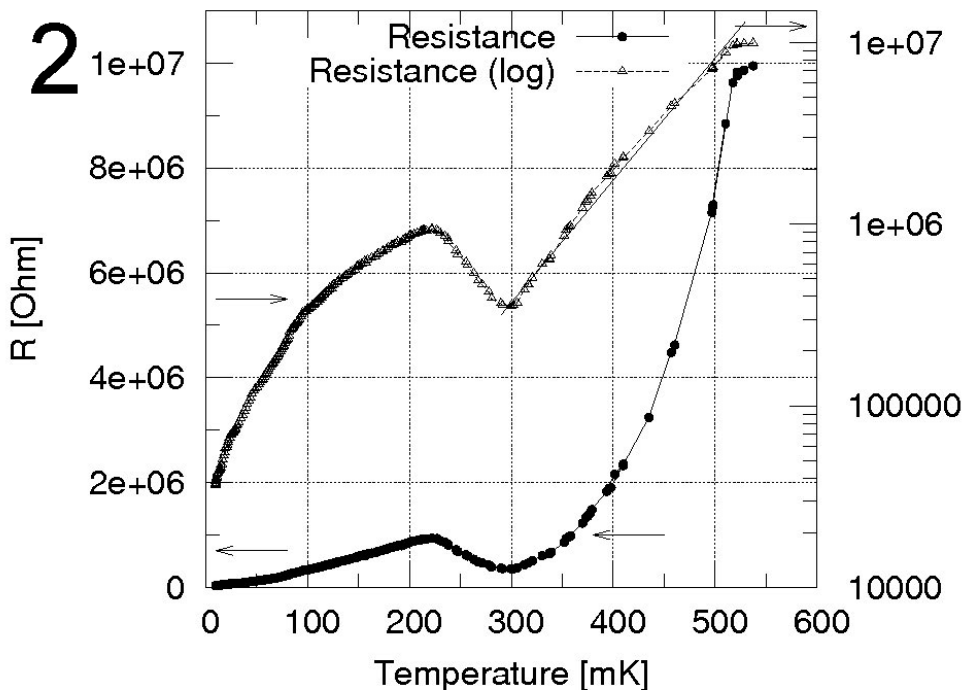
Fig. 5.6 #2, 75kHz measurement: Increase of resistance in the temperature region 270-220mK could be related to the possible electron (dimple) – ^3He quasiparticle scattering (another possibility was to relate it to Wigner crystallization jump, though it was necessary to mention, that for jump, this temperature range was too wide). Following two decreases, at 220mK and 70mK we cannot explain.

Fig. 5.6 #1, 100kHz measurement: Increase of the resistance in the temperature region 290-120mK could be related to the electron (in dimple) - ^3He quasiparticle scattering (though the temperature dependence was absolutely different from expected one). At 120mK we unexpectedly lost our electrons (we cannot explain why).



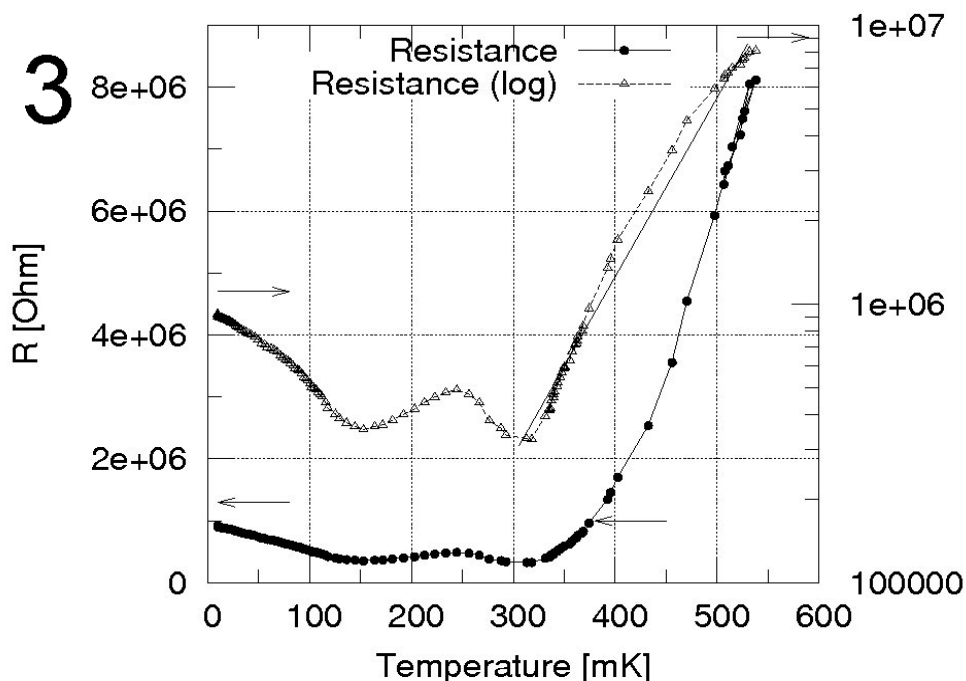
Density - $7.2 \cdot 10^6 \text{ cm}^{-2}$.
Frequency 100 kHz ,

Excitation voltage 10 mV ,
Film thickness 0.2 mm ,
Electrical field on middle
bottom electrode 0 V/cm .
Electrical field on top
electrode -8.5 V/cm .



Density - $5.8 \cdot 10^6 \text{ cm}^{-2}$.
Frequency 75 kHz ,

Excitation voltage 10 mV ,
Film thickness 0.2 mm ,
Electrical field on middle
bottom electrode 0 V/cm .
Electrical field on top
electrode -8.5 V/cm .



Density - $7.3 \cdot 10^6 \text{ cm}^{-2}$.

Frequency 50kHz,

Excitation voltage 10mV,

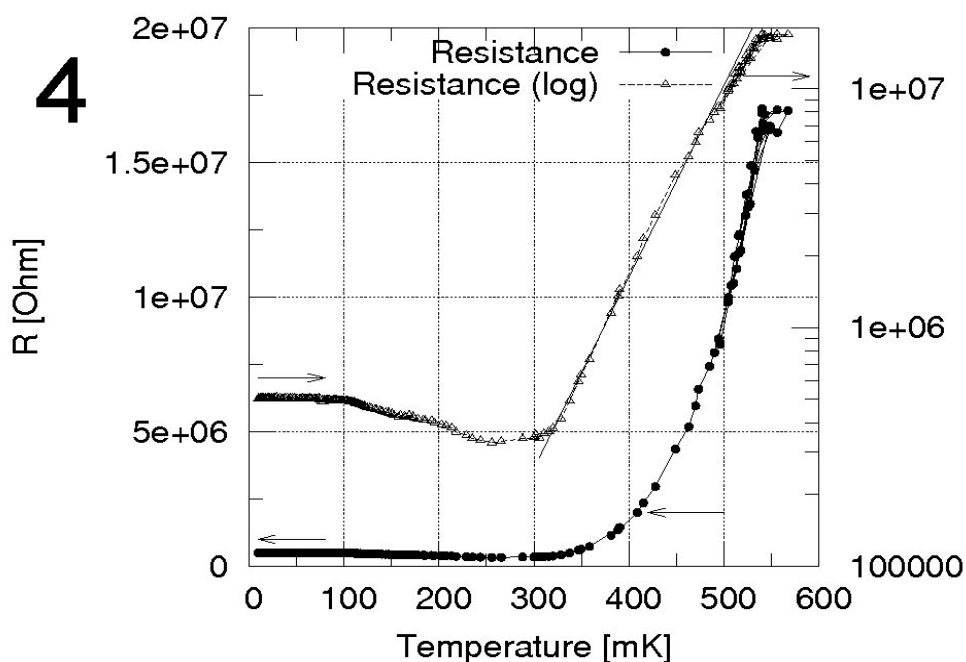
Film thickness 0.2mm,

Electrical field on middle

bottom electrode 0V/cm.

Electrical field on top

electrode -8.5 V/cm .



Density - $7.3 \cdot 10^6 \text{ cm}^{-2}$.

Frequency 10kHz,

Excitation voltage 10mV,

Film thickness 0.2mm,

Electrical field on middle

bottom electrode 0V/cm.

Electrical field on top

electrode -10 V/cm .

Fig. 5.6 Resistance of electron layer with different frequencies of excitation voltages. For 100kHz measurement (#1) at 120mK we lost our electrons. In temperatures 300 – 530mK we have scattering of electron on helium vapor-atoms and resistance has a power law dependence. Deviation from power law dependence at temperatures above 530mK we attribute to our experimental conditions (insensitive thermometer). Electron-ripplon and electron- ^3He quasiparticle scatterings (hydrodynamic and ballistic regimes) can not explain our data for temperatures below 300mK.

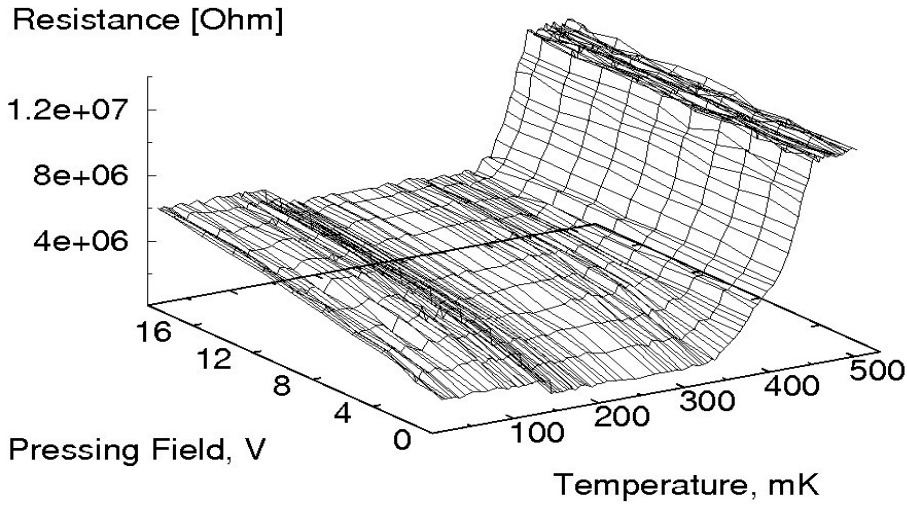
In before mentioned explanations we tried to explain our measurements basing on proposed by Kimitoshi Kono scattering mechanism, namely electron-rippon and electron in dimple - ^3He quasiparticle (hydrodynamic and ballistic regimes). Though our attempts to explain data failed very often. Further discussions are given in Chapter 6

5.5 Measurements with different pressing fields

We also carried out measurements with different pressing electrical field (as on the top electrode as well as on three bottom electrodes). The idea was to check the theory, made by M. Saito [Sai77], for electron-vapour and electron-rippon scattering for the case of ^3He . In his theory for ^4He M. Saito predicted that electron - ^4He -vapour-atom scattering should not depend on pressing electrical field. On the other side, in the electron-rippon scattering regime, the collision time should slightly increase with decreasing of temperature and decrease with increasing of pressing electrical field.

On the Fig. 5.7 we can see our resistance of electron layer versus pressing electrical field (positive) on three bottom electrodes. For the original data (X and Y components), please, see Appendix F, Fig. F7, p.120. The whole sweep in temperature was done in 10 hours from high to low temperatures and the pressing field (from 0 to 45V/cm) was increased from small to high values and back in one step. For each point in temperature the measurement of pressing field was done in 10 min. The top electrode was at -4V ($-10\text{V}/\text{cm}$) and the voltage of the guard electrode was at -6V . Concentration of electrons was $1.8 \cdot 10^6 (\pm 15\%)$ electrons/ cm^2 . Helium film thickness was 1.0mm. Signal decrease at 140mK was connected with the lose of a part of electrons (4%, the loose happened in time between the measurements).

R versus pressing electrical fields on bottom electrodes #1, #2, #3



R versus pressing electrical fields on bottom electrodes #1, #2, #3

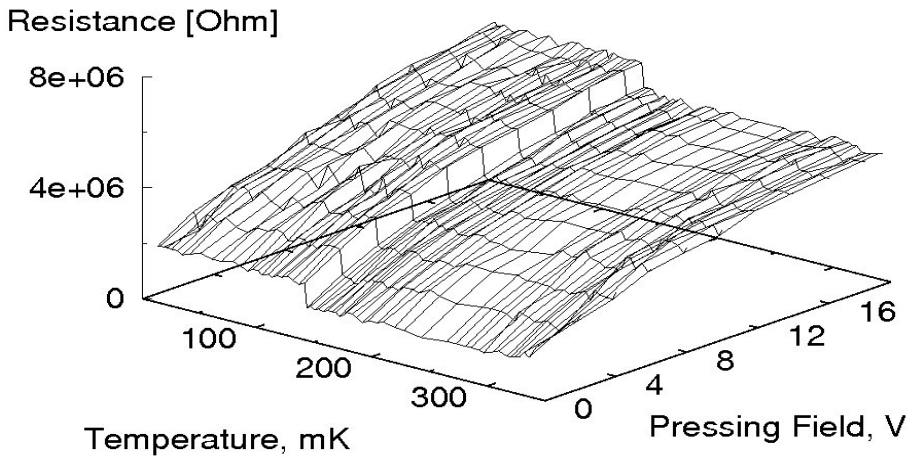


Fig. 5.7 Resistance of electron layer versus voltage on three bottom electrodes. Top: whole temperature range, bottom: low temperature one. Positive voltage was applied to three bottom electrodes from 0 to 18V (45V/cm). Density $1.8 \cdot 10^6 (\pm 15\%)$ electrons/cm². Helium film thickness was 1mm. A signal decrease at 140mK was connected with loose of part of electrons (4%). Excitation voltage – 10mV, frequency 100kHz. Voltage on the guard electrode was –6V and on top electrode –4V. Constant value of resistance above 490mK we attribute to our experimental condition (insensitive thermometer).

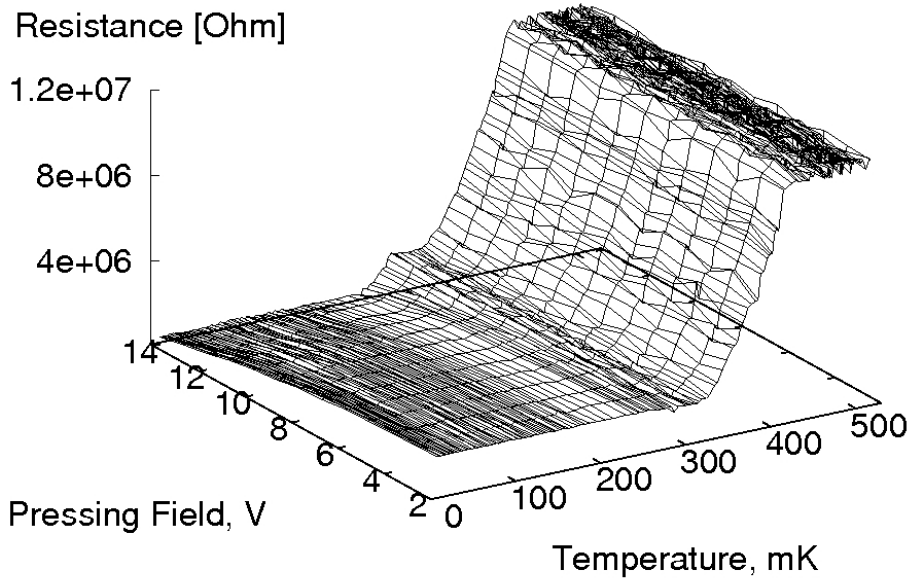
From our measurements of three bottom electrodes (Fig. 5.7) we can conclude: (i) below 350mK, increasing of pressing electrical field leads to

increasing of resistances that was predicted by M. Saito, (ii) we cannot see temperature dependence of resistance in the temperature 5-300mK (according to M.Saito, resistance should slightly decrease).

On the other hand, we also carried out measurements with pressing field (negative) on the top electrode, Fig 5.8 (and original data were presented in the Appendix F, Fig. F6, p.119). Electrical field was increased from -2V (-5V/cm) to -14V (-35V/cm). This measurement was done together with excitation voltage and frequency sweeps (for more details, see Chapter 5.3). Concentration was $1.04 \times 10^6 (\pm 15\%)$ electrons/cm², film thickness 1mm. Guard electrode voltage -6V . In this measurement we also observed that again, electron ³He-vapor atom scattering did not depend on pressing electrical field.

Though, our measurements in low temperature (below 300mK) were absolutely different from data predicted by M. Saito and our data, measured with three bottom electrodes. Instead of increasing of resistance, we obtained the decreasing (Fig. 5.8). We cannot explain this behavior, but we suspect that it is due to less homogenous field distribution inside the cell (our upper electrode was constructed as a circuit and moreover, did not cover three bottom electrodes, which were rectangular, see Appendix C, p.102). We think that increasing of pressing electrical fields led to electron moving toward the corners (which were not covered with top electrode) and in addition it also led to redistribution of electrons along the boundary (along guard electrode, which was square, for more discussion, please see Chapter 6, p.70 and Chapter 4.6, p.41).

R for pressing Fields on top electrode



R for pressing Fields on top electrode

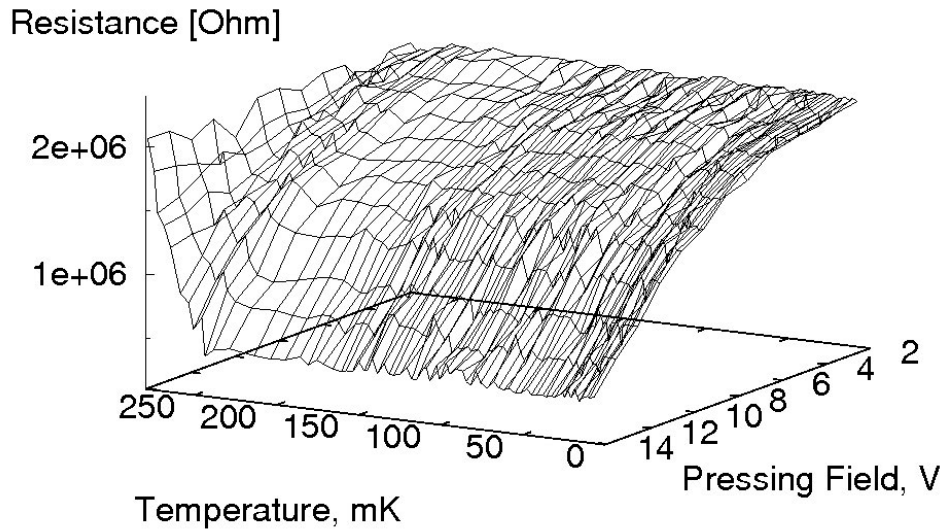


Fig. 5.8 Resistance of electron layer for different pressing field (from 0 to 35V/cm) on top electrode (negative voltage). Top: whole temperature range, bottom – low temperature one. Concentration $1.04 \cdot 10^6 (\pm 15\%)$ electrons/cm², film thickness 1mm. Excitation voltage 10mV, frequency 100kHz, voltages on the guard electrode – 6V and on three bottom electrodes – 0V. Constant value of resistance above 490mK we attribute to our experimental condition (insensitive thermometer).

5.6 Short Summary

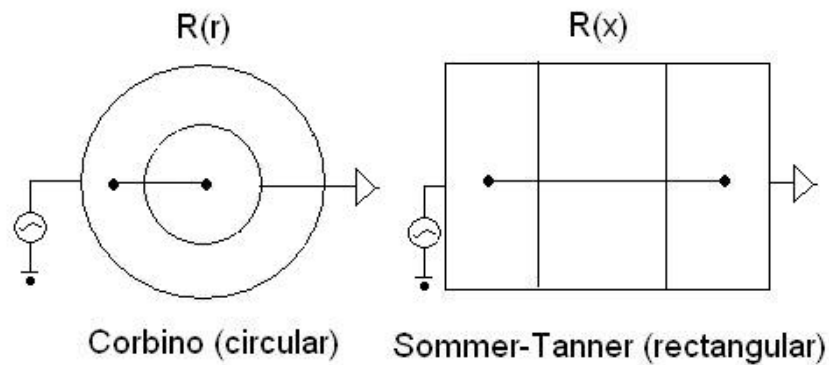
- i) Measurements with different frequencies (Chapter 5.4), film thicknesses (Chapter 5.2) and measurements similar to K. Kono's ones (Chapter 5.1) showed that we have electron-helium vapor atom scattering and resistance has power law dependence on temperature. At the same time, below 300mK we have different characteristics, which we can not explain with two scattering mechanisms, namely electron-rippions and electron- ^3He quasiparticle (hydrodynamic and ballistic regimes). Explanation of our data for temperatures below 300mK is still in need.
- ii) Measurements with different excitation voltages (Chapter 5.3) and pressing electrical fields (Chapter 5.5) showed that we have two scattering mechanisms, namely electron- helium vapor atom, at $T > 300\text{mK}$ and second, which we do not know. It is possible, that below 300mK we overheat electrons (see also Chapter 4.5, p.39) or we have sliding mode of SSE (in WS phase or without WS phase). Measurements with pressing field on top electrode showed that we could have redistribution of electrons inside the cell and possible increase of conductivity through the boundary layer of electrons (see also Chapter 4.6 p.41)

Chapter 6

Discussion

In this chapter we would like to analyze the data.

a) Geometry. We start with choosing of geometry. For measurement of electron mobility there are two possibilities, namely; circular (Corbino) and rectangular (Sommer-Tanner).



Each of geometries has advantages and disadvantages:

Circular geometry with two electrodes allows to measure mobility between these two electrodes not being afraid of boundary conditions (for example, conductivity along the guard electrode) or homogeneity of electrical (or magnetic) fields in the boundary (namely, in direction of signal propagation) between two measuring electrodes. It has another advantage: to obtain the resistance from measured signal, it is possible to use analytical functions (Bessel and Neumann). Recalculation of signal to resistance possibly needs adjusting of several parameters (capacitance of electron layer to ground and to top electrode, edge capacitance, mutual capacitance between two measuring electrodes), but nevertheless, it is much better than to numerically solve 3D (or sometimes 2D) Poisson

equation with boundary conditions. Next advantage is that in magnetic field it is possible to use the same formulas for recalculation of signal to resistance. The disadvantage of circular geometry is that it is not possible to measure edge effects, for example Hall effect (edge magnetoplasmons). Correspondingly the advantage of rectangular geometry is measurement of edge effects. The biggest disadvantage is that we lose 'symmetry'. We have boundary where we have changing of density from zero to maximal (which is in the middle of cell), electrical fields become non-homogeneous along the direction of signal propagation, 3D calculation of electrical field profiles (and correspondingly electron density) becomes almost impossible, recalculation of measured signal to resistance (or mobility) becomes very difficult and some approximations must be done (for more details, see [Lea91, Lea93]). Another advantage of rectangular geometry is measurements in temperature of ^3He A-phase. Magnetic field must be applied parallel to the direction of signal propagation, see also fig. 2.8 p.20 (magnetic field applied perpendicular to the helium surface leads to electron rotation).

From above mentioned, it becomes clear, that extensive measurements in circular geometry must be done first in order to determine electron mobility in "ideal", without edge effects conductivity. When everything is clear, next step could be measurements of edge effects in rectangular geometry (by the other words, when we know everything about ideal ("bulk") conductivity, where all boundary or inhomogeneous effects are excluded, than for rectangular geometry we would be able to distinguish "ideal" and "non-ideal" conductivities). Unfortunately, not everything was clear with circular geometry and this gave us problems in the future. Decision to make measurements in rectangular geometry was done in 1998 (group in Konstanz), cell was constructed in Konstanz and to 2001 was several times repaired and changed. Since August 2001 (when the author started to work in Bayreuth) cell was already installed

and not opened. After close examination of 16! articles (1995-2002) devoted to the problem of electrons on the surface of ^3He , it became clear that even with measurements in circular geometry, not everything is still understandable (see also Chapter 2.2 and 2.3) and further measurements in circular geometry were required. Several critical questions are still present: (i) existence of Wigner solid transition (namely, whether this transition is reproducible with changing of temperature in other direction) and for low density limit, observation of Wigner solid transition in the sliding regime, (see Fig 2.2 p.14) (ii) dependence on the pressing electrical field in normal fluid phase, 1-300mK; (iii) how good is statistics in the temperature region 1-300mK (namely, measurements, which show hydrodynamic and ballistic regimes of electron (in dimple) - ^3He quasiparticle scattering,); (iv) why there is the difference between “nice” (Fig. 2.4) and “non-linear” (Fig. 2.5) measurements in He superfluid phase temperature (and usually already these questions lead to further measurements in circular geometry); (v) particular question must be addressed to the method of signal to resistance recalculation. Answers on these questions were not stated before construction of rectangular cell (otherwise it would have led to the construction of the cell with circular geometry) and this led to some additional difficulties with interpretation and comparison of our data with measured previously in circular geometry.

b) *Discussion.* Our measurements are consistent with previously published (Kimitoshi Kono) in the high temperature region (300-550mK) where we have electron - ^3He -atom vapor scattering. This is shown by our measurements with different film thicknesses (0.2; 0.5 and 1.0mm), with (≈ 60 Gauss) and without magnetic field, with different pressing electrical fields (5V/cm - 45V/cm), and frequencies (10-100kHz) of excitation. On fig. 5.3 we can see that our measurements for the high temperature region agree quite good with each other (within our experimental errorbar) for different film thicknesses and magnetic fields. We also note that our data could be better fitted with formula $\sim \exp(-Q/T)$ then $T^{3/2}\exp(-Q/T)$, where T-temperature, Q- vaporization energy, though both

formulas could be used due to our errorbar for high temperatures. In addition, measurement with different excitation voltages (10mV-1V) are qualitatively in agreement with theory, proposed by M. Saito [Sait77], for two different mechanisms of scattering, namely electron - He-vapor atom and another one, which is still under the question.

On the other side, measurements in the low (1-300mK) temperatures are very different and sometimes not reproducible. Our attempts (Chapter 5.1) to interpret them as Wigner solid transition, electron-rippion or electron (in dimple) - He quasiparticle scattering (hydrodynamic and ballistic regimes) failed in many points. Often it is even difficult to notice any dependence, but anyhow, we presented some general features of measured signal.

First of all we notice that for electron concentrations below $2 \cdot 10^6$ electrons/cm² and temperature below 300mK, our signal (and correspondingly resistance and mobility) does not change (no other temperature dependence, except for electron - ³He vapor-atom scattering in the temperature region 300-550mK). For the concentration above $6 \cdot 10^6$ electron/cm² we observed temperature dependence of resistance (signal) and for concentrations $2-6 \cdot 10^6$ electrons/cm² we have sometimes temperature dependence and sometimes not. For example for 1mm film thickness, after the loading, concentration of electrons usually is relatively high (in our measurements above $6 \cdot 10^6$ electron/cm²) and during the sweep to the low temperatures we have losing of electrons (but not Wigner crystallization! - for more details, see Chapter 5.1). Density is decreased and after that, during sweep to the high temperatures (5-300mK) signal is slightly decreasing or staying constant. If concentration is below $2 \cdot 10^6$ electrons/cm², then there is no change of signal at all in the temperature region 5-300mK, signal is stable over few days and absolute reproducible in the following temperature sweeps. We also observed that losing of electrons never takes place in the temperature above 300mK where electron-Helium gas atom scattering is. Explanation is in need.

We tried to find explanations, why we have such a different behavior of electron signal in the temperature range 5-300mK (particular for the film thicknesses 0.2 and 0.5mm).

In our opinion, it is necessary to consider three possible explanations:

(i) It could be possible that we have situation when two conductivities play role, namely one through the center (“bulk”) layer and one through the boundary (“boundary”) layer along the guard electrode (where electron density changes from zero to maximum). Unfortunately, it is not known (theoretically and experimentally) how electron conductivity through the “bulk” and “boundary” depends on electron concentration. We only assume that conductivity through the boundary probably depend stronger on density, than that through the bulk. So, one our attempt to explain the results observed in the temperature region 5-300mK is based on two things: concentration and interplay of “bulk”-“boundary” conductivities. We think that for the concentration below $2 \cdot 10^6$ electrons/cm², conductivity through the boundary dominates (and from our measurements it implies that for such a low concentration conductivity through the boundary does not depend on the temperature in the range 5-300mK). In the concentration region $2-6 \cdot 10^6$ electrons/cm² we have interplay of two conductivities and which “wins” and how each conductivity depends on temperature we do not know. For the concentration region above $6 \cdot 10^6$ electron/cm we think that conductivity through “bulk” prevails and we have true “bulk” signal (see also Chapter .6 p.41). Unfortunately it is very difficult to check our theory due to two things: first, difficulties with exact determination (at least, no less than $\pm 15\%$, see also Chapter 4.1 and [Klier04]) of electron concentration and keeping of electron concentration (sometimes electrons can disappear by some unknown reasons), and second, to distinguish between “bulk” and “boundary” conductivities we should know “bulk” one but this was not all time the case because published data are still not extensive and clear.

(ii) Second possibility is appearance of imaginary component of resistance of electron layer. In the temperature below 280mK for the film thickness of 0.2 and 0.5mm some our data could be explained (at least qualitatively) if we assume, that resistance of electron layer has also imaginary part. Appearance of imaginary part of resistance may be interpreted as sign for Wigner crystallization (as it was done by K. Kono [Shir96, page 246]). Though in our opinion, change of imaginary part of resistance of electron layer is not absolutely necessary to be connected with Wigner crystallization and plausible explanation is still in need.

(iii) Another possible explanation is that we do not have coupling between helium surface and electrons on this surface. It could be, that electron conductivity is so high, that we overheat our electrons with 10mV signal and electrons are not “able” to thermalize to the surrounding temperature. For example, our two measurements in the temperature region below ^3He superfluid point transition for 1.0 mm film thickness. Each times, concentration was small $2 \cdot 10^6$ electrons/cm² and pressing field on top electrode was -15V (38V/cm) or -30V (75V/cm) (but also check for -4V (10V/cm) was done). Our signal was all time (0.6-1.3mK) stable. It is than possible, that our surface state electrons are in the sliding mode due to decoupling from helium surface and therefore, we do not see Wigner crystallization.

Chapter 7

Summary and Outlook

In this work, experiments with electron mobility on the surface of ^3He were carried out. Mobility measurements were done in the temperature range 0.6-600mK, the operating frequencies 1Hz-100kHz, the excitation voltage 4mV - 1V and pressing electrical fields 0-255V/cm on the top electrode and 0-47.5V/cm for three bottom electrodes. Films with different thicknesses 0.2, 0.5 and 1.0mm and magnetic field (approximately 60Gauss) were also under investigations.

In the temperature region above 300mK, electron scattering on ^3He vapor atoms was observed. Application of pressing electrical field to three bottom electrodes led to decrease of the electron mobility in the temperature region 5-300mK. Very often it was observed that at around 300mK, we had change of one type of scattering (^3He vapor atom) to another one (probably electrons in sliding regime) a kink like, not smooth change of signal (or mobility). Explanation is still in need.

In our measurements we failed to observe Wigner solid crystallization.

Possible explanations could be:

Interplay of two conductivities, namely conductivity through the electron layer in the center (“bulk”) and conductivity through the boundary layer of electrons (“boundary”). As evidence, that conductivity through the “bulk” and “boundary” could be present, could be our measurements with pressing electrical field on top electrode.

Another explanation could be overheating effect or sliding mode of Surface State Electrons, when electron layer was near decoupled from helium surface. In our opinion, it is most probable explanation. We also did measurements below temperature of the superfluid point transition, though we did not observed any change in the signal. Possible explanation could be overheating of electrons by excitation voltage or sliding mode.

As the next step one could make more extensive use of a magnetic field: measurements with higher valued in order to prove Drude's formula as well as measurements with higher magnetic fields. Another possibility is to use a circular geometry in order to exclude the effect of boundary conductivity.

Appendix A

Determination of electron concentration

In order to determine electron concentration we have to solve standart electrostatic task.

Let us consider the cell. For a fixed DC component we can use Gauss' law [for example, see [Val98], formula 3.11]

$$n = -\frac{e_0}{e} \left[\left(\frac{1}{D-d} + \frac{\epsilon_{He3}}{d} \right) V_e - \frac{V_t}{D-d} \right] \quad (*)$$

where V_t is the voltage on the top electrode, V_e is the voltage in the electron layer, D ist the distance between the top electrode and three bottom electrodes, d is the distance between low electrodes and helium film surface (electron layer), ϵ_{He3} is the dielectric constant of 3He .

Now we can consider the case, when we apply a negative voltage on the second (middle) bottom electrode. We consider a contour abcd (low middle electrode and a part of the top electrode).

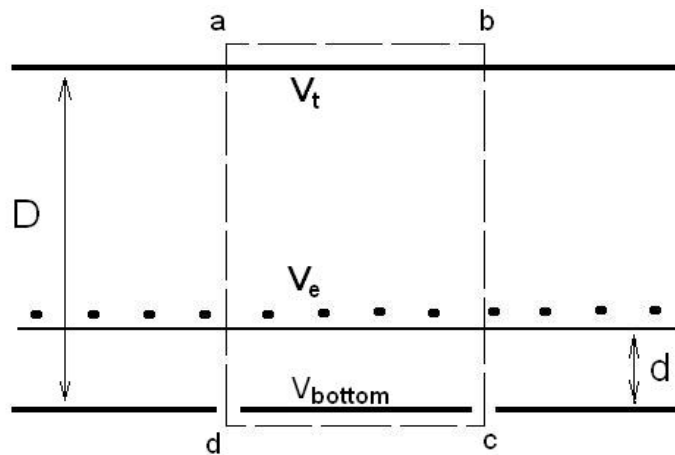


Fig. A1. *Electrical potentials in the cell*

This is again a capacitor, with $d=4\text{mm}$ and the length 17mm (the ratio between the thickness to the length is $4/17=0.235$)

We can use the same Gauss' law but with additional negative voltage on the bottom middle electrode.

$$n = -\frac{e_0}{e} \left[\left(\frac{1}{D-d} + \frac{e_{He3}}{d} \right) V_e - \frac{V_t}{D-d} + \frac{V_{bottom} e_{He3}}{d} \right] \quad (**)$$

Let us consider the case, when we have increased the voltage on the middle electrode V_{bottom} till the signal value beyond which we can see (so the density is zero above the middle electrode). Therefore we can find the density by a subtraction of the second equation ($n=0$) (***) from the first one (*).

$$n = \frac{e_0 e_{He3}}{e} \frac{V_{bottom}^0}{d} \quad (18)$$

(for a more detailed analysis, see [Wil88], [Dam87]). We also used this method for experimental determination of electron density (see also Fig. 4.2, p.32). The theoretical density is given by the formula of full screening of electrical field between electron layer and top electrode, $n_{theory} = \frac{e_0}{e} \frac{V_t}{D-d}$.

When electrons are loaded till the saturation we can use (with zero voltages on three bottom electrodes), for example, first formula (*), with $V_e = 0$ (V_e is not zero only in the boundary layer) in order to calculate the density

$$n = \frac{e_0 V_t}{e(D-d)} \quad (19)$$

And for our case, $V_e = 4V$, we have $n = 7.36 \cdot 10^{10} [m^{-2}] = 7.36 \cdot 10^6 [cm^{-2}]$. The corresponding temperature for the Wigner crystallization is 58mK.

$$T_{WignerCrystall} = \frac{e^2 \sqrt{n}}{137 * 4 \sqrt{p} e_0 k_B} \quad (20)$$

If we use positive voltage on the middle bottom electrode (typically it is +4V, for 1mm helium film, and after this loading this voltage was removed) then we can load more electrons $n = 36.8 \cdot 10^{10} [m^{-2}] = 36.8 \cdot 10^6 [cm^{-2}]$, and corresponding Wigner crystallization temperature is 130mK.

Appendix B

Calculation of cell impedances and comparison of different models for signal-resistance recalculations

B.1 General consideration of different models

B.1.1 (Lumped) Equivalent circuit.

The easiest way to calculate and model the surface electron layer and electrodes is to use equivalent circuit. It consists of two (or three, if the middle electrode is grounded) identical capacitors C that represent capacitive coupling of the excitation and the detection electrodes to the electron layer and one (or two, if we have three electrodes) resistor R , which represents the conductivity of electrons. Then the admittance Y is given by

$$Y \equiv \frac{I}{V_{ex}} = \frac{w^2 C^2 R}{4 + R^2 w^2 C^2} + i \frac{2wC}{4 + R^2 w^2 C^2} \quad (18)$$

R is directly related to the conductivity, $R = K/\sigma$, where K is a geometrical factor, which is not known, σ is the conductivity, which is for the case of a 2D geometry is simply the reversed resistance. This model is valid only for small phase shifts, i.e. $wCR \ll 1$ (for our case, it should be $R \ll 2M\Omega$). This model is independent of the geometry [rectangular or circular (Corbino)] because the geometrical factor K remains an unknown quantity. An example of usage of this model is presented on figure below.

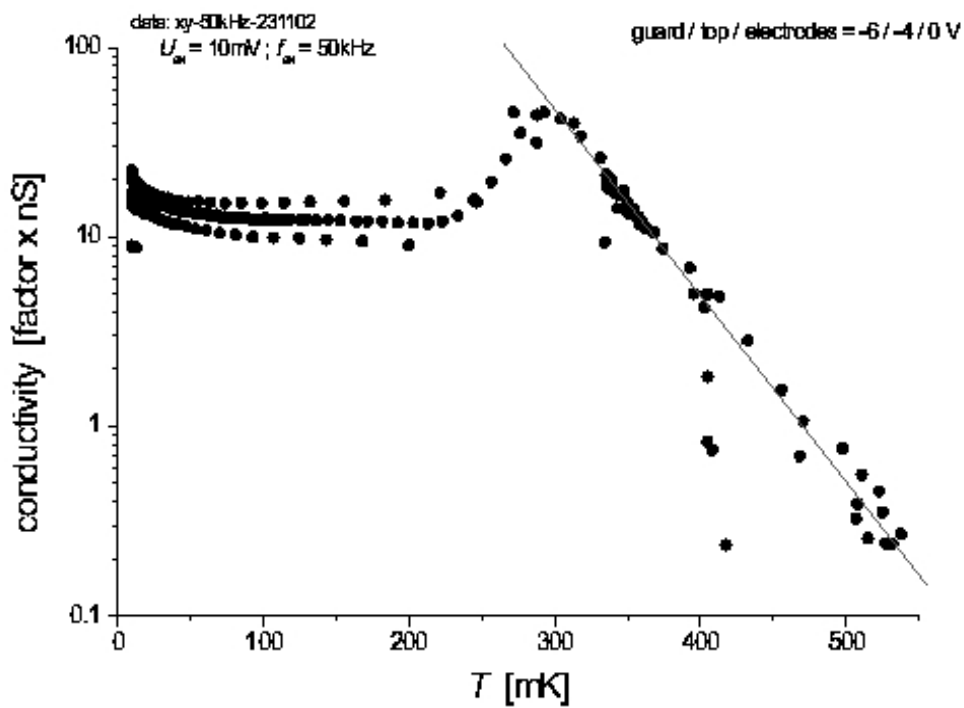
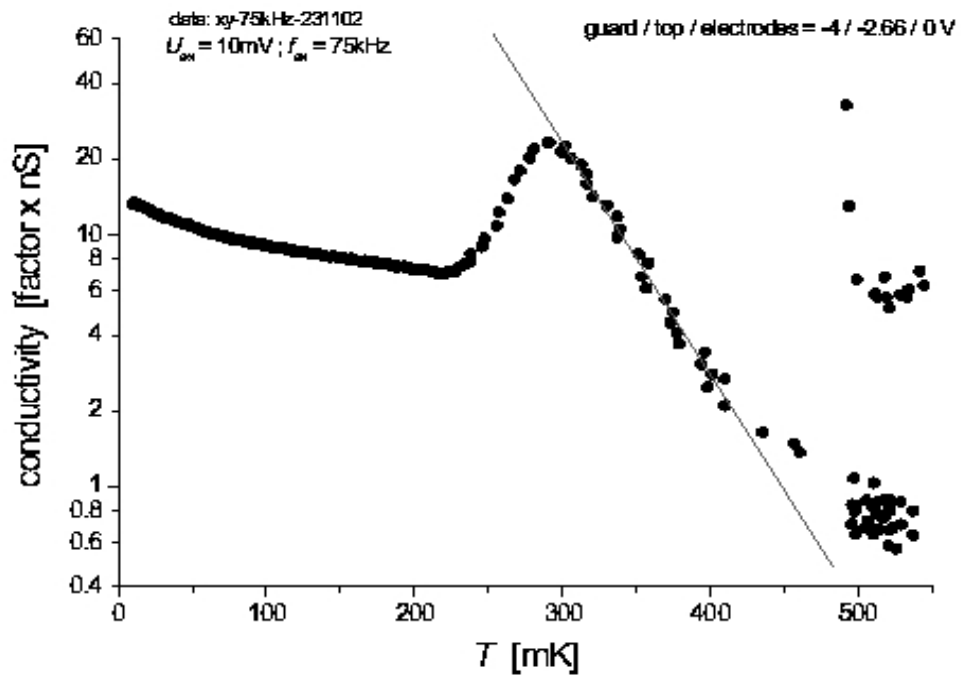


Fig. B.1 We can consider different way of impedance calculation using simple lumped impedance scheme (Juergen Klier, University of Konstanz)

B.1.2 Transmission line model

Sommer and Tanner [Som71] pointed out that electron layer can be considered as 2D transmission line with distributed resistance and capacitance. The theory for Corbino (circular) and Sommer-Tanner (rectangular) geometries was done by Dahm [Dam87, Met82, Met97] without any edge corrections, by Wilen [Wil88] for the Corbino geometry with edge corrections and by Lea [Lea91, Lea93] for the case of the rectangular geometry in the presence of the magnetic field only with a qualitatively estimation of the edge effects. An expression for the current in the cell of rectangular geometry (without edge effects) is given by

$$I = (1+i) \frac{wCV}{2} d \frac{\sinh^2((1+i)l/d)}{\sinh(3(1+i)l/d)} \quad (19)$$

where l is the length of electrode (all electrodes have the same length and width), V the input voltage, C the capacitance per unit area, $d = (2/RwC)^{1/2}$. δ is a characteristic length over which an excited wave can penetrate the electron layer [Dam87], ω - excitation frequency, R - resistivity of electron layer.

An example of this formula written in real (normal component of signal) and imaginary part (quadrature component) can be seen below:

For simplicity, dimensionless expression $l/d = l \sqrt{\frac{RwC}{2}}$ we denote as h

$$\begin{aligned} \text{Real component} \quad & -V/l * (9/2) * (2\omega C/R)^{1/2} [-2\sinh(h)\cos(h)\cos(h/3)^2 \cosh(h/3)^2 + \sinh(h)\cos(h)\cos(h/3)^2 \\ & + \sinh(h)\cos(h)\cosh(h/3)^2 - 2\sinh(h/3)\cos(h/3)\cosh(h/3)\sin(h/3)\cosh(h)\sin(h) - \\ & 2\cosh(h)\sin(h)\cos(h/3)^2 \cosh(h/3)^2 + \cosh(h)\sin(h)\cos(h/3)^2 \\ & + \cosh(h)\sin(h)\cosh(h/3)^2 + 2\sinh(h/3)\cos(h/3)\cosh(h/3)\sin(h/3)\sinh(h)\cos(h)] / (\cosh(h)^2 - \cos(h)^2) \end{aligned}$$

$$\begin{aligned} \text{Imaginary component} \quad & +V/l * (9/2) * (2\omega C/R)^{1/2} [-2\cosh(h)\sin(h)\cos(h/3)^2 \cosh(h/3)^2 + \cosh(h)\sin(h)\cos(h/3)^2 \\ & + \cosh(h)\sin(h)\cosh(h/3)^2 + 2\sinh(h/3)\cos(h/3)\cosh(h/3)\sin(h/3)\sinh(h)\cos(h) \\ & + 2\sinh(h)\cos(h)\cos(h/3)^2 \cosh(h/3)^2 - \sinh(h)\cos(h)\cos(h/3)^2 - \\ & \sinh(h)\cos(h)\cosh(h/3)^2 + 2\sinh(h/3)\cos(h/3)\cosh(h/3)\sin(h/3)\cosh(h)\sin(h)] / (\cosh(h)^2 - \cos(h)^2) \end{aligned}$$

(in order to obtain the measured voltage, we should multiply these values on the resistance of the cables, namely $1/i\omega C_{\text{cable}}$).

An expression for the current in the cell of Corbino geometry is

$$I = \frac{2wCV_{in}}{p} \frac{J_1\left(\frac{1+i}{\sqrt{2}} \frac{r_i}{d}\right)}{J_0\left(\frac{1+i}{\sqrt{2}} \frac{r_o}{d}\right)} \left[N_1\left(\frac{1+i}{\sqrt{2}} \frac{r_o}{d}\right) J_1\left(\frac{1+i}{\sqrt{2}} \frac{r_i}{d}\right) - J_1\left(\frac{1+i}{\sqrt{2}} \frac{r_o}{d}\right) N_1\left(\frac{1+i}{\sqrt{2}} \frac{r_i}{d}\right) \right] \quad (20)$$

where r_o and r_i are outer and inner radii of Corbino disk, respectively, and J_1 and N_1 are Bessel and Neumann function of the first order, respectively [Dam87]. (and, of course, if we write the real and imaginary part of signal it would be near the same big formula).

B.1.3 Our computations

Although it worth to mention, that for the rectangular geometry there is no paper available which considered the influence of edge (along the guard electrode) effects, we tried to measure and calculate the corresponding values of edge capacitance using our equivalent scheme. We used originally proposed by Sommer and Tanner [Som71] model as a basis and tried to recalculate it with additional parameters of our cell, Fig. B.2, which were measured.

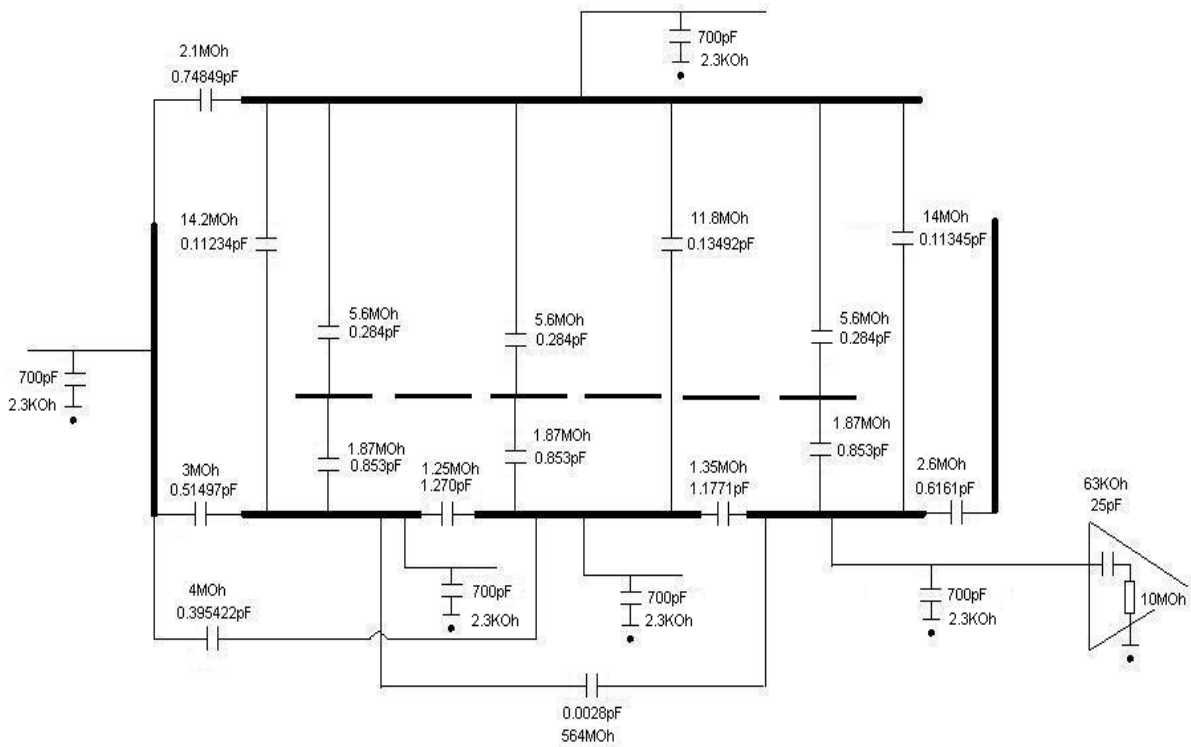


Fig. B.2 The characteristic impedances in the cell and its capacitance values for the frequency 100kHz. We usually denoted bottom left capacitor as 1, middle as 2 and right as 3. We applied signal to left capacitor (1) and pick up the signal at right one (3).

In order to calculate the resistance of electron layer from measured signal (for the scheme above) we should consider some simplifications otherwise recalculations becomes too difficult. First of all, all capacitances of the cables to ground are approximately 700pF (and corresponding resistance to ground 2.3kOhm). For typical measured resistances, 0.05-30MOhm, of electron layer, we could neglect this resistance and consider that electrodes are grounded. Special attention must be paid to two electrodes: excitation and pick-up ones. On pick-up electrode (number 3), we could not neglect capacitance of the cable, because it works as a “voltage divider” for the following high-ohmic Lock-In amplifier (see Fig B2). Cable capacitance at excitation electrode (number 1) we could neglect at all and we consider that our cable is absolute isolated from the ground. This simplification we can do, if we have good voltage source (that we have). In other words, voltage source tries to “keep” the necessary voltages, not

“looking” at all losses of signal to ground. In next approximation we can neglect the influence of guard electrode (guard “ring”). Capacitance between excitation and guard electrode is small (0.518pF) in comparison with the cable one (700pF), so it gives only small additional losses, but in any case, these losses are covered by voltage source, because he “keeps” voltages. We can neglect the influence of capacitance of guard electrode (0.516pF) to the third (pick-up) electrode. This only lightly increases capacitance of the third electrode to ground (700+0.5pF).

In our model we neglect “edge” capacitance, namely capacitance between electron layer and guard electrode. Calculation of this capacitance needs 3D calculation of electrical field profiles in the cell with rectangular geometry and need special attention in the future [Lea91]. We hope, that this capacitance does not influence much our results. One possible way to include this capacitance is to consider that our electrons do not cove all area of electrodes but only part of them (as usually done in lumped equivalent scheme, see the same Appendix, Chapter B.1.1).

After these simplifications, our equivalent scheme looks like on Fig. B.3 with the following system of equations.

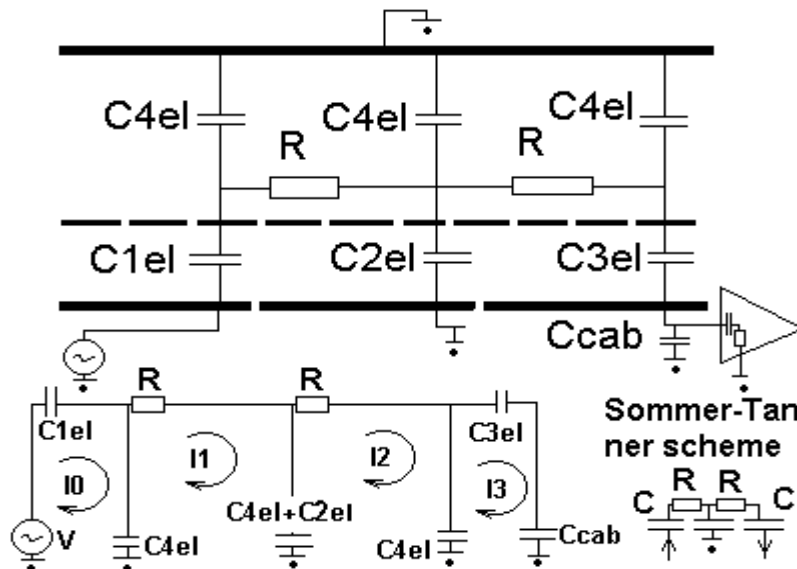


Figure. B.3 Our simplified scheme, Sommer-Tanner scheme and circuit scheme. Final voltage is measured on capacitor of cable (C_{cab}) and is $I3/(j*\omega*C_{cab})$.

For exact solution, the system of equations is:

$$\begin{aligned}
 & I_0 / (j \omega C_4 + j \omega C_1) + j I_1 / (\omega C_4) = V \\
 & -I_0 / (j \omega C_4) + I_1 / (j \omega C_4 + j \omega C_4 + j \omega C_2) + I_1 R - \\
 & I_2 / (j \omega C_4 + j \omega C_2) = 0 \\
 & -I_1 / (j \omega C_4 + j \omega C_2) + I_2 / (j \omega C_4 + j \omega C_4 + j \omega C_2) + I_2 R - \\
 & I_3 / (j \omega C_4) = 0 \\
 & -I_2 / (I \omega C_4) + I_3 / (I \omega C_4 + I \omega C_3 + I \omega C_{cab}) = 0
 \end{aligned}$$

the voltage that we measure is $I_3 / (j \omega C_{cab})$.

We used standard program Maple 6.0 for the solution

X-component of the signal is

$$\begin{aligned}
 x := & -V C_4^2 (4 C_4^4 + C_2^3 C_1 + 8 C_4^2 C_1 C_2 + 5 C_4 C_2^2 C_1 + 8 C_4^3 C_2 + 4 C_4^3 C_1 \\
 & + 5 C_4^2 C_2^2 + C_2^3 C_4) (C_4 + C_3 + C_{cab}) (6 R^2 \omega^2 C_4^5 C_2^3 + 13 R^2 \omega^2 C_4^6 C_2^2 \\
 & + 3 C_4^6 + R^2 \omega^2 C_4^4 C_2^4 - 6 C_4 C_2^3 C_1 C_3 - C_2^4 C_1 C_3 - C_2^4 C_1 C_{cab} \\
 & + 4 R^2 \omega^2 C_4^8 + 12 R^2 \omega^2 C_4^7 C_2 - 6 C_4 C_2^3 C_1 C_{cab} - 13 C_4^2 C_1 C_2^2 C_3 \\
 & - 13 C_4^2 C_1 C_2^2 C_{cab} - 5 C_4^2 C_2^3 C_1 - 12 C_4^3 C_1 C_2 C_3 - 12 C_4^3 C_1 C_2 C_{cab} \\
 & - C_2^4 C_4 C_3 - C_2^4 C_4 C_{cab} - 4 C_4^4 C_1 C_3 - 4 C_4^4 C_1 C_{cab} - 9 C_4^3 C_1 C_2^2 \\
 & - 5 C_4^2 C_2^3 C_3 - 5 C_4^2 C_2^3 C_{cab} - 7 C_4^4 C_2 C_3 - 7 C_4^4 C_2 C_{cab} - 9 C_4^3 C_2^2 C_3 \\
 & - 9 C_4^3 C_2^2 C_{cab} - 7 C_4^4 C_1 C_2 - C_2^4 C_1 C_4 - 2 C_4^5 C_3 - 2 C_4^5 C_{cab} \\
 & - 5 C_4^4 C_2^2 - 4 C_4^3 C_2^3 - 2 C_4^5 C_1 - C_2^4 C_4^2) / (((6 R^2 \omega^2 C_4^5 C_2^3 \\
 & + 13 R^2 \omega^2 C_4^6 C_2^2 + 3 C_4^6 + R^2 \omega^2 C_4^4 C_2^4 - 6 C_4 C_2^3 C_1 C_3 - C_2^4 C_1 C_3 \\
 & - C_2^4 C_1 C_{cab} + 4 R^2 \omega^2 C_4^8 + 12 R^2 \omega^2 C_4^7 C_2 - 6 C_4 C_2^3 C_1 C_{cab} \\
 & - 13 C_4^2 C_1 C_2^2 C_3 - 13 C_4^2 C_1 C_2^2 C_{cab} - 5 C_4^2 C_2^3 C_1 - 12 C_4^3 C_1 C_2 C_3 \\
 & - 12 C_4^3 C_1 C_2 C_{cab} - C_2^4 C_4 C_3 - C_2^4 C_4 C_{cab} - 4 C_4^4 C_1 C_3 - 4 C_4^4 C_1 C_{cab} \\
 & - 9 C_4^3 C_1 C_2^2 - 5 C_4^2 C_2^3 C_3 - 5 C_4^2 C_2^3 C_{cab} - 7 C_4^4 C_2 C_3 - 7 C_4^4 C_2 C_{cab} \\
 & - 9 C_4^3 C_2^2 C_3 - 9 C_4^3 C_2^2 C_{cab} - 7 C_4^4 C_1 C_2 - C_2^4 C_1 C_4 - 2 C_4^5 C_3 \\
 & - 2 C_4^5 C_{cab} - 5 C_4^4 C_2^2 - 4 C_4^3 C_2^3 - 2 C_4^5 C_1 - C_2^4 C_4^2)^2 + (\\
 & 13 R \omega C_4^4 C_2^2 C_{cab} + 18 R \omega C_4^5 C_2^2 + R \omega C_4^2 C_2^4 C_{cab} + R \omega C_4^2 C_2^4 C_3 \\
 & + 6 C_4^3 C_2^3 C_1 R \omega + C_2^4 C_1 R \omega C_4^2 + 4 R \omega C_4^6 C_3 + 4 R \omega C_4^6 C_{cab} \\
 & + 14 R \omega C_4^6 C_2 + 13 R \omega C_4^4 C_2^2 C_3 + 12 R \omega C_4^5 C_2 C_3 + 12 C_4^5 C_1 R \omega C_2 \\
 & + 13 C_4^4 C_1 R \omega C_2^2 + 12 R \omega C_4^5 C_2 C_{cab} + 6 R \omega C_4^3 C_2^3 C_3 + 4 C_4^6 C_1 R \omega \\
 & + 10 R \omega C_4^4 C_2^3 + 2 R \omega C_4^3 C_2^4 + 6 R \omega C_4^3 C_2^3 C_{cab} + 4 R \omega C_4^7)^2) C_{cab}
 \end{aligned}$$

and Y-component

$$\begin{aligned}
y := & V C4^2 (4 C4^4 + C2^3 C1 + 8 C4^2 C1 C2 + 5 C4 C2^2 C1 + 8 C4^3 C2 + 4 C4^3 C1 \\
& + 5 C4^2 C2^2 + C2^3 C4) (C4 + C3 + Ccab) (13 R \omega C4^4 C2^2 Ccab + 18 R \omega C4^5 C2^2 \\
& + R \omega C4^2 C2^4 Ccab + R \omega C4^2 C2^4 C3 + 6 C4^3 C2^3 C1 R \omega + C2^4 C1 R \omega C4^2 \\
& + 4 R \omega C4^6 C3 + 4 R \omega C4^6 Ccab + 14 R \omega C4^6 C2 + 13 R \omega C4^4 C2^2 C3 \\
& + 12 R \omega C4^5 C2 C3 + 12 C4^5 C1 R \omega C2 + 13 C4^4 C1 R \omega C2^2 \\
& + 12 R \omega C4^5 C2 Ccab + 6 R \omega C4^3 C2^3 C3 + 4 C4^6 C1 R \omega + 10 R \omega C4^4 C2^3 \\
& + 2 R \omega C4^3 C2^4 + 6 R \omega C4^3 C2^3 Ccab + 4 R \omega C4^7) / (((6 R^2 \omega^2 C4^5 C2^3 \\
& + 13 R^2 \omega^2 C4^6 C2^2 + 3 C4^6 + R^2 \omega^2 C4^4 C2^4 - 6 C4 C2^3 C1 C3 - C2^4 C1 C3 \\
& - C2^4 C1 Ccab + 4 R^2 \omega^2 C4^8 + 12 R^2 \omega^2 C4^7 C2 - 6 C4 C2^3 C1 Ccab \\
& - 13 C4^2 C1 C2^2 C3 - 13 C4^2 C1 C2^2 Ccab - 5 C4^2 C2^3 C1 - 12 C4^3 C1 C2 C3 \\
& - 12 C4^3 C1 C2 Ccab - C2^4 C4 C3 - C2^4 C4 Ccab - 4 C4^4 C1 C3 - 4 C4^4 C1 Ccab \\
& - 9 C4^3 C1 C2^2 - 5 C4^2 C2^3 C3 - 5 C4^2 C2^3 Ccab - 7 C4^4 C2 C3 - 7 C4^4 C2 Ccab \\
& - 9 C4^3 C2^2 C3 - 9 C4^3 C2^2 Ccab - 7 C4^4 C1 C2 - C2^4 C1 C4 - 2 C4^5 C3 \\
& - 2 C4^5 Ccab - 5 C4^4 C2^2 - 4 C4^3 C2^3 - 2 C4^5 C1 - C2^4 C4^2)^2 + (\\
& 13 R \omega C4^4 C2^2 Ccab + 18 R \omega C4^5 C2^2 + R \omega C4^2 C2^4 Ccab + R \omega C4^2 C2^4 C3 \\
& + 6 C4^3 C2^3 C1 R \omega + C2^4 C1 R \omega C4^2 + 4 R \omega C4^6 C3 + 4 R \omega C4^6 Ccab \\
& + 14 R \omega C4^6 C2 + 13 R \omega C4^4 C2^2 C3 + 12 R \omega C4^5 C2 C3 + 12 C4^5 C1 R \omega C2 \\
& + 13 C4^4 C1 R \omega C2^2 + 12 R \omega C4^5 C2 Ccab + 6 R \omega C4^3 C2^3 C3 + 4 C4^6 C1 R \omega \\
& + 10 R \omega C4^4 C2^3 + 2 R \omega C4^3 C2^4 + 6 R \omega C4^3 C2^3 Ccab + 4 R \omega C4^7)^2) Ccab)
\end{aligned}$$

This was the case, when we assumed, that capacitances of three bottom electrodes are different.

Solution looks simpler if we consider that three capacitances C1, C2 and C3 are equal (by the other words, we do not consider changing of electron density at the boundary, we simply consider, that electrons cover all surfaces of electrode and recalling, that physical dimensions of all three bottom electrodes are equal).

For simplicity we denote the following:

$$A=Ccab/C4, \quad B=C1/C4, \quad D=C1\omega R, \quad E=C4\omega R$$

$$\text{And } F=[4+12B+13B^2+6B^3+B^4]*(1+A+B)$$

$$G=6AB^2D+13ABD+12AD+AB^3D+42BD+22D+2B^4D+4AE+14B^3D+36B^2D+4E$$

$$H=-23B^2+B^2D^2+6BD^2-4B+13D^2+12DE+4E^2-2A-7AB^4-34B^3-21AB^2-AB^5-B^6-11AB-8B^5-24B^2-18AB^3+3$$

Then the final X-component of signal is $+V \cdot A^{-1} \cdot F \cdot H / (G^2 + H^2)$

And Y-component of signal is $-V \cdot A^{-1} \cdot F \cdot G / (G^2 + H^2)$

We also note, that as X as well as Y-components are linear on excitation voltage (that greatly simplifies recalculation of our measurements with different excitation voltages).

In our calculations of resistance R we used measured signal and then we adjusted resistance to fit the theoretical curve.

B.1.4 Comparison of different models for resistance recalculation

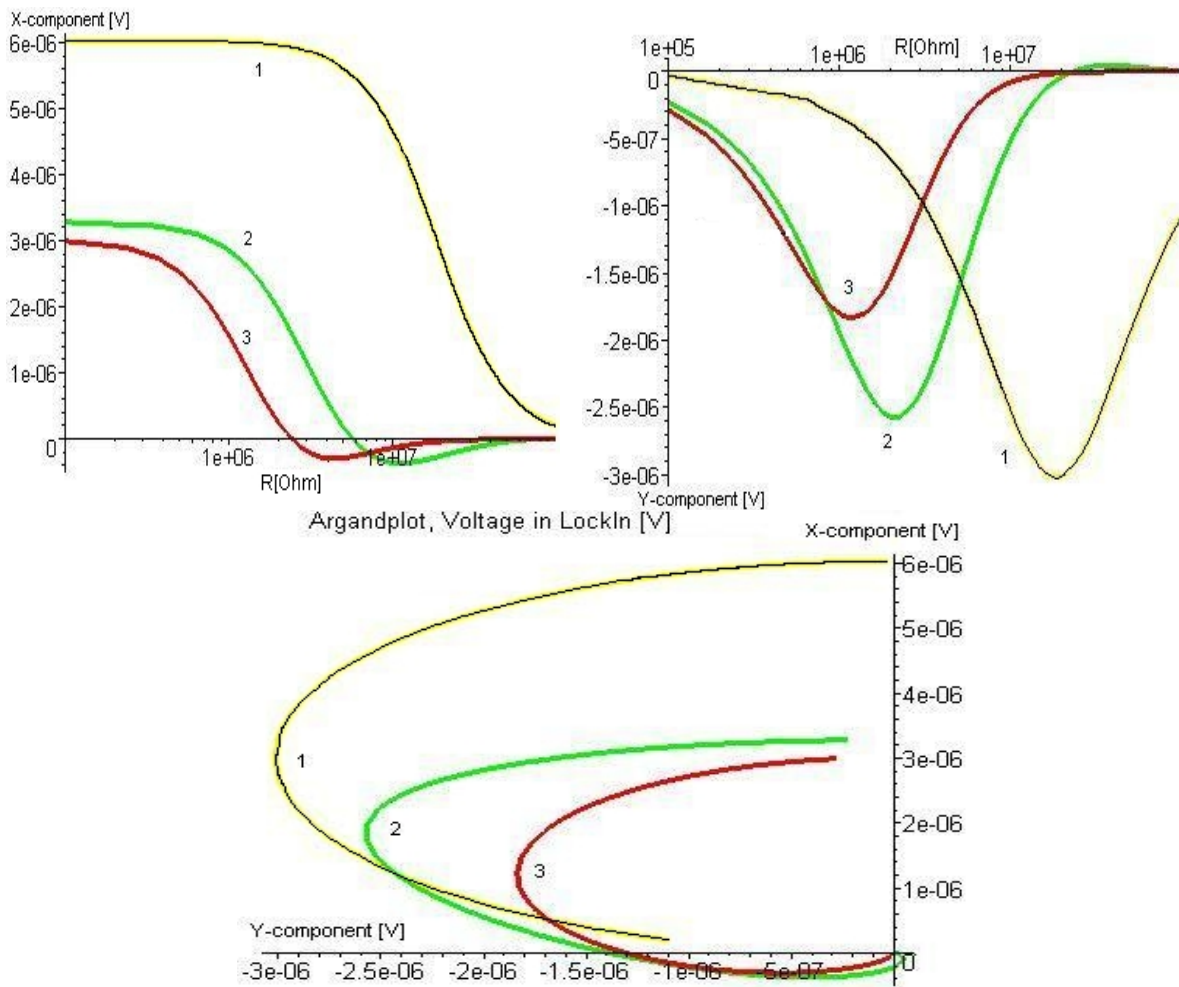


Fig. B.4 Comparison of different models: 1- lumped equivalent scheme, 2- transmission line model, 3-our calculation. Upper-left figure – X-component of the signal, upper-right – Y-component of the signal, bottom plot – Argand plot.

As it can be seen in Fig. B.4 there is not much difference between our calculation and the results of the transmission line model (difference is very big comparison with lumped equivalent scheme, but in any case, an equivalent lumped scheme is valid in the range of resistances below 2M Ω). The difference in absolute voltages is within 10% in the maximum and minimum for the x-component and does not exceed 40% for the minimum in the y-component (difference in Y component we attribute to fact, that in our equivalent scheme we included all parasitic capacitances between measuring electrode and top and guard electrode). Once we consider the same voltages in the x and y components for our and transmission line models, differences in resistances differs maximum by a factor of 2.5-3 times (in our calculation resistances are smaller). Therefore we can consider that our model (our recalculations of signal to resistance) could be quite similar to previously done by transmission line model ([Lea 91, Lea 93]) and difference in absolute values would not be worse than a factor of 3.

B.1.5 Resistance of electron layer as a complex value

In some our measurements we observed that for low temperatures below 300mK, our signal deviates from expected one (X component of signal should be constant, Y one should be zero). This can be seen, for example, on Fig. F2, F5, Appendix F. This behavior cannot be explained by the model, assuming the resistance of electron layer as pure resistive (no imaginary component).

So, we assume that imaginary component of signal, jZ , should be included in the resistance of electron layer, $R+jZ$, and we obtain the following formulas for X and Y components of signal (we also assume that electrons completely cover surface of electrodes).

For simplicity we denote the following (the same definitions as in Chapter B.1.3):

$$A=Cc_{ab}/C^4, \quad B=C_1/C^4, \quad D=C_1\omega R, \quad E=C^4\omega R \quad K=Z/R$$

$$\text{And } F=[4+12B+13B^2+6B^3+B^4]*(1+A+B)$$

$$H=-23B^2+B^2D^2+6BD^2-4B+13D^2+12DE+4E^2-2A-7AB^4-34B^3-21AB^2-AB^5-B^6-11AB-8B^5-24B^2-18AB^3+3$$

$$G=6AB^2D+13ABD+12AD+AB^3D+42BD+22D+2B^4D+4AE+14B^3D+36B^2D+4E$$

$$M=-H+12ADK+13ABDK+6AB^2DK+AB^3DK+B^2D^2K^2+22DK+42BDK+36B^2DK+14B^3DK+2B^4DK+4AEK+12DEK^2+13D^2K^2+6BD^2K^2+4EK+4E^2K^2$$

$$N=-G-2B^2D^2K-12BD^2K-8E^2K-24EDK-26D^2K$$

Then the final X-component of signal is $-V*A^{-1}*F*G/(M^2+N^2)$

And Y-component of signal is $+V*A^{-1}*F*N/(M^2+N^2)$

And X and Z component of signal are plotted on the figure below.

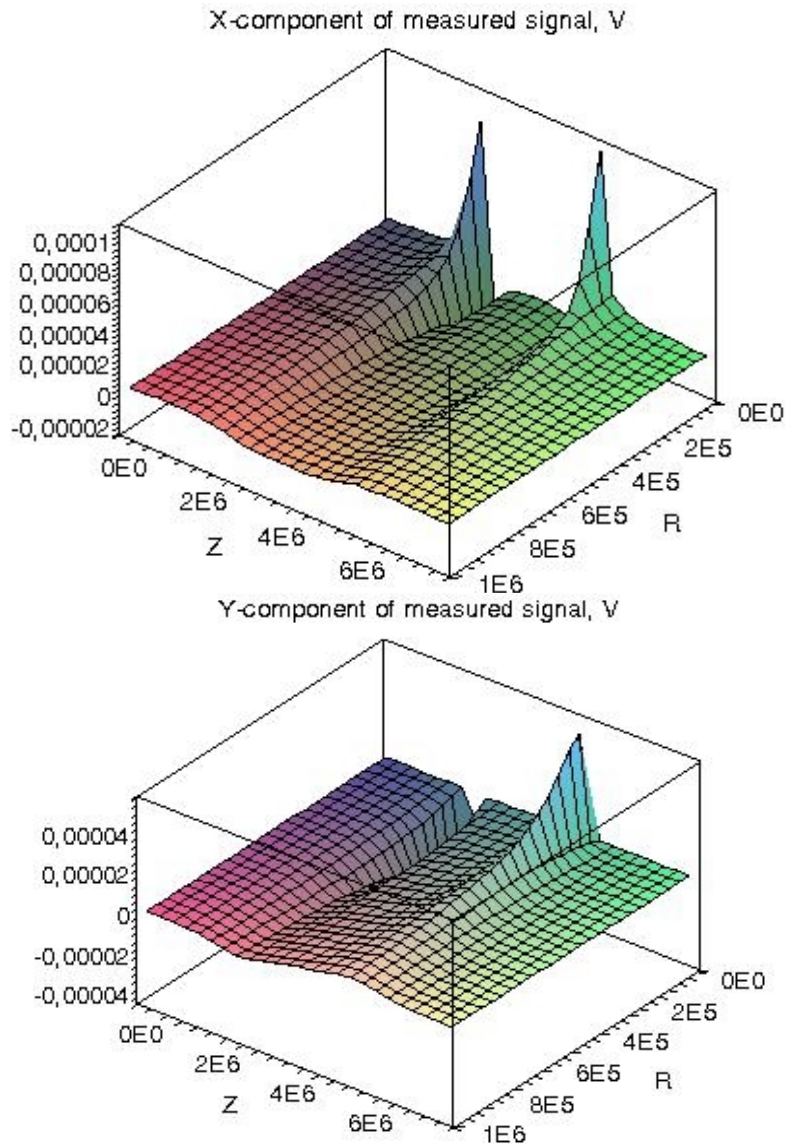


Fig. B.5 *X and Y components (Volt) of measured signal. (In calculations it was assumed, that electrons cover all surface of three bottom electrodes). We noted R as a real part of resistance of electron layer, and Z as a imaginary part of resistance of electron layer*

For example, measurement for 0.2mm He film, Chapter 5.2, Fig. 5.4 #1 and also Appendix F, Fig. F.2, for temperature below 300mK could be explained, if we assume an appearance of imaginary component of $-200\text{K}\Omega$, see figure below.

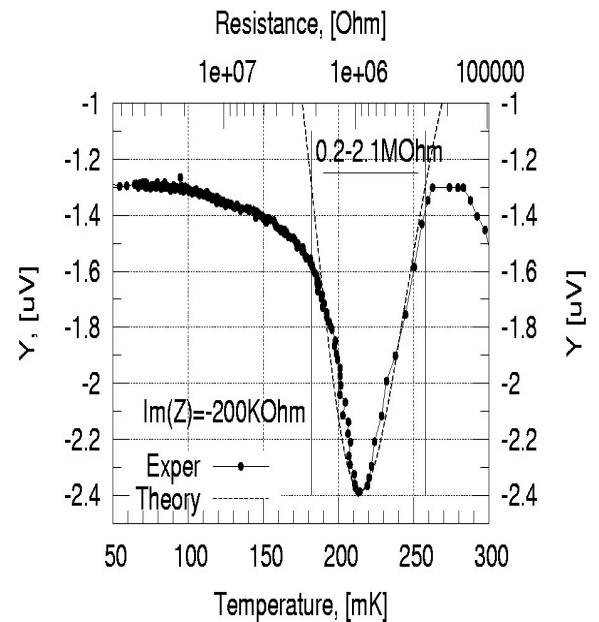
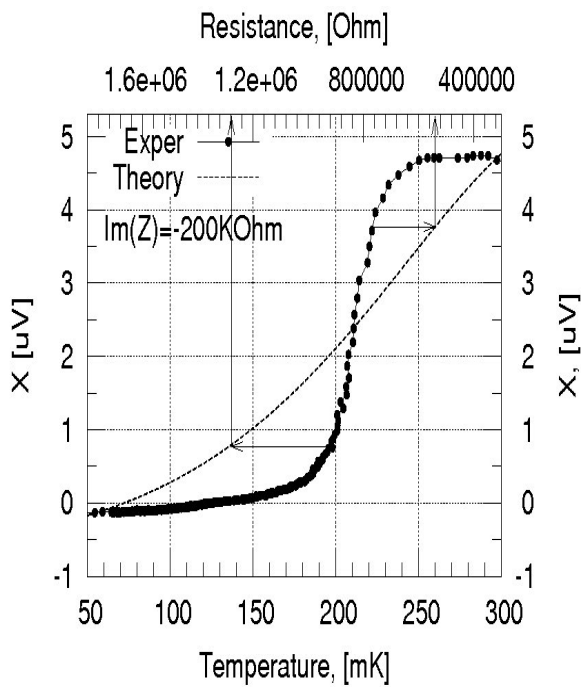
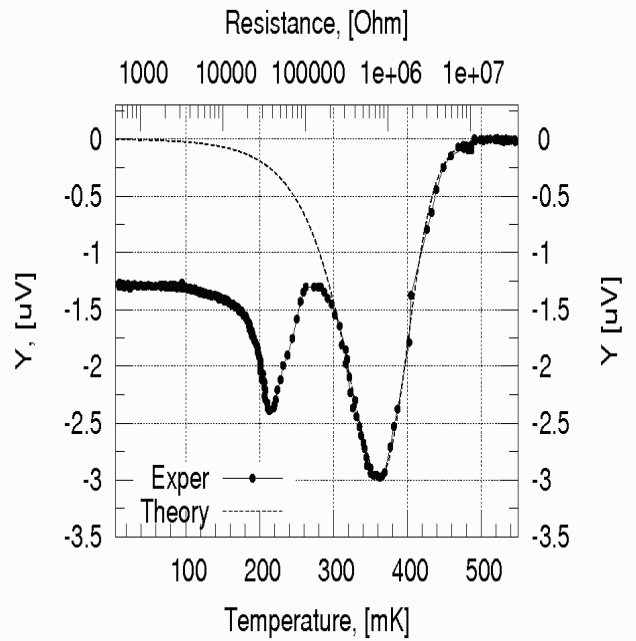
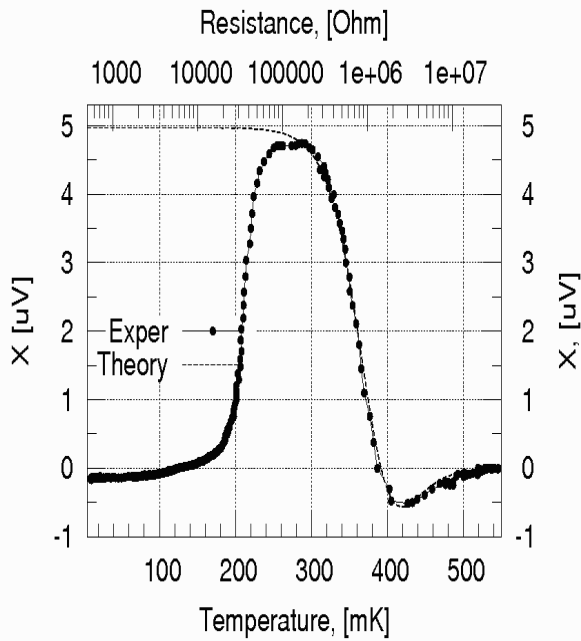


Fig. B.6 Left top and bottom – X component of experimental and theoretical curves. Right top and bottom – Y ones. In high temperature range (above 300mK), resistance can be explained as having pure resistive part (top scale is exponential except for the down left picture), in low temperature range, below 250mK, an imaginary component of resistance occurs (-200KW) and resistance changes in the range 0.3-1.8MW

On Fig. B.6 top and bottom, we can see, that for temperature region above 300mK, our experimental data could be explained, assuming , that resistance of electron layer is pure resistive (we also note, that during this measurement, our dilution unit was quite stable in the range 450-550mK and we observed power law dependence of resistivity in this temperature).

On the other side, if we assume, that in temperature region 250-300mK, imaginary component of resistance of electron layer appears, namely, $-200\text{K}\Omega$, then we can explain low temperature (below 250mK) behavior, see figure above, bottom left and right. Resistance changes in the range 0.3-1.8M Ω (real part, imaginary part is fixed at the value of $-200\text{K}\Omega$) and shows no more exponential behavior. Final dependence of resistance on the temperature is presented on the Fig. 5.4, #1.

Here we would like also to note, that in order to explain our low temperature part we tried to adjust real and imaginary parts of resistance of electron layer, and for example signal can be explained assuming the imaginary part as a constant ($-200\text{K}\Omega$) and than varying only R, real part of resistance. For this plot there are other possibilities to fit the experimental curve, varying real as well as imaginary part of resistance (and accordingly, dependence of resistance on temperature could be different). So, in our opinion, it is difficult to say about exact power low dependence of resistance of electron layer on temperature.

To summarize, we can say, that if our experimental data are not explained by the simple assumption, that resistance of electron layer is pure resistive than we should assume, that imaginary component of resistance is also present. Though, then, exact power low of resistance of electron layer on temperature is difficult to determine, due to several possibilities of adjusting of real and imaginary parts of resistance of electron layer.

B.2 Qualitative analysis of our cell

As the next step we can consider our cell with different film thickness for our equivalent scheme.

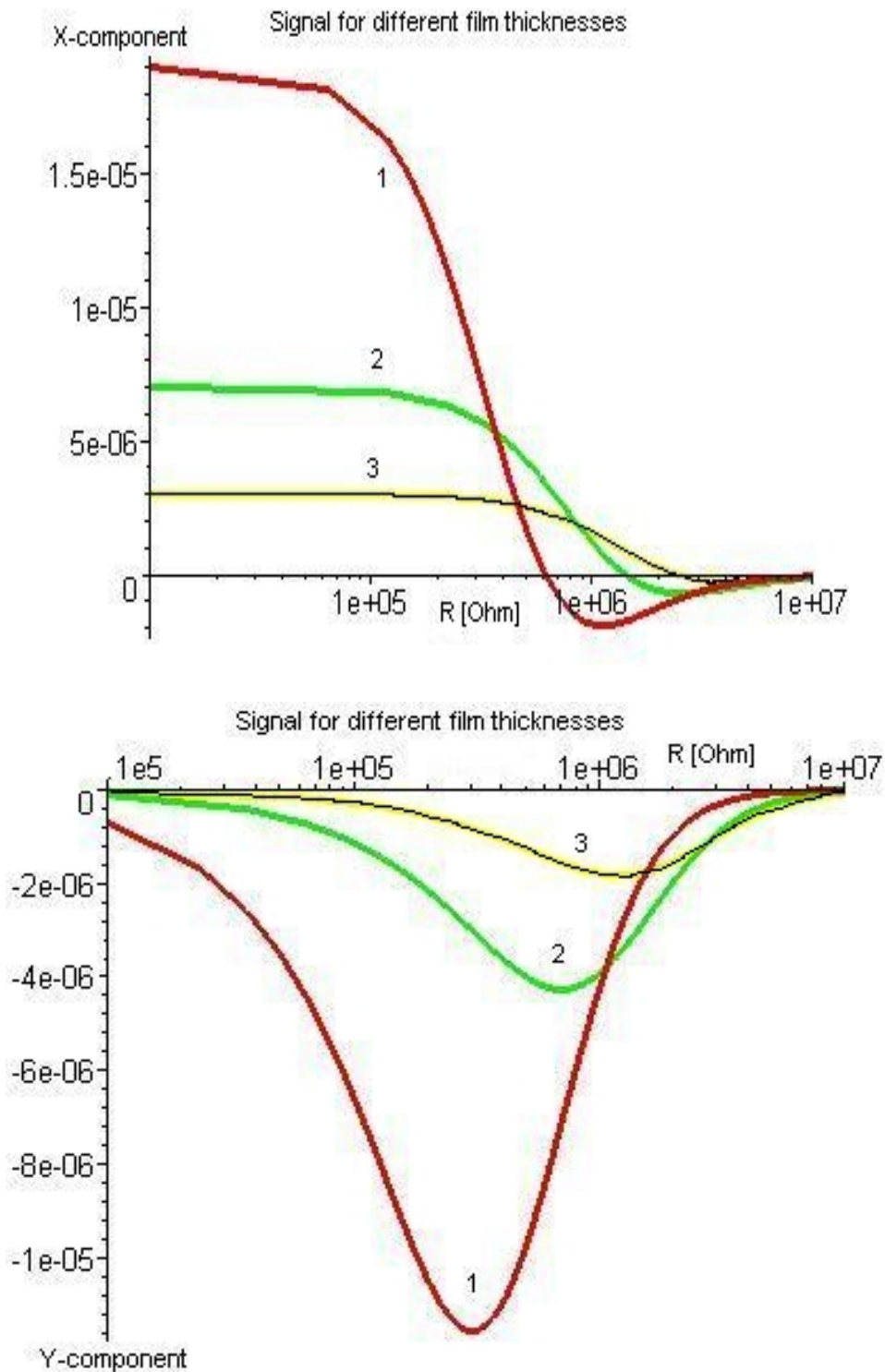


Fig. B.7 Comparison of cell sensitivity for different helium film thicknesses, Top – X-component of the signal, bottom - Y-component of the signal. 1-0.2mm, 2-0.5mm, 3-1.0mm, measurement from two opposite electrodes.

Table 3. *Qualitative comparison of our cell with different film thicknesses.*

	0.2mm		0.5mm		1mm	
	X	Y	X	Y	X	Y
Absolute voltages, in maximum	19.0 μV	11.5 μV	7.02 μV	4.27 μV	3.01 μV	1.84 μV
Resistance value in maximum, in Y-component.	-	0.31 $\text{M}\Omega$	-	0.70 $\text{M}\Omega$	-	1.20 $\text{M}\Omega$
For low resistances, value, at which cell is not sensitive (changes are less then 10% from maximum or minimum)	0.097 $\text{M}\Omega$	0.016 $\text{M}\Omega$	0.224 $\text{M}\Omega$	0.038 $\text{M}\Omega$	0.384 $\text{M}\Omega$	0.064 $\text{M}\Omega$
For high resistances, value, at which cell is not sensitive (changes are less then 10% from maximum or minimum)	6.0 $\text{M}\Omega$	1.86 $\text{M}\Omega$	3.8 $\text{M}\Omega$	4.27 $\text{M}\Omega$	23.6 $\text{M}\Omega$	7.3 $\text{M}\Omega$
Useful range, 10-90% of resistance changes, $\text{M}\Omega$	0.097 -6.0	0.016 -1.86	0.224 -13.8	0.038 -4.27	0.384 -23.6	0.064 -7.3

On Fig. B.7 and Table 3 we can see calculated signal for three different thicknesses: 0.2mm, 0.5mm and 1.0mm.

As we can see (Table 3), a decrease in a helium film thickness leads to the higher voltage measured and increased sensitivity in low resistances range.

We can calculate and compare how good our theoretical model fits experimental data basing on the measurements with different film thickness. If we take maximum value of experimental data for x-component for different film thicknesses 1.0mm:0.5mm:0.2mm 1:2.05:6.97 (we took maximum of x-component of 1mm film thickness as unity) and compare to the theoretical curve 1:2.39:6.31 we can see that our experimental data are within 15% of theoretical curves (Fig. B.13).

We also found that for our geometry (and for circular also) signal changes only within 10% (gets higher) if we increase distance between electron layer and top electrode from 3.0 to 6.0mm (which is quite understandable, because capacitive losses of signal to top electrode becomes smaller). So, distance from electron layer to top electrode is not critical.

A next very important parameter is the boundary layer between the guard electrode and electrons' layer. The electron density in this layer changes from zero to maximum (for convenience we can take as a boundary a position at which the electron layer density is half of maximum). To find this boundary one has to solve static task with fixed potentials at all electrodes (for this calculation we can neglect the excitation voltages). This is standard task for 2D geometry (but only for 2D, for 3D it is still not solved) and we used program written by group of Juergen Klier (University of Konstanz) for x-z plane.

For example, on Fig. B.8, We can see density profile in the cell (Annemarie Valkering, University of Konstanz, where U_t – voltage on the top electrode, U_g - voltage on the guard electrode).

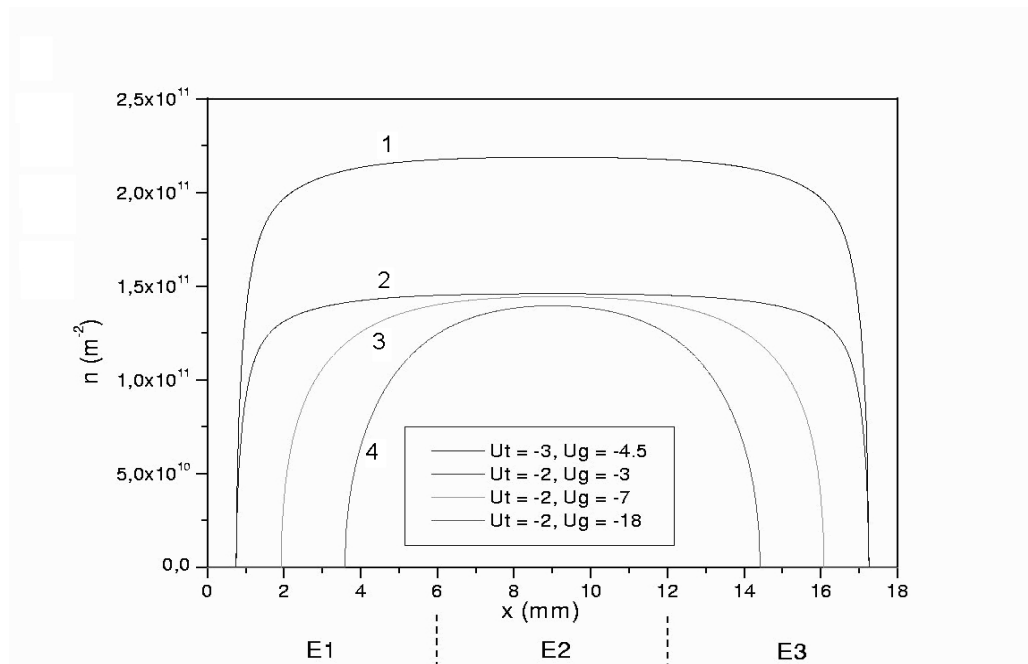


Fig. B.8 Typical density profile in the cell. 1- $U_{top} -3V$, $U_{gate} -4.5V$; 2 - $U_{top} -2V$, $U_{gate} -3V$; 3 - $U_{top} -2V$, $U_{gate} -7V$; 4 - $U_{top} -2V$, $U_{gate} -18V$

Then we can define the effective capacitance between the electron layer and the upper and lower electrodes (it is convenient to normalize it to the maximal possible capacitance, when there is no boundary layer, the density is constant everywhere).

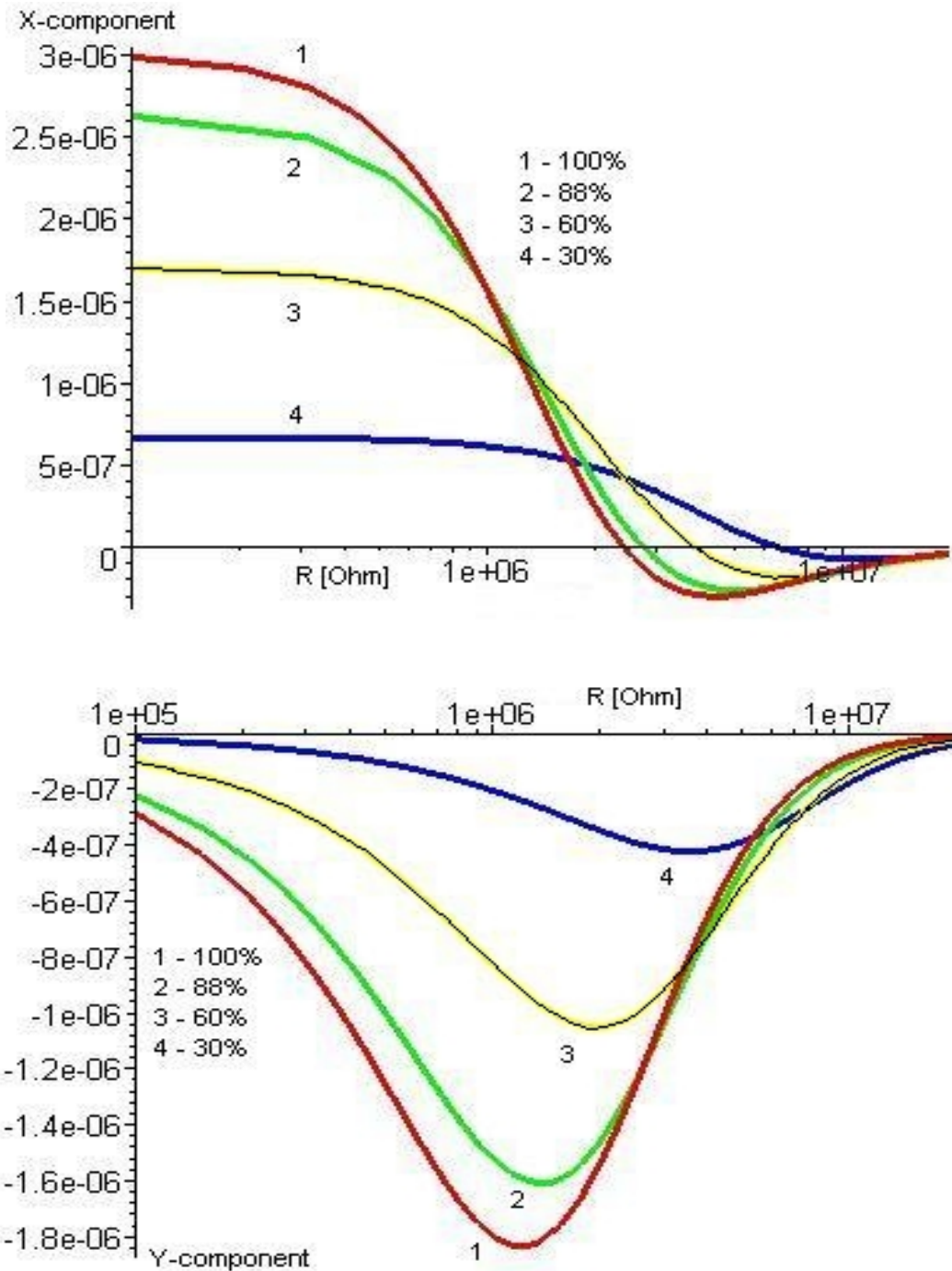


Fig B.9 Comparison of cell sensitivity for different percentage of electron layer. 100% - all electrodes are covered with electron layer, other percentages - electrons cover partly the electrodes. Top - X-component, bottom - Y-component. 1-100%, 2-88%, 3-60%, 4-30%, measurement from two opposite electrodes.

Table 4. *Quantitative comparison of cell with different percentages of electron layer.*

	100%		88%		60%		30%	
	X	Y	X	Y	X	Y	X	Y
Absolute voltages, in maximum	3.01 μV	1.84 μV	2.64 μV	1.61 μV	1.70 μV	1.05 μV	0.67 μV	0.42 μV
Res. value in max., in Y-component.	-	1.20 $\text{M}\Omega$	-	1.36 $\text{M}\Omega$	-	1.95 $\text{M}\Omega$	-	3.57 $\text{M}\Omega$
For low resistanc., value, at which cell is not sensitive (changes are less than 10% from max. or minimum)	0.384 $\text{M}\Omega$	0.064 $\text{M}\Omega$	0.434 $\text{M}\Omega$	0.073 $\text{M}\Omega$	0.632 $\text{M}\Omega$	0.105 $\text{M}\Omega$	1.40 $\text{M}\Omega$	0.197 $\text{M}\Omega$
For high resistanc., value, at which cell is not sensitive (changes are less than 10% from max. or minimum)	23.6 $\text{M}\Omega$	7.3 $\text{M}\Omega$	26.7 $\text{M}\Omega$	8.30 $\text{M}\Omega$	36.6 $\text{M}\Omega$	11.5 $\text{M}\Omega$	58.4 $\text{M}\Omega$	19.3 $\text{M}\Omega$
Useful range, 10-90% of resistance changes, $\text{M}\Omega$	0.384 - 23.6	0.064 - 7.3	0.434 - 26.7	0.073 - 8.30	0.632 - 36.6	0.105 - 11.5	1.40- 58.4	0.197 - 19.3

We can note (Table 4 and Fig. B.9) that decreasing of capacitance (electrons do not cover all surface of electrodes) leads to shifting of our measured signal to higher resistance values (so, we can measure higher resistances) and lower amplitudes of signal.

The same analysis is applicable to our measurement with two adjust electrodes. We do not present whole analysis for two adjust electrodes (#2 and #3) we would like only to point out that it is very similar to three electrodes measurement (#1 and #3), the biggest difference – we do not have negative voltage on x-component of signal.

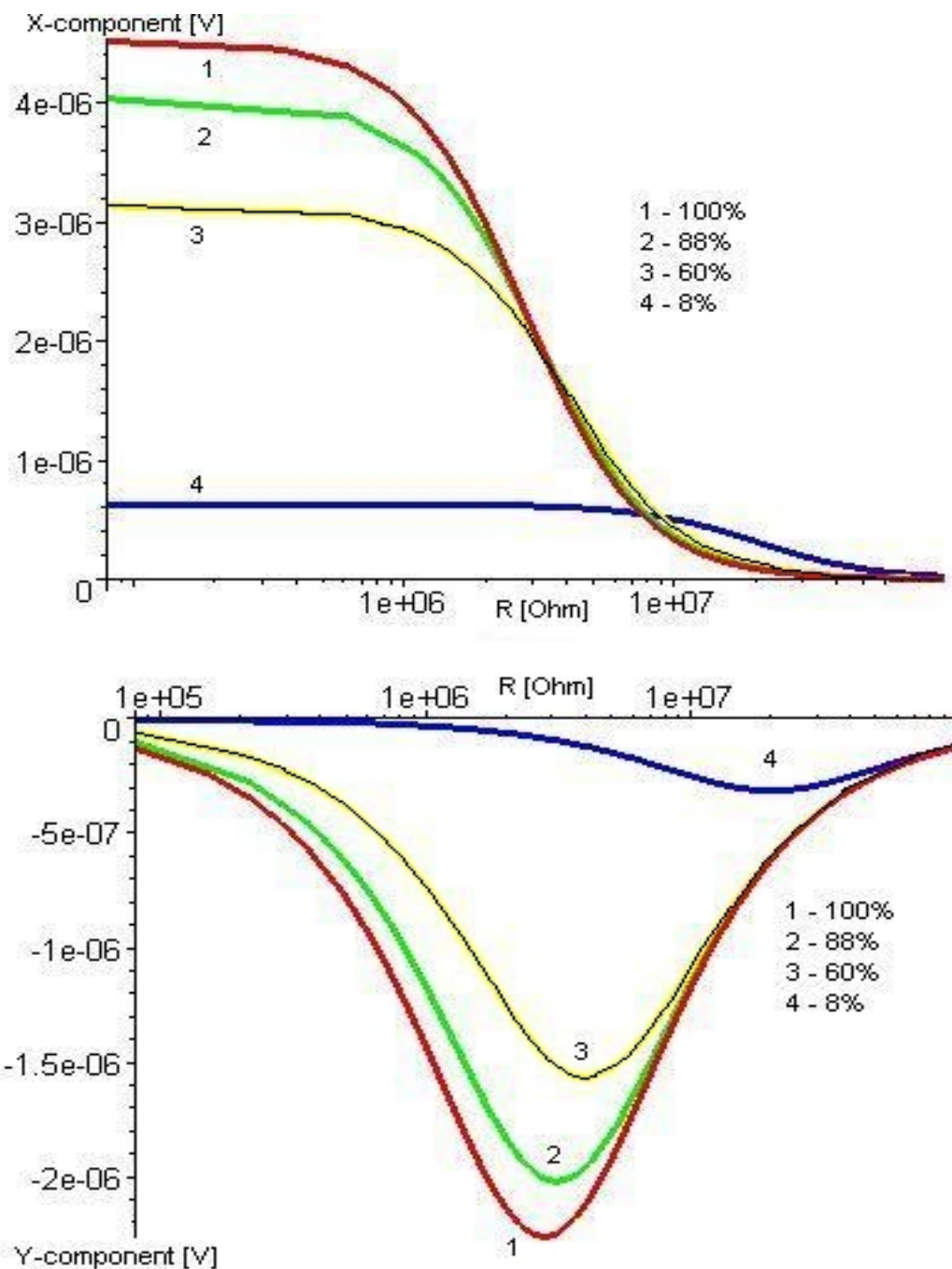


Fig. B.10 Comparison of sensitivity of cell with measurements of two adjacent electrodes. 100% - all electrodes are covered with electron layer, other percentages - electrons cover partly electrodes. 1-100%, 2-88%, 3-60%, 4-8%.

Next critical question could be the absolute value (and sometimes even power law) of obtained resistances. Deviation of experimental curve from theoretical one, Fig. B.11, B.12 and B.13 could be big (sometimes even an order of

magnitude, Fig. B.11) and further explanation or, maybe, even better model should be done.

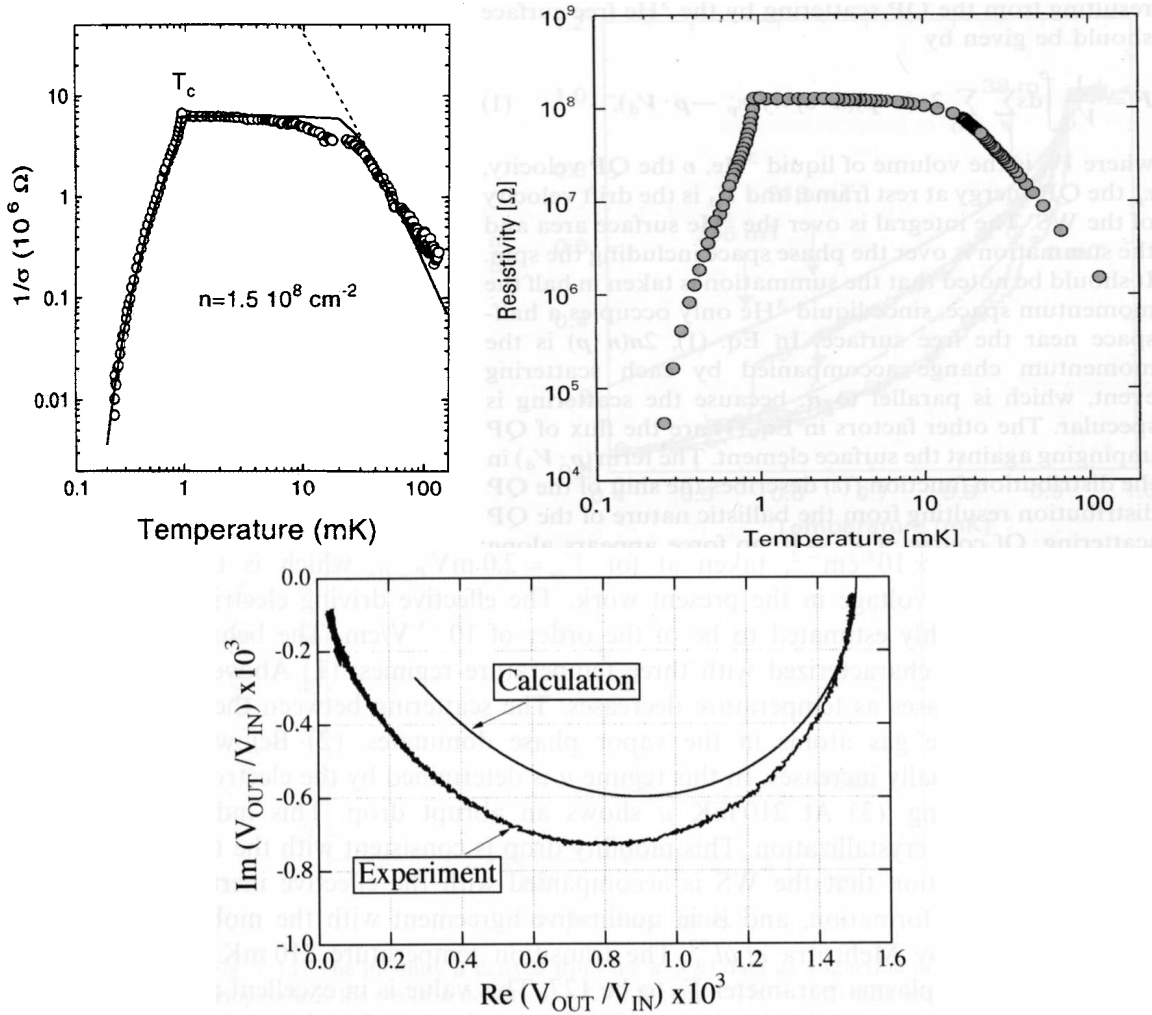


Fig. B.11 Comparison (top left and right) of measured resistances. Electron density is the same $1.5 \cdot 10^8 \text{ cm}^{-2}$, the only pressing fields are different. Left [Mon98], $E=135\text{V/cm}$, right [Kon00], $E=488\text{V/cm}$, down adjustment of experimental data to theoretical curve in order to obtain resistances [Sh95, Shir96].

On the Fig. B.12, we can see a theoretical curve (transmission line model) and the experimental data for rectangular geometry (Sommer-Tanner).

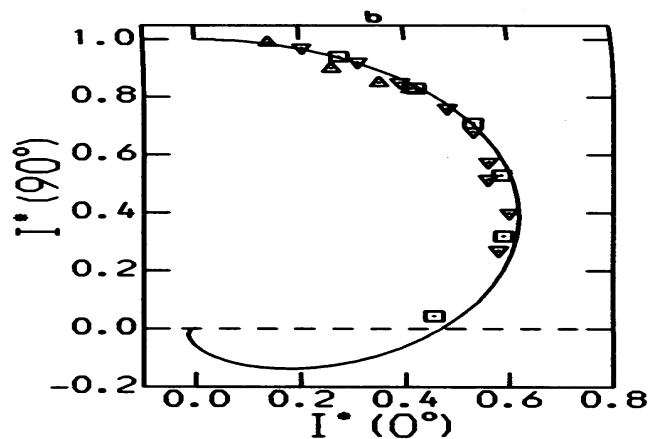


Fig. B.12 Comparison of measured signal and theoretical curves (transmission line model) for rectangular geometry (Sommer-Tanner scheme) [Lea91]

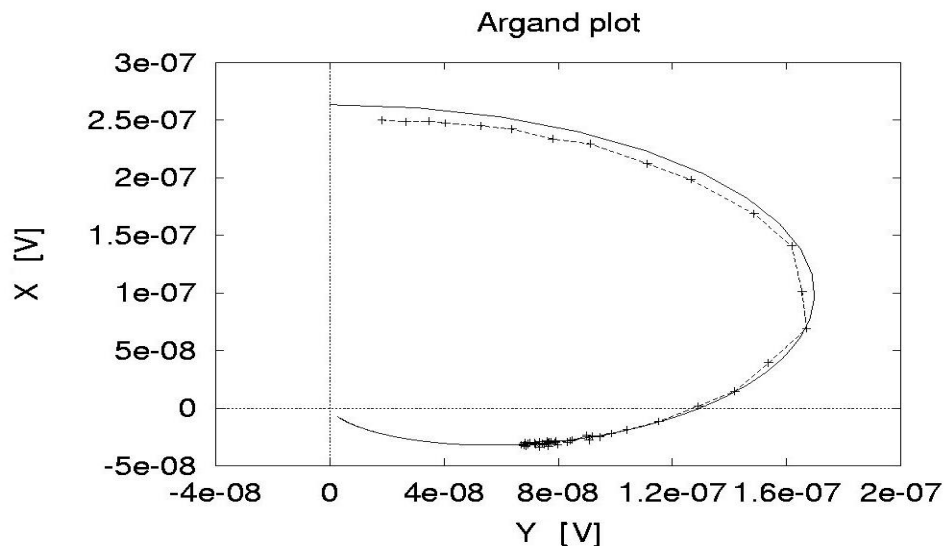


Fig. B.13 Comparison of our measured signal and theoretical curves (improved Sommer-Tanner model using our equivalent scheme). In comparison with fig. B.4 we inverted imaginary component (Y) of signal.

On Fig. B.13 we presented typical our adjusting curves.

To conclusion: deviation between measured signal and theoretical curves (for circular geometry – K. Kono’ measurement using transmission line model; for rectangular geometry – M. Lea’s measurements using transmission line model, and our rectangular geometry using our improved equivalent scheme) can be large (and nonlinear!) and the improved or new model of recalculation of measured signal to resistance values is necessary.

Appendix C

Description of the cell

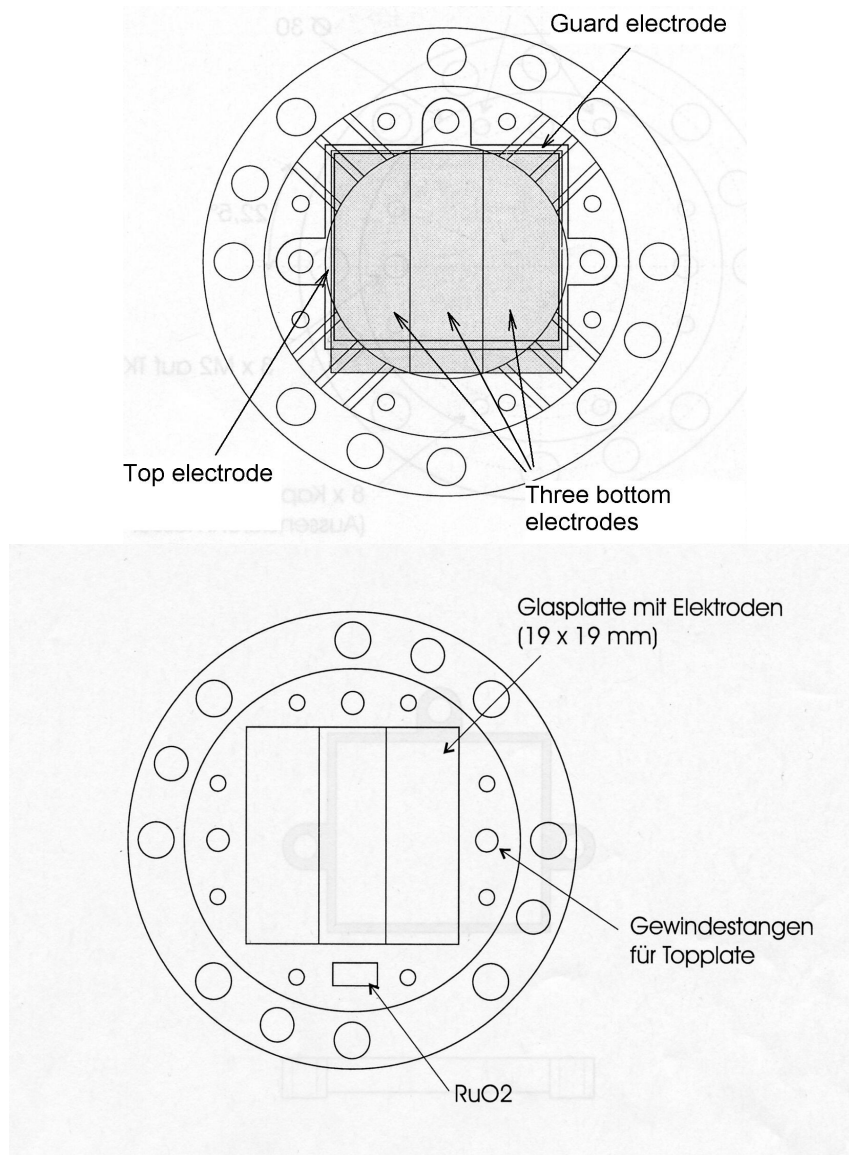


Fig. C1. Real view of the cell (see also Fig. 3.2). Top electrode is round and does not cover all area of three bottom electrodes.

Appendix D

Observed instability

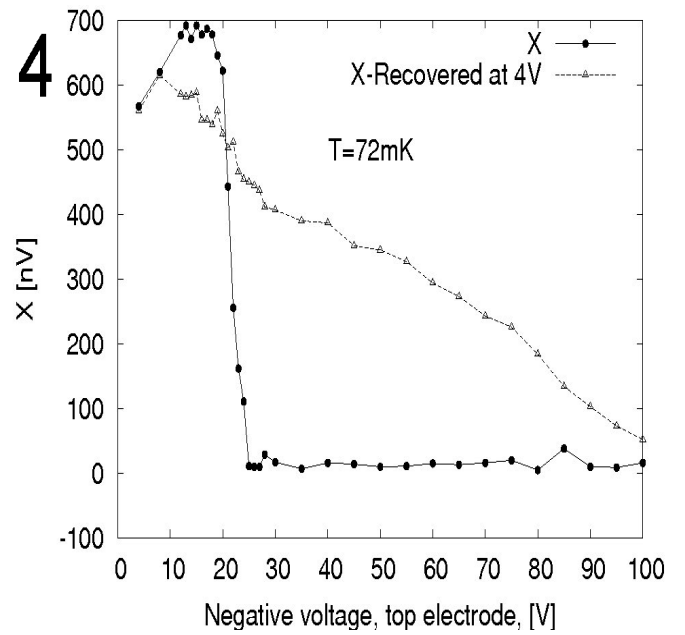
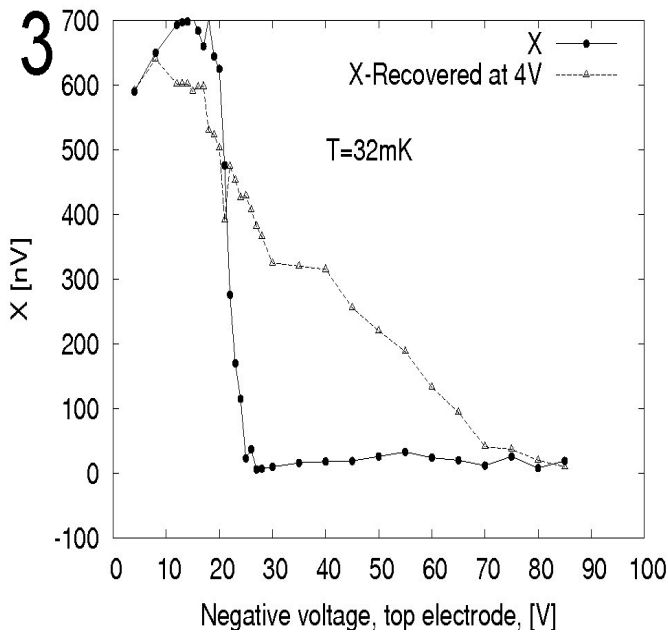
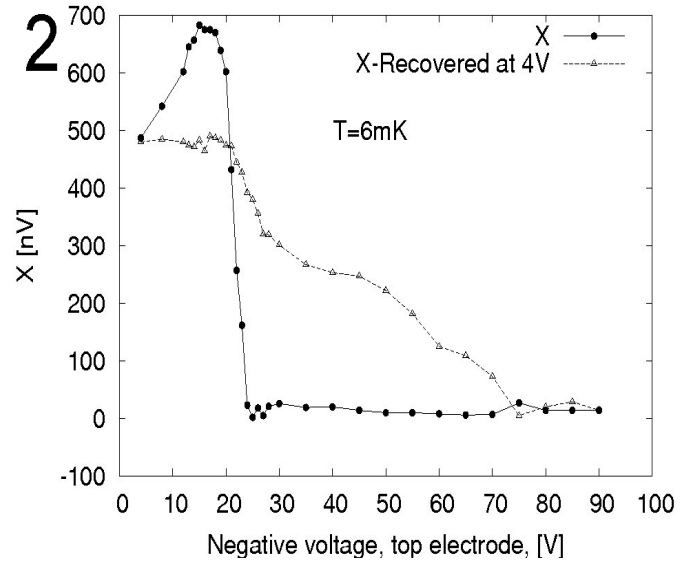
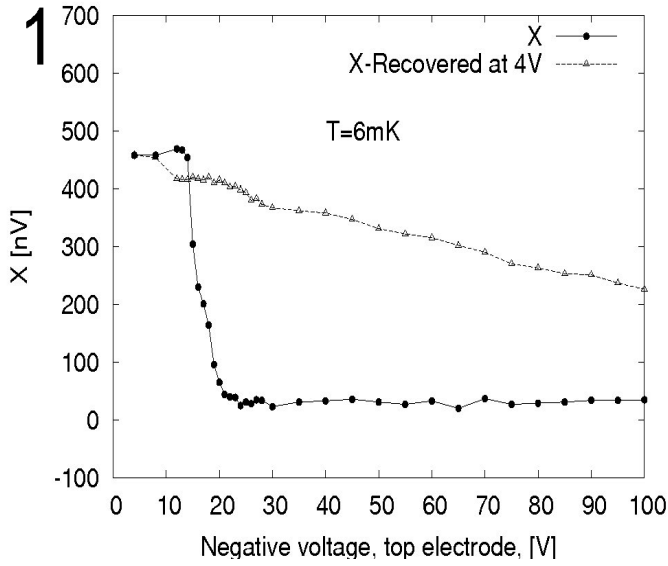
We also performed measurements with high pressing electrical field (top electrode) from -4V (-10V/cm) up to -100V (-250V/cm). A sweep in the field was done in the following way: In one step we increased negative voltage, then again, in one step, voltage was decreased to -4V , then voltage was again increased to the next negative value and again decreased to -4V and so on. Three bottom electrodes were at zero potential and voltage at the guard electrode was -6V . The initial (after the loading) density was $7.3(\pm 15\%)10^6\text{electrons/cm}^2$. In the Fig D1 and D2 the same Appendix D we plotted the x-component of signal (except for the 480mK), because it was more sensitive than y-component at these temperatures.

The measurements were carried out in two days. First the measurement at high temperatures (above 250mK) were performed followed by the measurements at lower temperatures (below 250mK) where we observed recovered signal (signal was fully or partly recovered after applying more than -20V (-50V/cm)). After these measurements there was a brake of 4 hours during which no parameters were changed. Next, the measurements at lower temperatures (where we did not observed recovered signal) were done once more (Please, see data in Fig. D1 and D2, where for each temperature, we plotted one curve for signal at high negative voltage and another curve for the recovered signal at -4V after this high voltage. So, for each pressing voltage we had two characteristic points: the signal corresponding to this voltage and signal, at -4V , but recovered after applying this high negative voltage). So, for high temperatures we observed that signal (electrons) disappeared at $19\text{-}21\text{V}$ and never came back. For lower temperature (below 250mK) we had two sets of data: the signal could totally disappear at $19\text{-}21\text{V}$ or signal could be partly recovered. We would like also to notice that recovering of signal was observed even during the measurement of whole sweep (usual measurements when

temperature was changed from 5 till 500mK). For example, we loaded electrons and made two sweeps one with -4V and second with -15V on top electrode and the signal was present. Then we applied -30V and during the sweep we had not observed any signal. Decreasing of voltage to -10V recovered the signal and we again measured the signal in the whole temperature region. We repeated such kind of measurements once more for another electron concentration, for the -8V , -12V on top electrode (signal was present), -20V (no signal) and -4V (signal was present again). As we can see there was a principal difference between these two data sets. We interpreted this as following: starting from -20V (or Field -50V/cm) we squeeze the electrons that were in the center of electrode to the helium surface (and dimple was increased), resistance of these electrons became very high so that we did not see any conductivity. The conductivity can be small and non-zero due to the electrons that were near the edge of the guard electrode, where electric pressing field was not so high. For some reasons, we lost electrons that were in this boundary layer near the guard electrode (though it is worth to mention that our fields were not so strong to make a helium bubble with electrons inside, which can move to the bottom electrode and annihilate or it is hardly possible that electrons moved to the guard electrode). As a next step we removed a high field and accordingly electrons moved from the center to the boundary (and now density became lower). Next negative applied voltage did not influence the electrons near to the center, whereas the electrons near the boundary disappeared. The procedure was repeated till all electrons were lost.

To check this hypothesis attempting to explain, why there were two different behaviors at low (below 250mK) temperature, we made two tests: (i) fast (less than one hour) and slow (five-six hours) cool-down and then measurements, and (ii) a fast cool-down and then either we measured immediately or after waiting several hours. Our results was that this behavior did not depend on the prehistory – whether we had a fast or slow cool-down or whether we waited

several hours before the measurements. Therefore, we considered it as an intrinsic, not yet completely understood property of the system.



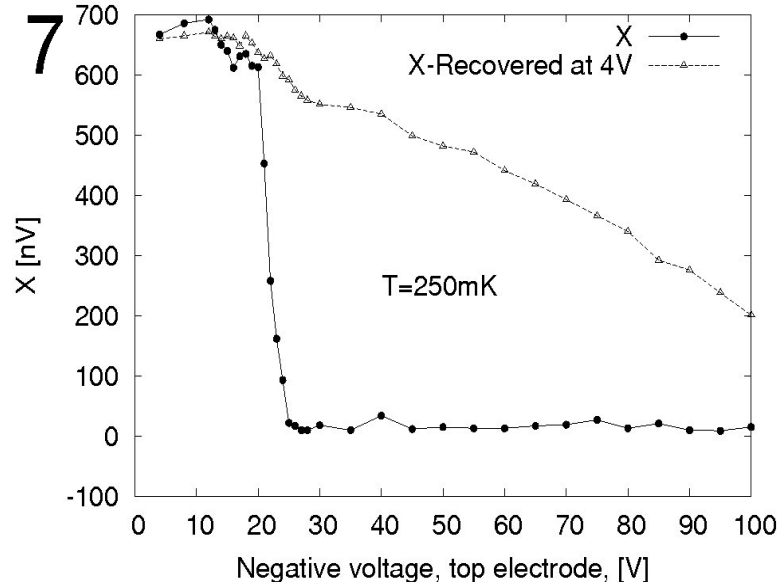
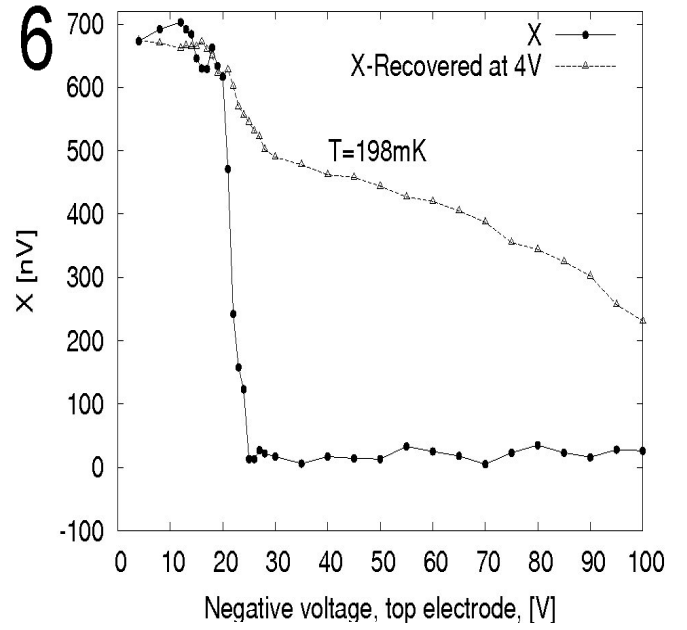
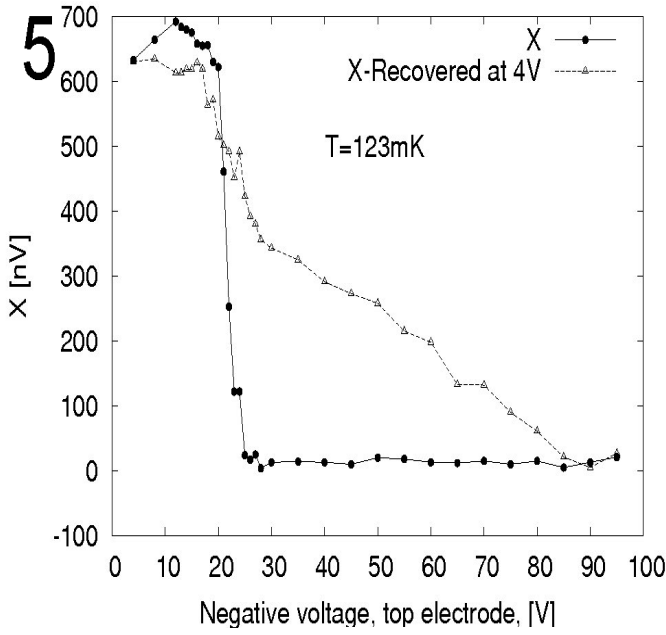
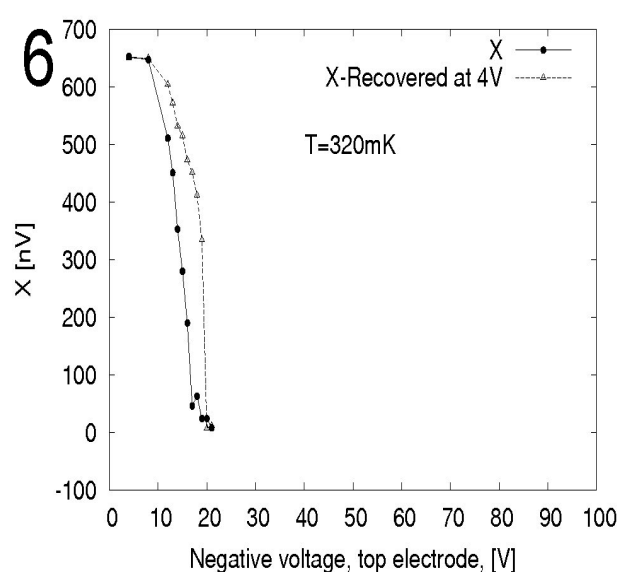
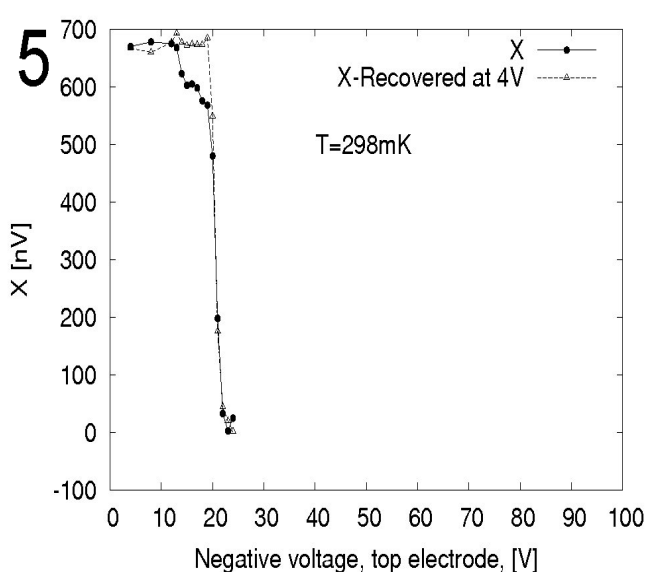
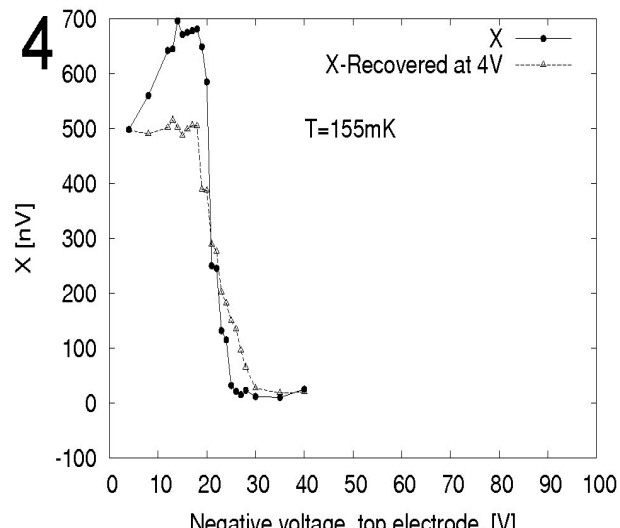
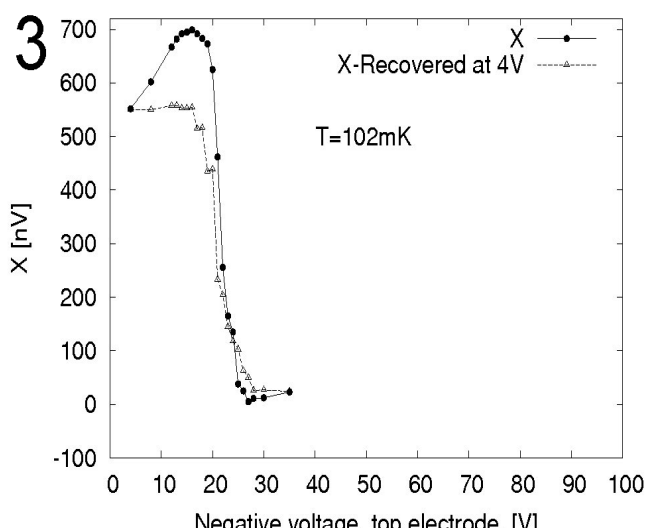
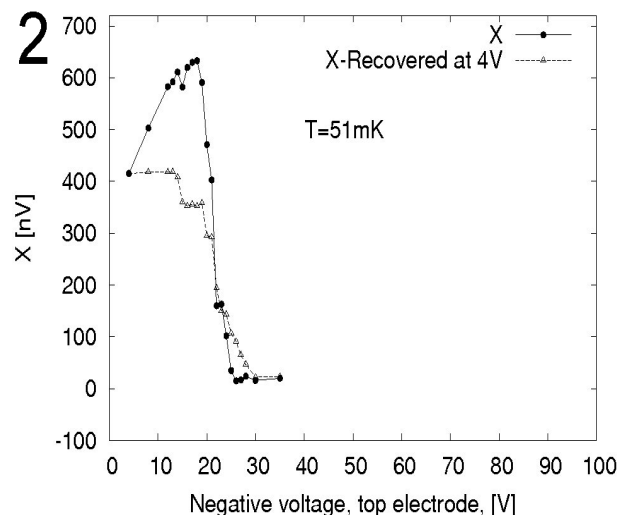
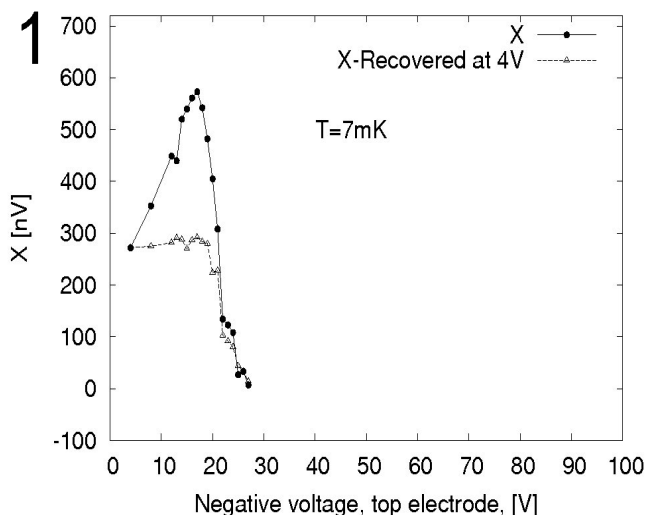


Fig. D.1 *X*-component of signal versus different negative voltages on the top electrode. Electrons were loaded at 300mK and initial signal 660nV, frequency 100kHz. 1 – 6mK, 2-6mK, 3-32mK, 4-72mK, 5-123mK, 6-198mK, 7-250mK. Voltage on the guard electrode $-6V$, initial (after loading) density at 300mK - $7.3 \cdot 10^6$ electrons/cm². For each temperature, we plotted one curve for signal at high negative voltage and another curve for the recovered signal at $-4V$ after this high voltage.



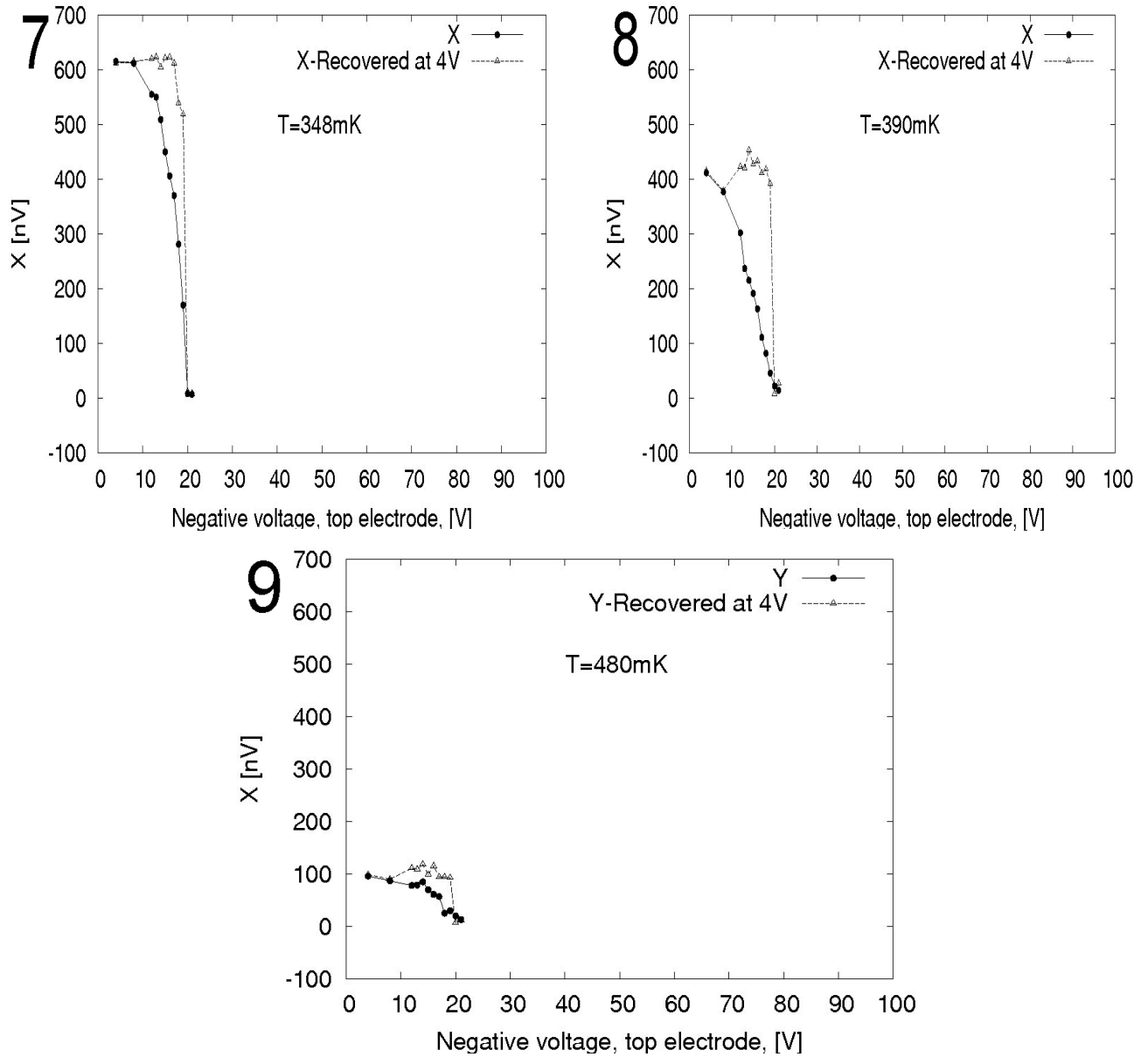


Fig. D.2 X-component of signal versus different negative voltages on the top electrode. Electrons were loaded at 300mK and initial signal 660nV, frequency 100kHz. 1 – 7mK, 2-51mK, 3-102mK, 4-155mK, 5-298mK, 6-320mK, 7-348mK, 8-390mK, 9-480mK. Voltage on the guard electrode –6V, initial (after loading) density at 300mK - $7.3 \cdot 10^6$ electrons/cm². For each temperature, we plotted one curve for signal at high negative voltage and another curve for the recovered signal at –4V after this high voltage.

Appendix E

Wigner solid phase

If we consider several our measurements, that were not explained with simple model, which considered electron scattering as only real part of resistance than we can not explain whole our data. Although qualitatively our data could be explained as we consider also imaginary part of resistance of electron layer.

Including imaginary part should be explained, at least qualitatively.

We consider an assumption, that at the moment, when imaginary part of resistance started play a role, we could have Wigner crystallization.

This assumption was used by Kimitoshi Kono et all [Shir96]. In his measurements for ^4He he used another method for obtaining of resistance and mobility. For each point he used sweep in magnetic field, and assuming that Drude formula worked, he was able to obtain mobility and electron concentration independently. Though he had found that in the Wigner Solid phase, resistance (or conductivity) did not obey the Drude formula. To obtain resistance (or conductivity) he fitted the signal with formula $R = a_0 + a_1 B + a_2 B^2$, where B – magnetic field, R – resistance of electron layer, a_1 , adjusting parameter. He also suggested, that mobility obtained in Wigner solid phase with the help of Drude formula was not physically meaningful. Furthermore, he noted that the transport was not Ohmic in the Wigner solid phase.

We did not observe abrupt jump in Wigner Solid transition (as K Kono) but it could be explained either, that we had less homogeneous electron density distribution inside the cell: in center it could be maximal concentration (and Wigner solid transition started earlier) and along the boundary concentration could be smaller and accordingly Wigner solid transition at lower temperatures or we do not have coupling between electrons and helium surface. If we look at

the published experimental data (Fig.2.2) we can notice, that mobility decrease during the Wigner solid crystallization transition was 2-3 times in absolute value and after that mobility smoothly decreased. We also observed smooth decrease of mobility (increase of resistance), for example on Fig. F2 #3, F2 #5, F5 #1, F5 #3, Appendix F.

Then next question could be of concentration of electrons.

It could be also possible that our determination of electron concentration for 0.2 and 0.5mm helium film was not right (unfortunately, we checked electron densities only for 1.0 mm film thickness, see also Chapter 4.1). Probably, our standard method for determination of electron concentration (loading till saturation of signal, so concentration was determined by voltage on the top electrode during the loading) was not valid for smaller films as 1.0mm (group in Uni Konstanz, Prof. Paul Leiderer, Juergen Klier had similar problems with determination of electron concentration, but it is necessary to mention, that they worked with film thicknesses usually much less than 0.1mm, Juergen Klier, private communication). One possibility to determine electron concentration would be measurement in magnetic field, if we assume that Drude formula valid (as K. Kono did, but we would like also to point out again, that K. Kono claimed that Drude formula was not valid in Wigner Solid phase) and than we could separately determine electron concentration and mobility.

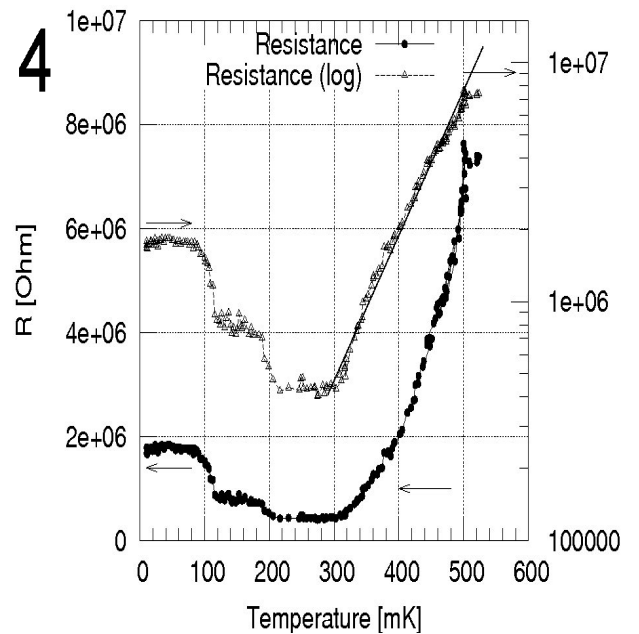
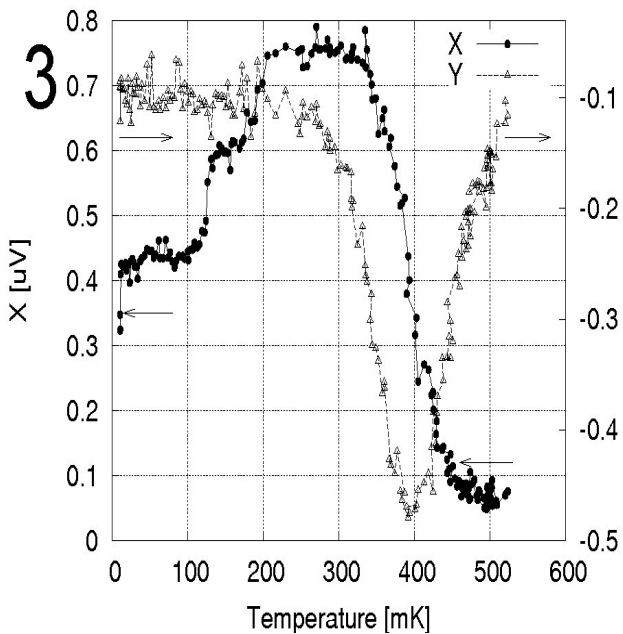
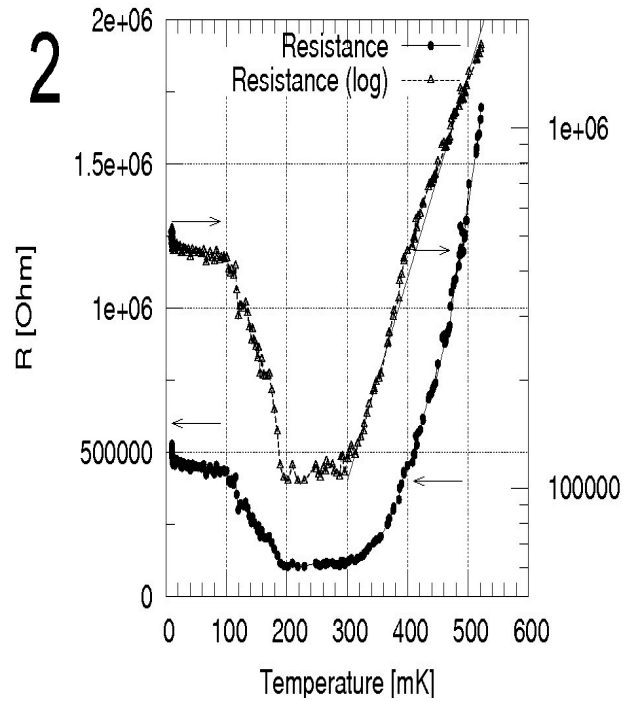
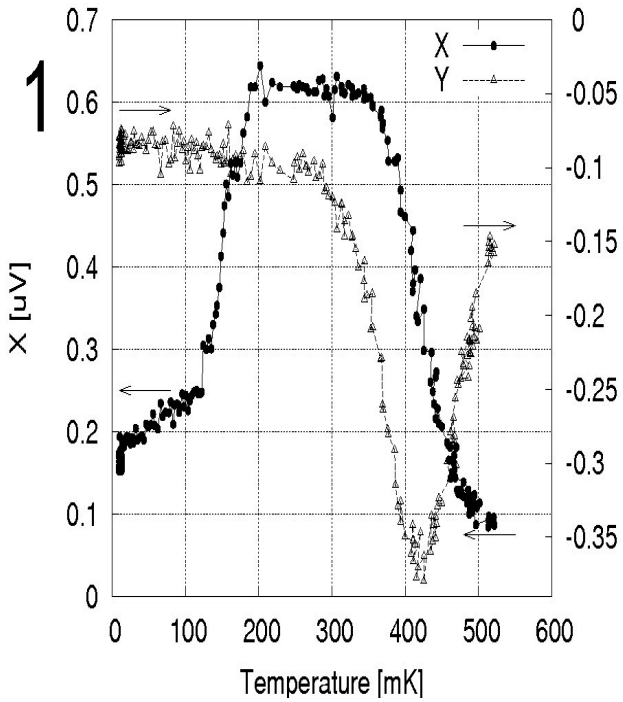
We would like to note, that all these consideration applied to the measurements of 0.2mm helium film thickness and to 0.5mm one. For 1.0mm film we did not observed any anomalous behavior of signal (by the other word, signal (or mobility) could be explained, assuming that resistance of electron layer was pure resistive).

So, from our measurements we cannot conclude that we have observed Wigner crystallization.

Appendix F

Original Data (X and Y Components)

F.1 Some our additional measurements (data for the Chapter 5.1)



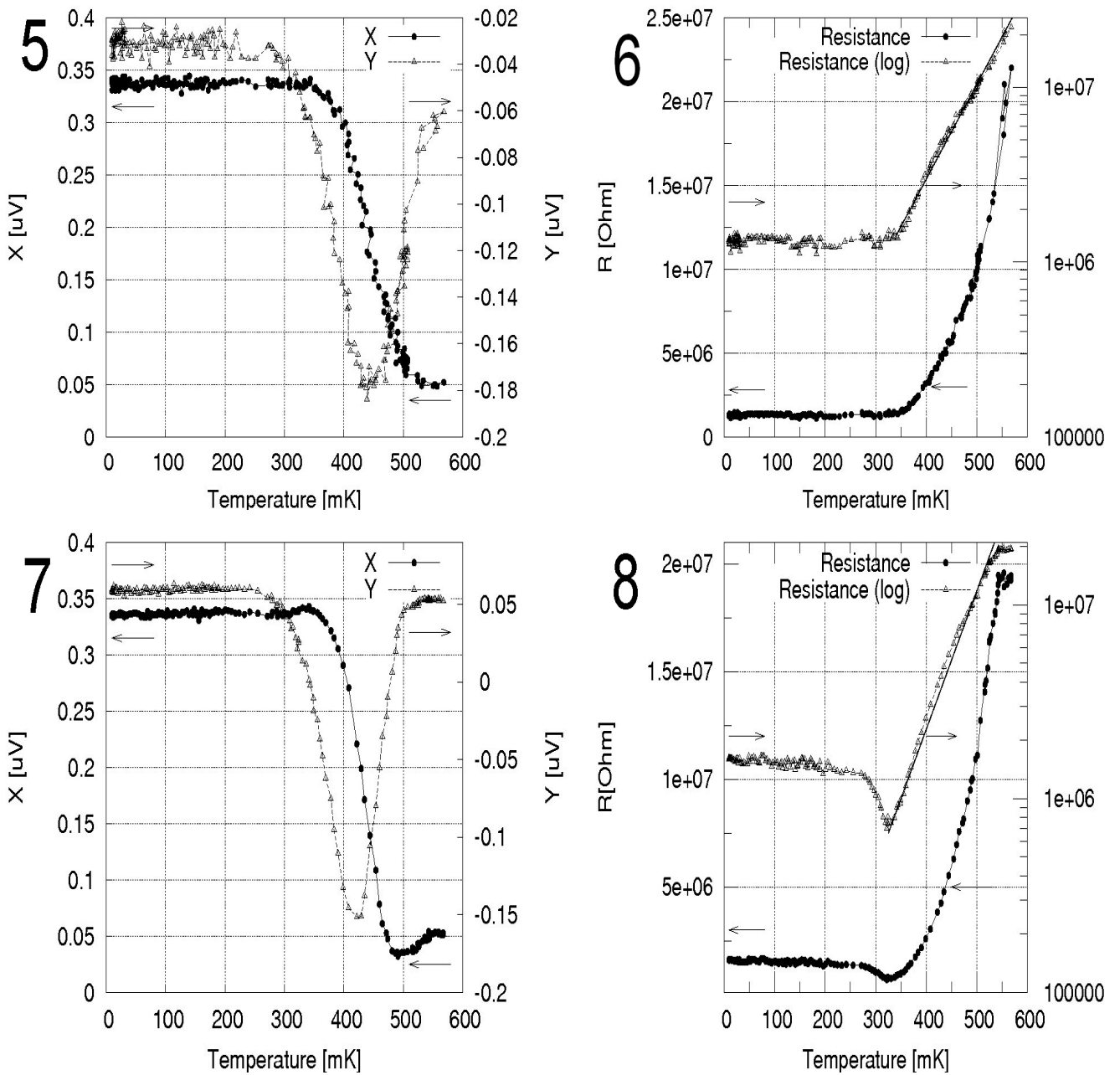
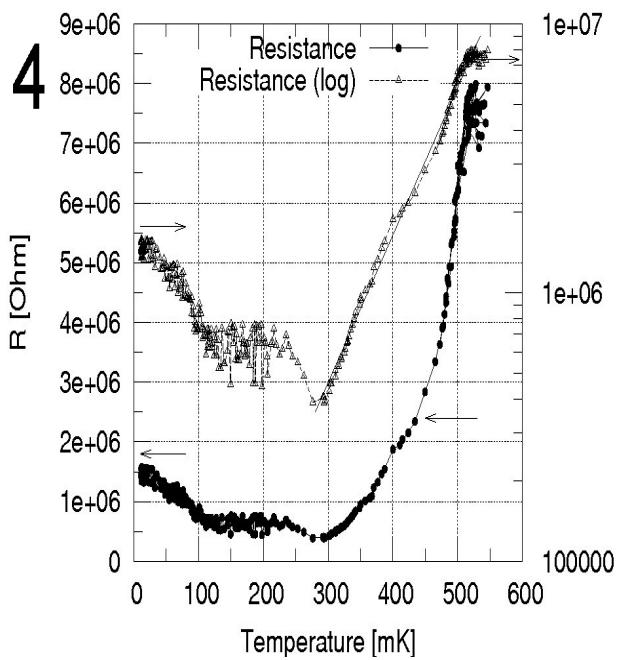
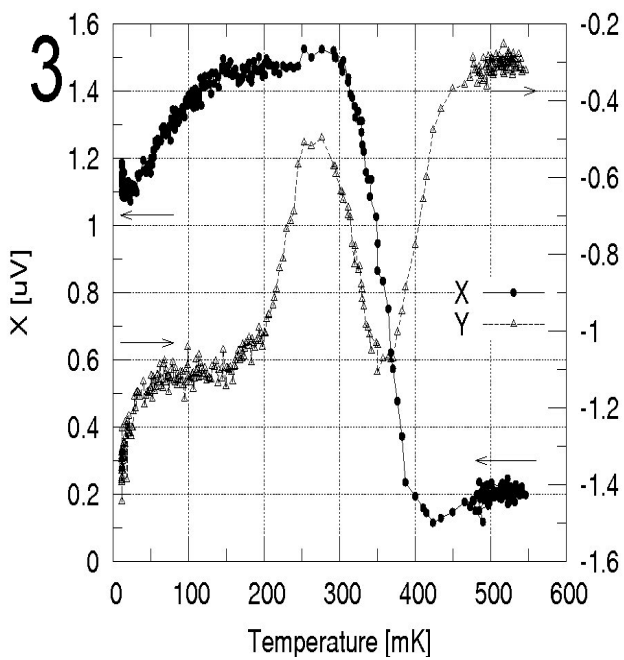
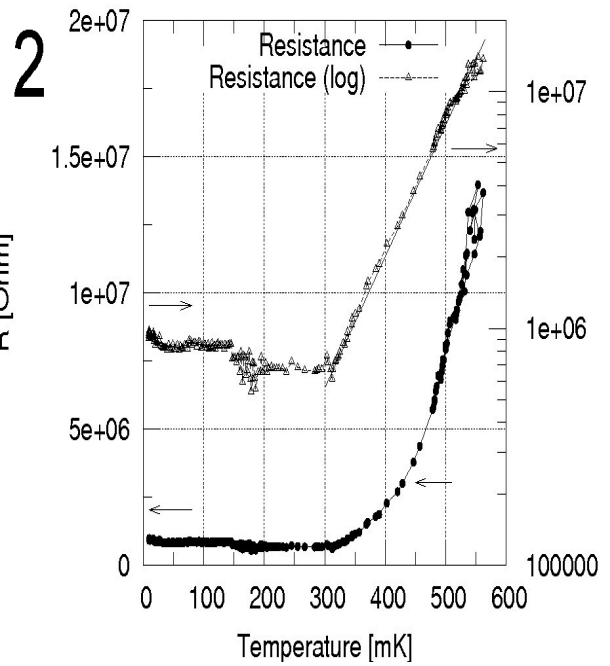
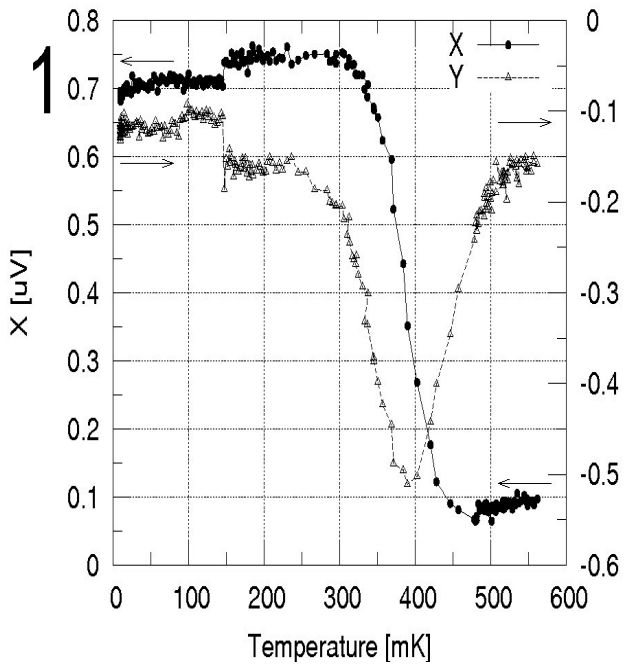


Fig. F.1 Some our measurements with 100 kHz frequency, 10mV excitation voltage, helium film thickness 1.0mm. Voltage on the guard electrode -6V , on the top electrode -4V . 1 – signal and 2 – resistance, Stanford SR850 Lock-In, density $3.6 \cdot 10^7$ electrons/cm², and voltage on the middle bottom electrode $+6\text{V}$; 3 – signal and 4 – resistance, Stanford SR850, density $7.3 \cdot 10^6$ electrons/cm², and voltage on the middle bottom electrode 0V ; 5 – signal and 6 – resistance, Stanford SR850, density $4.5 \cdot 10^6$ electrons/cm², and voltage on the middle bottom electrode 0V ; 7 – signal and 8 – resistance, Ithaco3961B, density $3.2 \cdot 10^6$ electrons/cm², and voltage on the middle bottom electrode 0V .

F.2 Measurements with different film thicknesses (data for the Chapter 5.2)



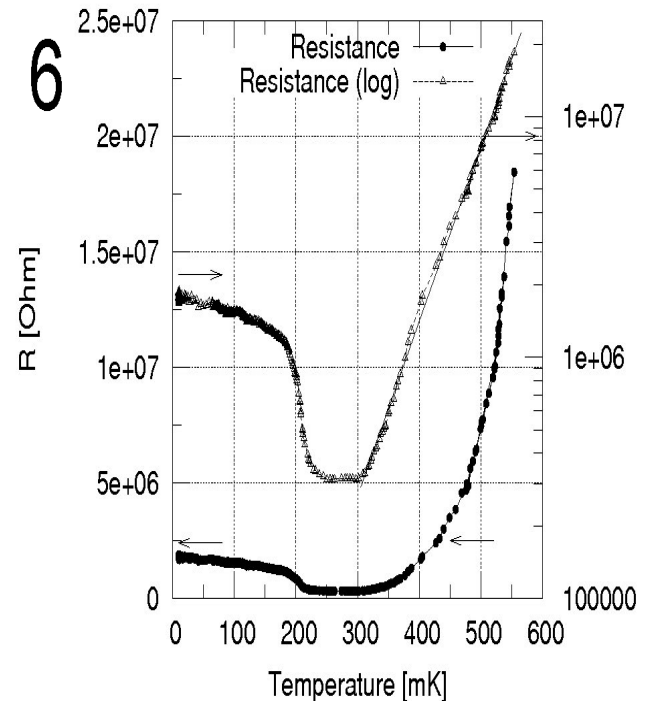
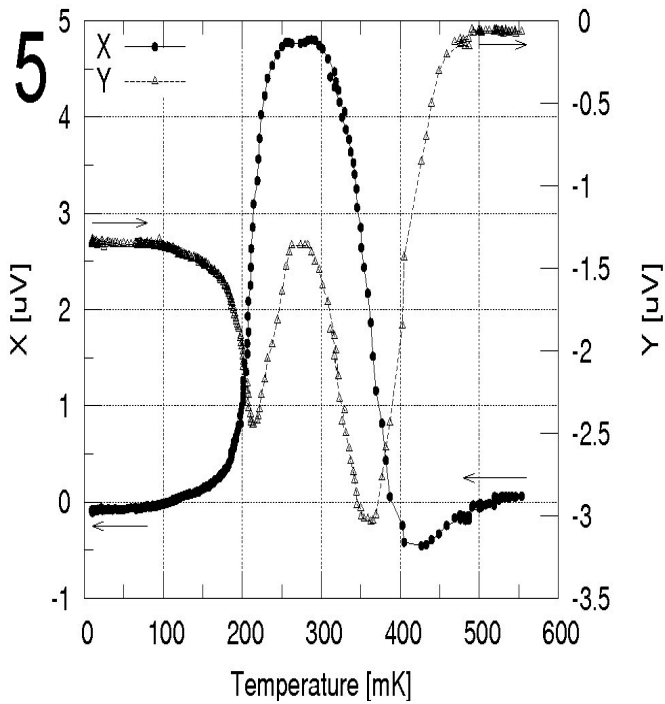
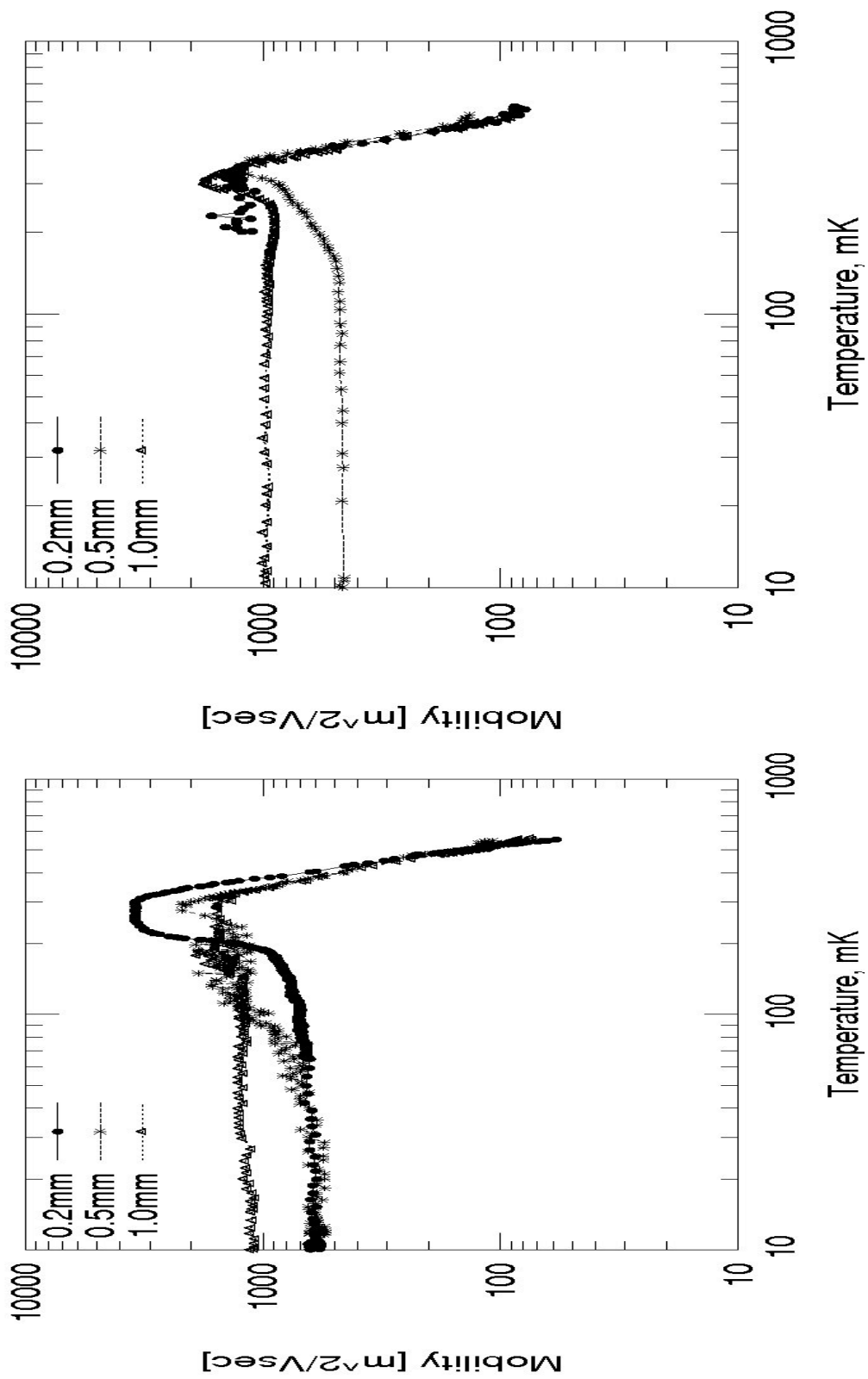


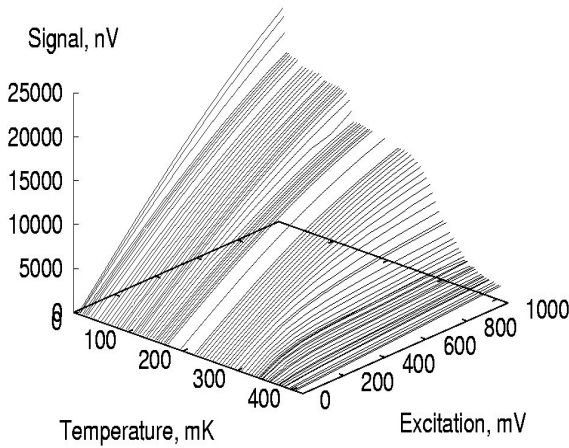
Fig. F.2 Measurement of electron layer on ^3He films of different thicknesses, for 100kHz. 1 – signal and 2 - resistance for 1.0mm, density $-5.8 \cdot 10^6$ electrons/cm 2 , 3 – signal and 4 - resistance for 0.5mm film, density $-7.3 \cdot 10^6$ electrons/cm 2 , 5 – signal and 6 - resistance for 0.2mm film, density $-6.1 \cdot 10^6$ electrons/cm 2 . Excitation voltage – 10mV. Voltages on the top, guard and three bottom electrodes were -4 ; -6 and 0 V correspondingly for film thicknesses 0.5 and 1.0mm and -2.6 ; -4 ; 0 for 0.2 mm film thickness.



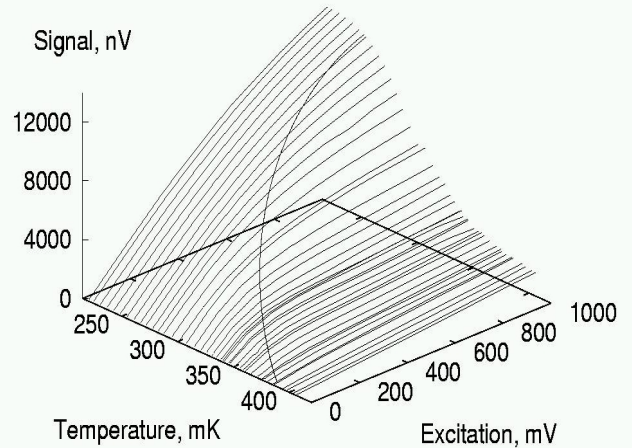
F.3. Mobility measurements for helium films with different thicknesses. Left without magnetic field and right with magnetic field (approximately 60Gauss). See also Fig 5.3, Chapter 5.2

F.3 Measurement with different excitation voltages (data for the Chapter 5.3)

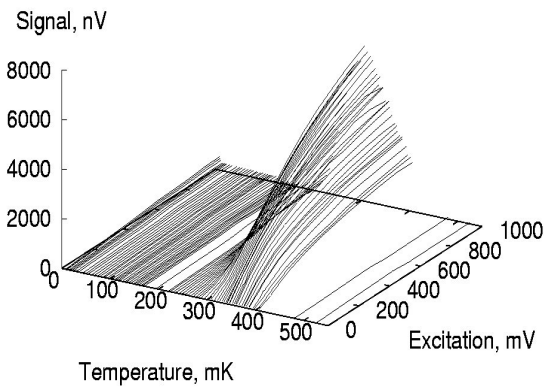
X-component of Signal for different excitation and Temperatures



X-component of Signal for different excitation and Temperatures



Y-component of Signal for different excitation (mV) and Temperature



Y-component of Signal for different excitation (mV) and Temperature

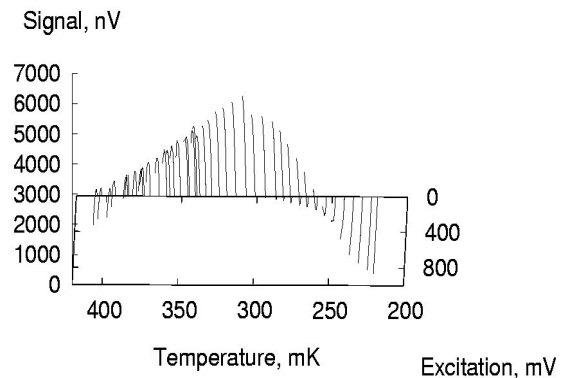
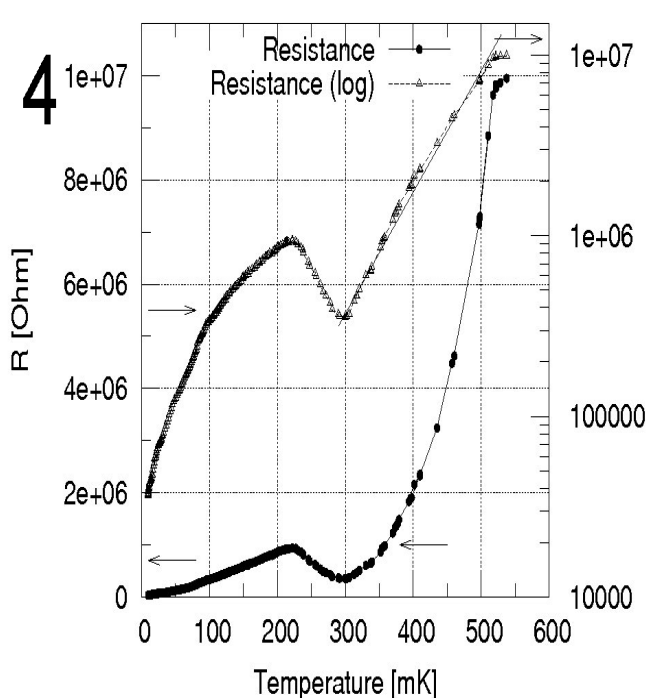
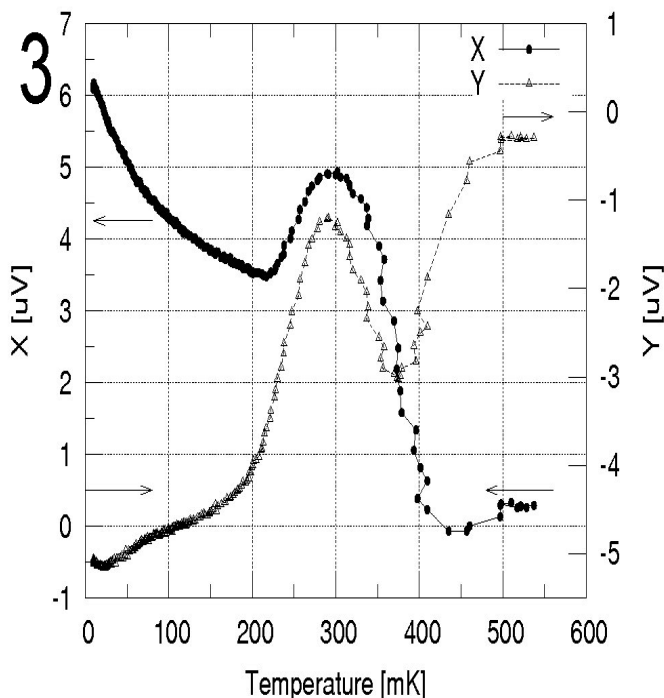
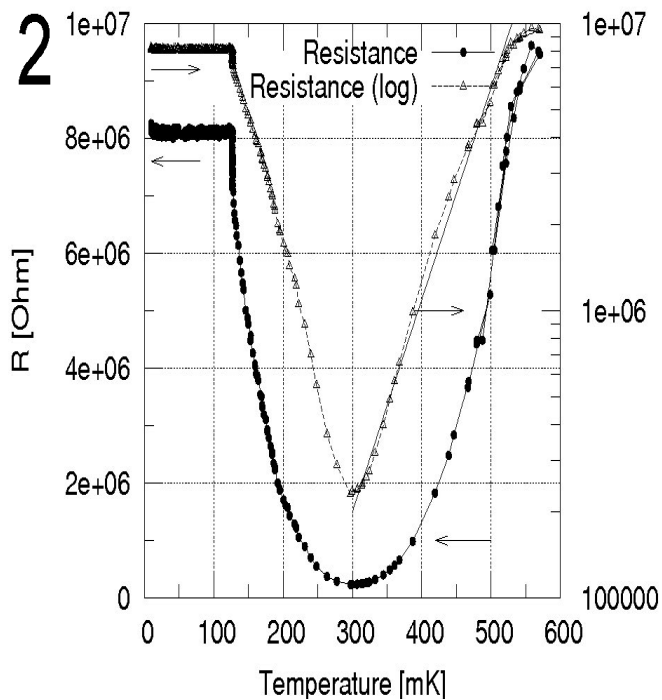
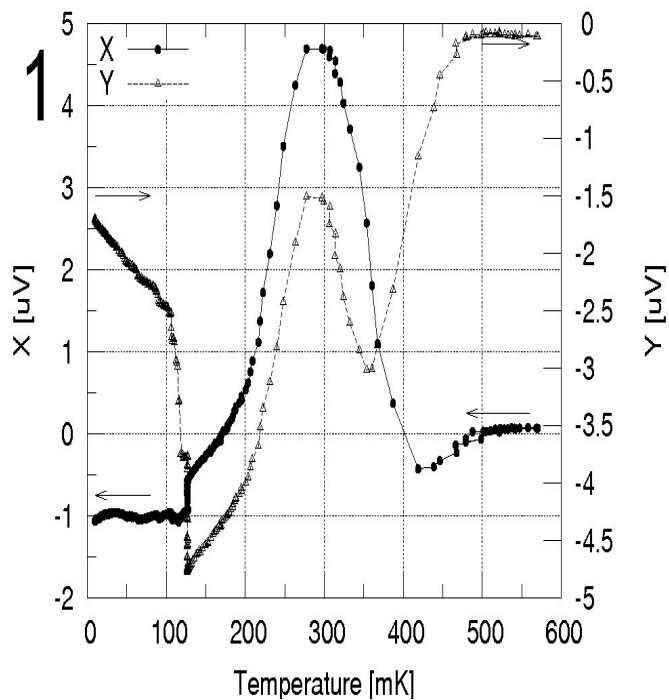


Fig. F.4 Measurement of electron signal with different excitations voltages. Top left and right – x-component of signal, bottom left and right – y-component. Two decreases at 10mK and 130mK are connected with losing of small part of electrons (5%). Density - $1.04 \cdot 10^6 (\pm 15\%)$ electrons/cm². On the right plots for each component we can see how the signal changes the slope for different excitations. Line separates regions with different slopes of measured signal. We can see, that decreasing of signal takes place as on x as well as on y component of signal (for y-component it is difficult to see, but it is present). See also Fig. 5.5 for more details.

F.4 Measurements with different excitation frequencies (data for the Chapter 5.4)



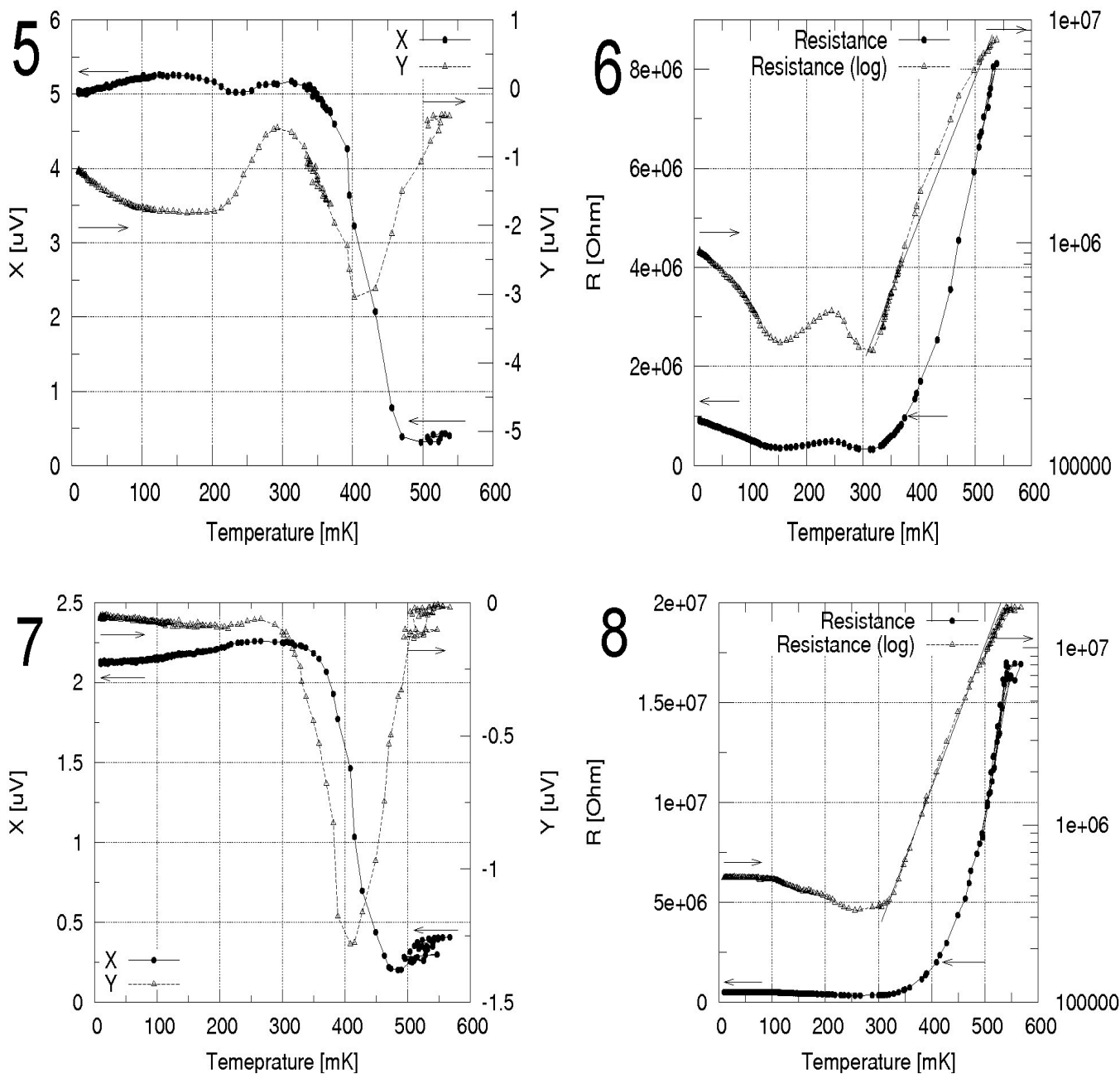
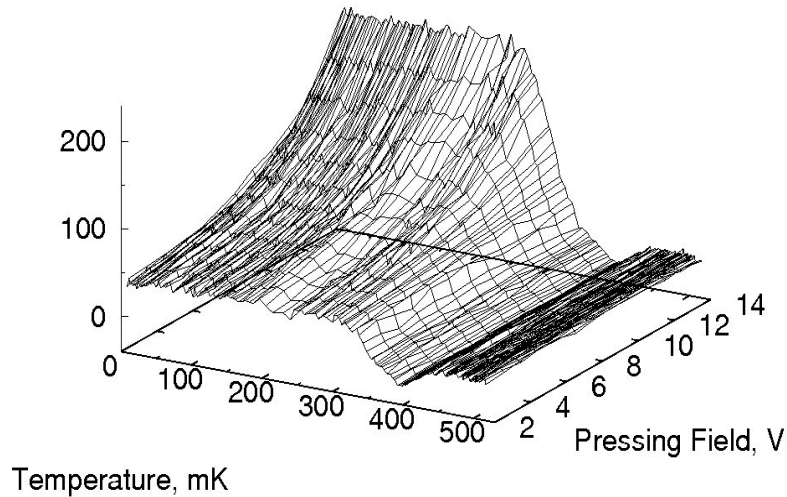


Fig. F.5 Measurement with different excitation frequencies for 0.2mm helium film. 1 – signal and 2 - resistance for 100kHz (at 120mK we have loose of electrons), density - $7.2 \cdot 10^6$ electrons/cm², 3 – signal and 4 - resistance for 75kHz, density - $5.8 \cdot 10^6$ electrons/cm², 5 – signal and 6 - resistance for 50kHz, density - $7.3 \cdot 10^6$ electrons/cm², 7 – signal and 8 - resistance for 10kHz density - $7.3 \cdot 10^6$ electrons/cm². Excitation voltage – 10mV. Voltages on the top, guard and middle bottom electrodes were –2.6; -4 and 0 V correspondingly.

F.5 Measurements of different pressing voltages on top and bottom electrodes (data for the Chapter 5.5)

X versus pressing fields on top electrode and Temperatures



Y versus pressing fields on top electrode and Temperatures

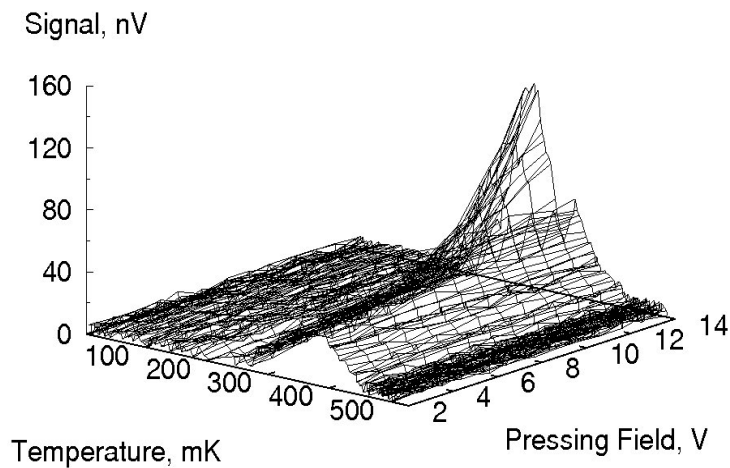
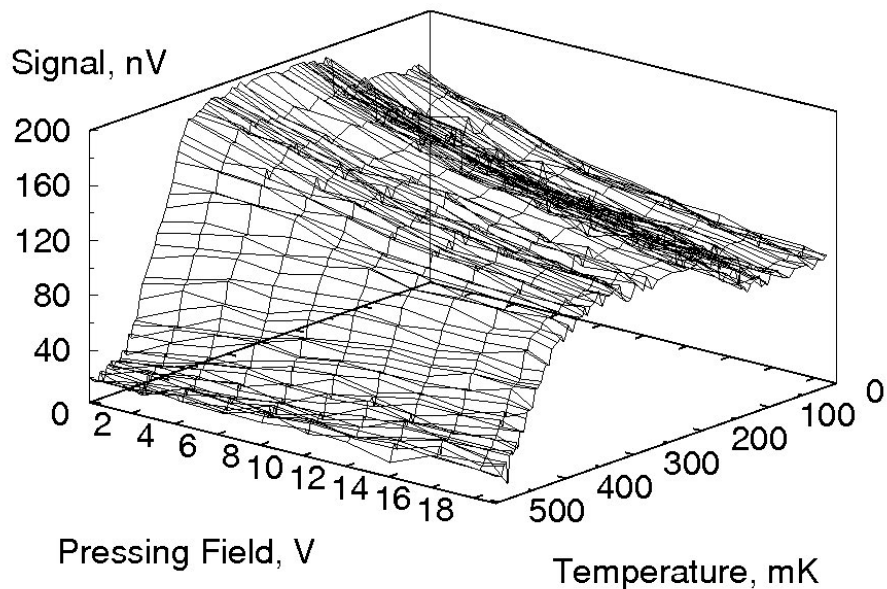


Fig. F.6 Electron signal for different pressing field (from 0 to 35V/cm) on top electrode (negative voltage). Top: x-component of signal, Bottom: y-component. Density - $1.04 \cdot 10^6 (\pm 15\%) \text{ electrons/cm}^2$. For more detail, see also Fig. 5.8

X versus pressing field on three bottom electrodes and Temperature



Y versus pressing field on three bottom electrodes and Temperature

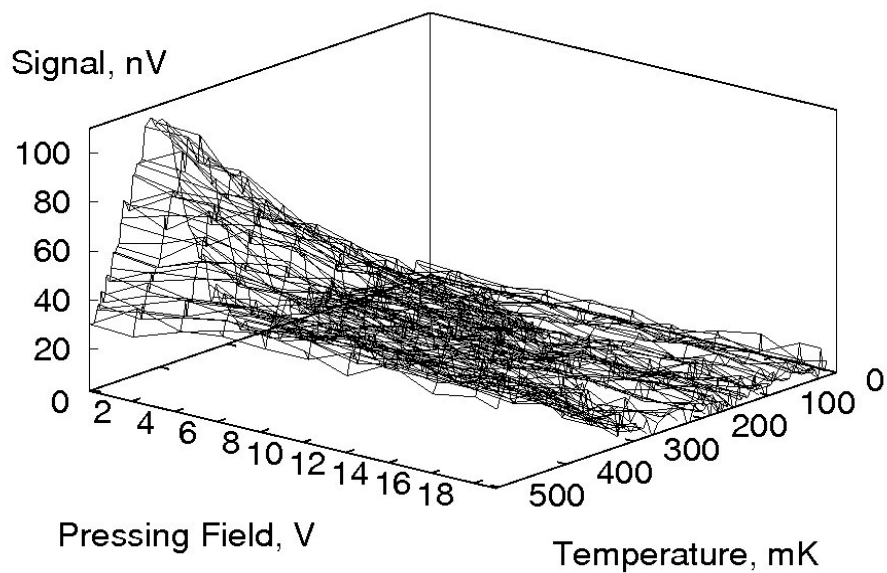
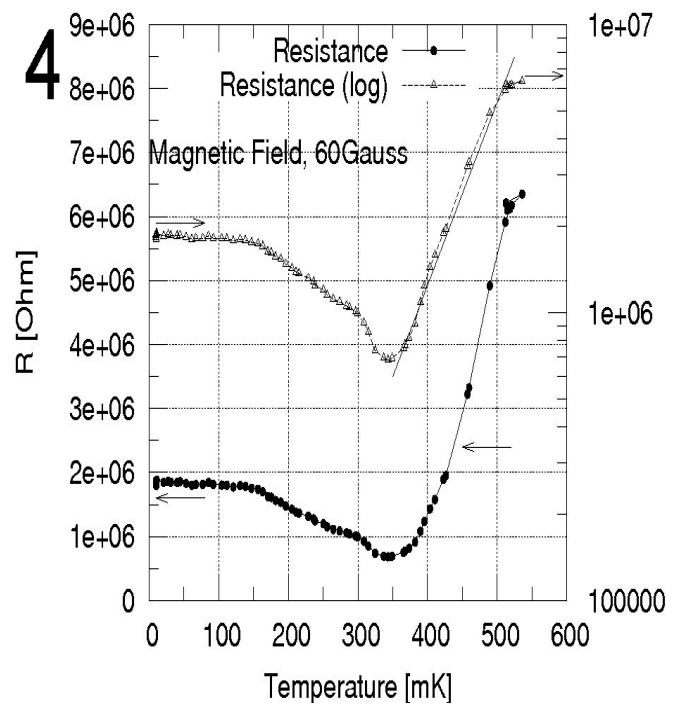
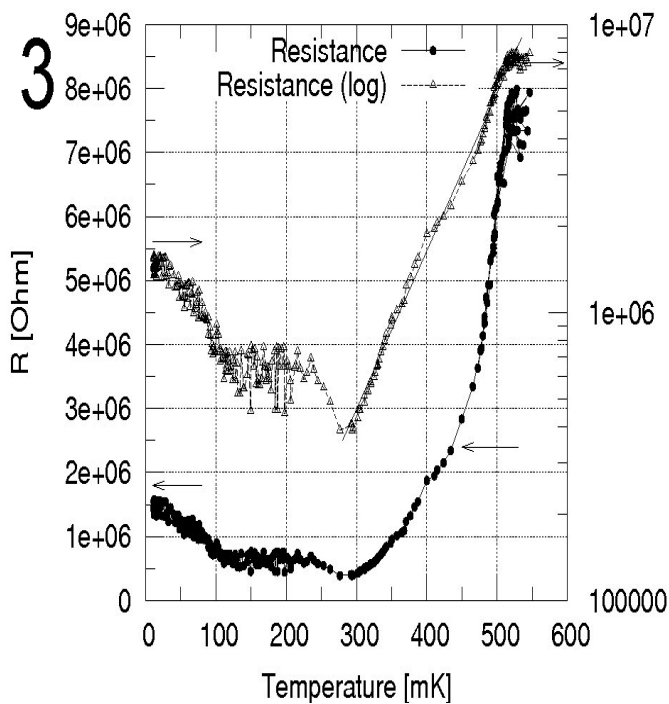
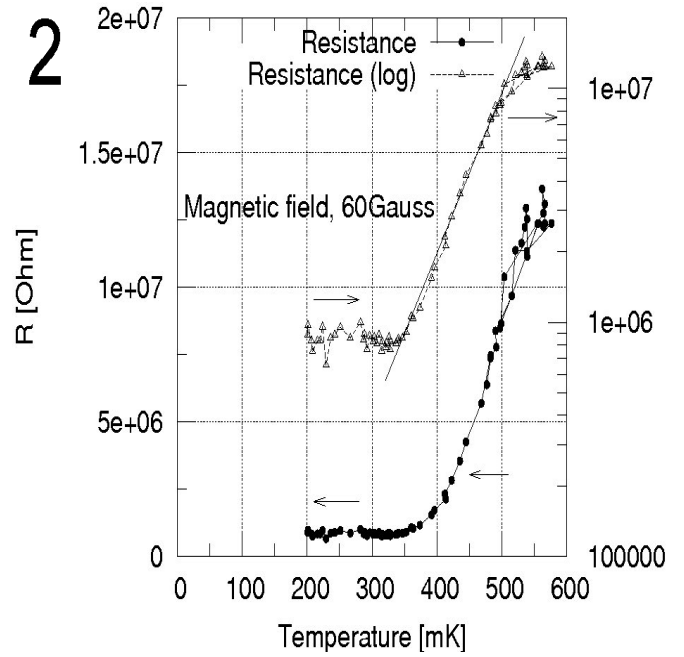
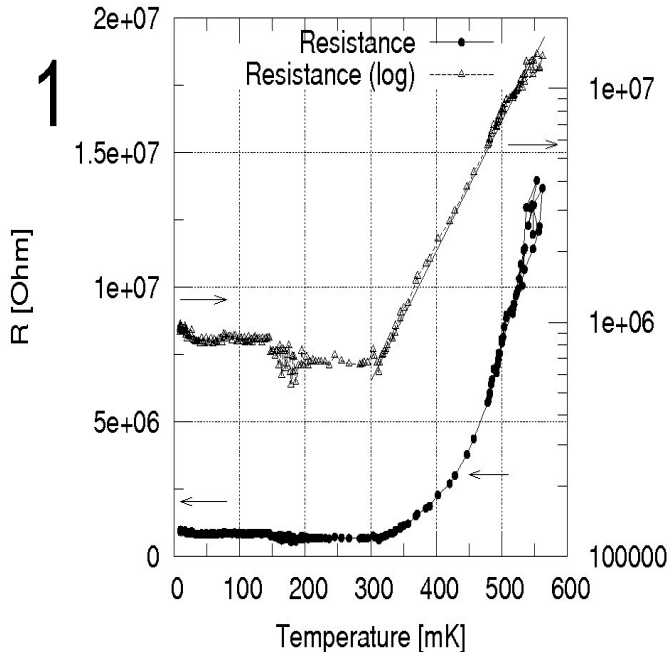


Fig. F.7 Electron signal for different electrical pressing field on three bottom electrodes. Top - X-component of signal, bottom - Y-component. Density - $1.8 \cdot 10^6$ electrons/cm². Signal decrease at 140mK is connected with loose of part of electrons (18%). See also Fig. 5.7

F.6 Measurements with magnetic field



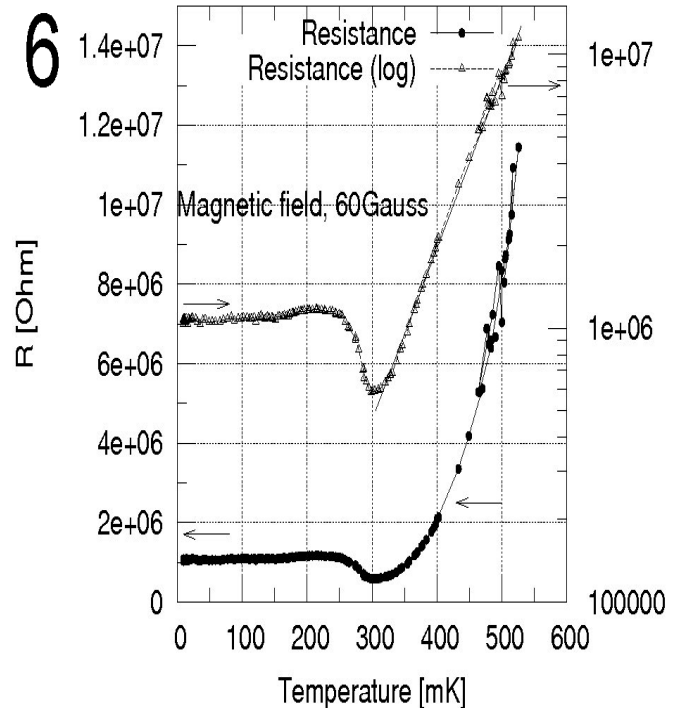
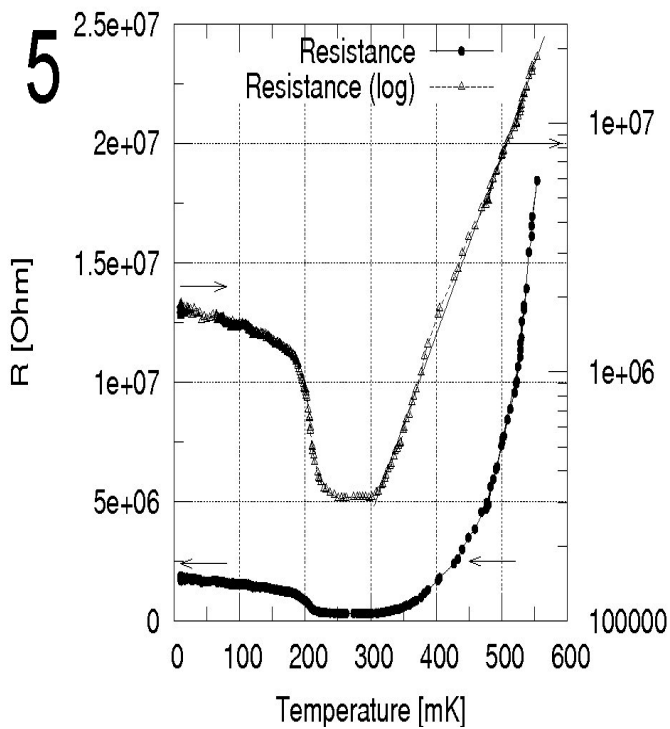


Fig. F.8 Magnetic field measurement (less than 92Gauss, approximately 60Gauss) for 100kHz and different film thicknesses. 1 – resistance without and 2 - with magnetic field for 1.0mm film, density - $6.1 \cdot 10^6$ electrons/cm²; 3 – resistance without and 4- with magnetic field for 0.5mm film, density - $7.3 \cdot 10^6$ electrons/cm²; 5- resistance without and 6- with magnetic field for 0.2mm film, density - $5.8 \cdot 10^6$ electrons/cm². Excitation voltage – 10mV. Voltages on the top, guard and middle bottom electrodes were -4; -6 and 0 V correspondingly for film thicknesses 0.5 and 1.0mm and -2.6; -4; 0 for 0.2 mm film thickness.

Bibliography

- [All66] *Superfluid Helium*, ed. by J.F. Allen, Academic Press, London and New York, 1966
- [Arm75] *The helium Liquids*, ed. by Jonathan G.M. Armitage, and Ian E. Farquhar, Academic Press, 1975
- [Bet76] D.S. Betts *Refrigeration and Thermometry below One Kelvin*, Sussex University Press, Sussex, 1976
- [Dam87] R. Mehrotra, A.J.Dahm *J. Low Temp. Phys.* **67**, 115-121 (1987)
- [Dob00] E.R. Dobbs, *Helium Three*, Oxford University Press, 2000
- [Edw75] D.O. Edwards, S.Y. Shen, J.R. Eckard, P.P. Fatouros, and F.M. Gasparini, *Phys. Rev. B* **12**, 892 (1975)
- [Edw78] D.O. Edwards and W.F. Saam, *Progress in Low Temp. Phys.*, **VIIA**, D.F.Brewer, ed. (North-Holland), 283 (1978)
- [Eska04] G.Eska, *private communication*
- [Eska88] G.Eska, *J. Low Temp. Phys.* **73**, Nos ¾, 207-221, (1988)
- [Fee69] Eugene Feenberg, *Theory of Quantum Fluids*, Academic Press, 1969
- [Fra84] H. Franco, J. Bossy, and H. Godfrin *Properties of sintered powders and their application in heat exchangers at millikelvin temperatures.*, *Cryogenics*, p. 477, (1984)
- [Gly94] Henry R. Glyde, *Excitations in Liquid and Solid Helim*, Clarendon Press, Oxford 1994

- [Gri79] C.C: Grimes and G. Adams: *Phys.Rev.Lett.* **42** (1979) 795
- [Handbo] Handbook of Chemistry and Physics, David R. Linde, 85th edition
2004-2005, CRS Press
- [Iino85] M. Iino, M. Suzuki, A.J.Ikushima, and J.Okuda, *J. Low Temp. Phys.*, **59**, 291-304 (1985)
- [Iye80-1] Y.Iye, K.Kono, K.Kajita, W.Sasaki, *J. Low Temp. Phys.* **38**, 293 (1980)
- [Iye80-2] Y.Iye, *J. Low Temp. Phys.* **40**, 441 (1980)
- [Kel69] *Helium 3 and Helium 4*, ed. by E. Keller, Plenum Press, New York 1969
- [Kha65] I.M.Khalatnikov, *An Introduction to the Theory of Superfluidity*, W.A. Benjamin INC.1965
- [Kir98] O.I. Kirichek, K.Shirahama, and K.Kono, *J. Low Temp. Phys.* **113**, 1103 (1998)
- [Kir00] O.I. Kirichek, K.Shirahama, F.I.B. Williams, M. Saitoh, K.Kono, *Physica B*, **284-288**, 279 (2000)
- [Kir01] O.I.Kirichek, M.Saitoh, and K.Kono, *Phys.Rev.Lett.* **86**, N18, 4064-4067 (2001)
- [Kir02] O. Kirichek, M. Saitoh, and K. Kono *J. Low Temp. Phys.*, **126**, 97-102 (2002)
- [Kir04] Oleg Kirichek, *Privat communication*
- [Klier04] Juergen Klier, Universitz of Konstanz. *Private communication.*

- [Kon00] K. Kono, *Physica B* **280**, 112-116 (2000)
- [Kon02] K. Kono, *J. Low Temp. Phys.* **126**, 467 (2002)
- [Land59] L.D. Landay and M. Lifshitz, *Fluid Mechanics*, (Pergamon, Oxford, 1959), p.237
- [Lea91] M. J. Lea, A. O. Stone, P. Fozooni, and J. Frost *J. Low Temp. Phys.*, **85**, 67-89 (1991)
- [Lea93] M. J. Lea, P. Fozooni, and J. Frost *J. Low Temp. Phys.*, **92**, 189-199 (1993)
- [Leid92] P. Leiderer, *J. Low Temp. Phys.* **87**, 247 (1992); P. Leiderer, in *Two-dimensional Electron Systems on Helium and other Substrates*, edited by E.Y.Andrei (Kluwer Academic Publishers, Netherlands, 1997)
- [Lou74] O.V. Lounasmaa, *Experimental Principles and Methods Below 1K*, Academic Press, London and New York, 1974
- [Mat01] K.Matsumoto, Y.Okuda, M.Suzuki, and S.Misawa *J. Low Temp. Phys.* **112**, 59 (2001)
- [Met82] R. Mehrotra, B.M. Guenin, and A.J.Dahm *Phys. Rev. Lett.* **48**, 641 (1982)
- [Met87] R. Mehrotra, *J. Low Temp. Phys.*, **67**, 123-142 (1987)
- [Mon91] Yu.P. Monarkha and V.B. Shikin, *Sov. J. Low.Tem. Phys.* **17**, 487 (1991)
- [Mon01] Yu.P. Monarkha and K. Kono: *J. Phys. Soc. Jpn*, **70** (2001) 1617-1626

- [Mon97] Yu. Monarkha and K. Kono: *J. Phys. Soc. Jpn*, **66** (1997) 3901-3907
- [Mon98] Yu. Monarkha, K. Shirahama, O.I. Kirichek, K. Kono *Physica B* **249-251** (1998) 636-639
- [Mor00] T. Morita, .Shirahama, F.I.B. Williams, K.Kono, *Physica B* **284-288**, 281-282 (2000)
- [Nom80] H.Nomaizawa : *Solid State Commun.* **34** (1980) 607
- [Noz99] Phillipe Noziekes and David Pines, *The Theory of Quantum Liquids*, Advanced Book, Classics, Dresher Book, 1999
- [Pere04] S. Pereversev, *private communication*
- [Pob92] F.Pobell *Matters Methods at Low Temperatures*, Springer Verlag, Berlin, Springer Textbook Edition, 1992
- [Phy81] W.A. Phyllips (ed.): *Amorphos Solids*, Topics Curr. Phys., Vol.24 (Springer, Berlin, Heilderberg, 1981)
- [PPE] Sergiy Putselyk, Sergey Pereversev, Georg Eska, *experimental observation*
- [Sait77] M.Saitoh, *J. Phys. Soc. Jpn*, **42** (1977) 201-209
- [Shii02] T.Shiino, H.Mukuda, K.Kono and W.F.Vinen *J. Low Temp. Phys.* **126**, 493 (2002)
- [Sh95] Keya Shirahama and Kimitoshi Kono *Phys.Rev.Lett.* **74**, N21, 781-784 (1995)
- [Shir95] K.Shirahama, S.Ito, H. Suto, and K.Kono, *J. Low Temp. Phys.* **101**, 439 (1995)

- [Shir96] K.Shirahama and K.Kono *J. Low Temp. Phys.* **104**, 237 (1996)
- [Shir97] K.Shirahama, O.Kirichek and K.Kono *Phys.Rev.Lett.* **79**, N21, 4218-4221 (1997)
- [Shir98] K.Shirahama, O.Kirichek and K.Kono *J. Low Temp. Phys.* **110**, 179 (1998)
- [Shir00] K.Shirahama, H.Suto, O.Kirichek and K.Kono *Physica B* **284-288**, 277-278 (2000)
- [Som71] W.T.Sommer and D.J.Tanner, *Phys. Rev. Lett.* **27**, 1345 (1971)
- [Sti86] Stiver W. Van Sciver, *Helium Cryogenics*, Plenum Press, New York, 1986
- [Suto96] H. Suto, K. Shirahama, and K. Kono *Czechoslovak Journal of Physics*, Vol. 46 (1996), Suppl.S1
- [Val98] A.M.C. Valkering, Doctoral Thesis, Technische Universitaet Eindhoven, 1998
- [Wag95] T. Wagner, *Experimente mit gepulster NMR zur Spin-Spin-Wechselwirkung in den Metallen Platin und AuIn₂ bei tiefen Temperaturen*, Dissertation, Universität Bayreuth, 1995
- [Wil67] Wilkins, *The properties of Liquid and Solid Helium*, Clarendon Press, Oxford 1967
- [Will82] F.I.B. Williams, *Surf.Sci.* **113**, 371 (1982)
- [Wil88] Wilen and R. Gianetta *J. Low Temp. Phys.* **72**, 353-369 (1988)

List of Figures

2.1	<i>Schematic diagram of gas-liquid (and electrons) interface.</i>	7
2.2	<i>Mobility as a function of temperature for three electron densities [Shir95]</i>	14
2.3	<i>Mobility of ^3He and ^4He [Shir95] in the vapor-atom regime as a function of vapor density.</i>	15
2.4	<i>WS resistivity versus temperature for the saturation case, $E=2\text{pen}$.</i>	16
2.5	<i>WS resistance in the nonlinear regime.</i>	18
2.6	<i>(a) Collision time of surface electrons on the ^4He surface obtained from the linewidth of coupled plasmon-riplon resonance as a function of temperature (opened circle). The low frequency data of Corbino measurements (solid circles). (b) The collision time of surface electrons on ^3He surface as a function of temperature for two different densities [Kir98]</i>	19
2.7	<i>Collision time t of surface electrons obtained from the line width of transverse optical-plasma resonance as a function of temperature.</i>	19
2.8	<i>The Wigner Solid resistance $R(T)$ normalized by $R(T_c)$, as a function of T/T_c, at $0T$ (filled circles), 218mT (opened circles), 256mT (crosses).</i>	20
3.1	<i>Schematic drawing of the cryostat.</i>	23
3.2	<i>Schematic diagram (sketch) of the cell for mobility measurement.</i>	27
3.3	<i>Schematic diagram (sketch) of the cell for capacitance measurement</i>	27
4.1	<i>Dependence of the X and Y components of the signal versus the pulse duration.</i>	31
4.2	<i>Electron density versus the voltage at the top electrode.</i>	32
4.3	<i>Typical measured X (top) and Y (bottom) components of electron layer resistance.</i>	34
4.4	<i>Schematic picture of cell tilting and forces acting on electrons.</i>	35
4.5	<i>Electrical signal (X-component) versus applied positive electrical field on one of the bottom electrodes.</i>	37
4.6	<i>Filament schema for calculation of filament temperature and relaxation time.</i>	38

4.7	<i>Temperature increase of electrons, due to overheating by excitation voltages.</i>	40
5.1	<i>Our resistance measurements for 100 kHz frequency, 10mV excitation voltage, helium film thickness 1.0mm, voltage on the guard electrode – 6V, on the top electrode –4V.</i>	50
5.2	<i>Top – Mobility for three electron densities [Shir95], bottom our measurements.</i>	52
5.3	<i>Electrons’ mobility for helium films with different thicknesses (0.2. 0.5 and 1.0mm). Left without magnetic field and right with magnetic field</i>	54
5.4	<i>Measurements of electron layer resistance with ³He films with different thicknesses.</i>	56
5.5	<i>Resistance of electron layer versus different excitation voltages.</i>	59
5.6	<i>Resistance of electron layer with different frequencies of excitation voltages for the helium film of 0.2mm.</i>	64
5.7	<i>Resistance of electron layer versus voltage on three bottom electrodes.</i>	66
5.8	<i>Resistance of electron layer for different pressing field (from 0 to 35V/cm) on top electrode (negative voltage)</i>	68
A1	<i>Electrical potentials in the cell</i>	78
B.1	<i>We can consider different way of impedance calculation using simple lumped impedance scheme (Juergen Klier, University of Konstanz)</i>	81
B.2	<i>The characteristic impedances in the cell and its capacitance values for the frequency 100KHz</i>	84
B.3	<i>Our simplified scheme, Sommer-Tanner scheme and circuit scheme.</i>	85
B.4	<i>Comparison of different models.</i>	88
B.5	<i>X and Y components (Volt) of measured signal</i>	91
B.6	<i>Left top and bottom – X component of experimental and theoretical curves. Right top and bottom – Y ones.</i>	92
B.7	<i>Comparison of cell sensitivity for different helium film thicknesses</i>	94
B.8	<i>Typical density profile in the cell.</i>	96
B.9	<i>Comparison of cell sensitivity for different percentage of electron layer.</i>	97

B.10	<i>Comparison of sensitivity of cell with measurements of two adjust electrodes.</i>	99
B.11	<i>Comparison (top left and right) of measured resistances</i>	100
B.12	<i>Comparison of measured signal and theoretical curves (transmission line model) for rectangular geometry (Sommer-Tanner scheme) [Lea91]</i>	101
B.13	<i>Comparison of our measured signal and theoretical curves (improved Sommer-Tanner model using our equivalent scheme)</i>	101
C.1	<i>Real view of the cell (see also Fig. 3.2)</i>	102
D.1	<i>X-component of signal versus different negative voltages on the top electrode.</i>	106
D.2	<i>X-component of signal versus different negative voltages on the top electrode.</i>	108
F.1	<i>Some our measurements with 100 kHz frequency, 10mV excitation voltage, helium film thickness 1.0mm.</i>	112
F.2	<i>Measurement of electron layer on ³He films of different thicknesses.</i>	114
F.3	<i>Mobility measurements for helium films with different thicknesses. Left without magnetic field and right with magnetic field</i>	115
F.4	<i>Measurement of electron signal with different excitations voltages.</i>	116
F.5	<i>Measurement with different excitation frequencies for 0.2mm helium film.</i>	118
F.6	<i>Electron signal for different pressing field (from 0 to 35V/cm) on top electrode (negative voltage).</i>	119
F.7	<i>Electron signal for different electrical pressing field on three bottom electrodes.</i>	120
F.8	<i>Magnetic field measurement (less than 92Gauss, approximately 60Gauss) for 100KHz and different film thicknesses.</i>	122

List of Tables

- 1 Critical values for instability phenomena of ^3He and ^4He 9
- 2 Quantitative comparison of different damping coefficients of 44
gravitational-surface waves versus different temperatures and
frequencies
- 3 Qualitative comparison of our cell with different film thicknesses 95
- 4 Quantitative comparison of cell with different percentages of 98
electron layer.

Danksagung

Mein besonderer Dank gilt Herrn Prof. Dr. G. Eska für die Betreuung dieser Arbeit. Seine Unterstützung und zahlreiche klärende Diskussionen waren mir stets eine große Hilfe.

Herrn Prof. P. Leiderer danke ich sehr für die Übernahme des Korreferats.

Herrn Prof. W. Brand und Prof. L. Kador danke ich für die Abnahme der Doktorprüfung.

Dem Postdoc unserer Arbeitsgruppe, Dr. S. Pereversev, danke ich für die Beratung zu experimentellen Fragen der Ultratieftemperaturtechnik.

Stellvertretend für die Mitarbeiter der feinmechanischen und der Elektrowerkstatt möchte ich Herrn H.-J. Wehner, und Herrn K. Ötter für die gute und schnelle Bearbeitung aller Aufträge danken.

Des Weiteren gilt mein besonderer Dank Herrn Piotr Sekowsky für seine Freundlichkeit mir immer wieder etwas Neues über Kälte- und Vakuumtechnik zu erzählen und seine allzeitige Bereitschaft zu helfen. Verzeihe er mir alle leere Kannen!

Nicht zuletzt, möchte ich Frau C. Linser für die Hilfe bei meinem ständigen Kampf mit der deutschen Bürokratie danken! Auch besonderen Dank für die Teeecke!

Und endlich möchte ich meinen Eltern für die dauerhafte moralische Unterstützung während allen diesen Jahren danken.